2007

Structural and magnetothermal properties of compounds: Yb5Si[subscript x]Ge4â^'[subscript x], Sm5Si[subscript x]Ge4â^'[subscript x], EuO, and Eu3O4

Kyunghan Ahn
Iowa State University

Structural and magnetothermal properties of compounds: $Yb_5Si_xGe_{4-x}$, $Sm_5Si_xGe_{4-x}$, EuO, and Eu_3O_4

by

Kyunghan Ahn

A dissertation submitted to the graduate faculty

in partial fulfillment of the requirements for the degree of

DOCTOR OF PHILOSOPHY

Major: Materials Science and Engineering

Program of Study Committee:
Vitalij K. Pecharsky, Major Professor
Karl A. Gschneidner, Jr.
Ralph W. McCallum
Paul C. Canfield
David C. Johnston

Iowa State University

Ames, Iowa

2007

UMI Number: 3259437

UMI Microform 3259437

ProQuest Information and Learning Company
300 North Zeeb Road
P.O. Box 1346
Ann Arbor, MI 48106-1346

TABLE OF CONTENTS

ABSTRACT

The family of $R_5Si_xGe_{4-x}$ alloys demonstrates a variety of unique physical phenomena related to magneto-structural transitions associated with reversible breaking and reforming of specific bonds that can be controlled by numerous external parameters such as chemical composition, magnetic field, temperature, and pressure. Therefore, $R_5Si_xGe_{4-x}$ systems have been extensively studied to uncover the mechanism of the extraordinary magneto-responsive properties including the giant magnetoresistance (GMR) and colossal magnetostriction, as well as giant magnetocaloric effect (GMCE). Until now, more than a half of possible $R_5Si_xGe_{4-x}$ pseudobinary systems have been completely or partially investigated with respect to their crystallography and phase relationships (R = La, Pr, Nd, Gd, Tb, Dy, Er, Lu, Y). Still, there are other $R_5Si_xGe_{4-x}$ systems (R = Ce, Sm, Ho, Tm, and Yb) that are not studied yet. Here, we report on phase relationships and structural, magnetic, and thermodynamic properties in the $Yb_5Si_xGe_{4-x}$ and $Sm_5Si_xGe_{4-x}$ pseudobinary systems, which may exhibit mixed valence states.

The crystallography, phase relationships, and physical properties of $Yb_5Si_xGe_{4-x}$ alloys with $0 \leq x \leq 4$ have been examined by using single crystal and powder x-ray diffraction at room temperature, and dc magnetization and heat capacity measurements between 1.8 K and 400 K in magnetic fields ranging from 0 to 7 T. Unlike the majority of $R_5Si_xGe_{4-x}$ systems studied to date, where R is the rare earth metal, all Yb-based germanide-silicides with the 5:4 stoichiometry crystallize in the same Gd_5Si_4-type structure. The magnetic properties of $Yb_5Si_xGe_{4-x}$ materials are nearly composition-independent, reflecting the persistence of the same crystal structure over the whole range of x from 0 to 4. Both the crystallographic and magnetic property data indicate that $Yb_5Si_xGe_{4-x}$ alloys are mixed valence systems, in which the majority (60%) of Yb atoms is divalent, while the minority (40%) is trivalent. This finding is supported by recent Mössbauer spectroscopy data.

The crystallography, phase relationships, and physical properties of the $Sm_5Si_xGe_{4-x}$ alloys with $0 \leq x \leq 4$ have been investigated by using variable temperature x-ray powder

diffraction, dc magnetization and heat capacity measurements between 3.5 K and 350 K in magnetic fields ranging from 0 to 10 T. Similar to the $Gd_5Si_xGe_{4-x}$ system, there are three distinct phase regions in the paramagnetic state in the $Sm_5Si_xGe_{4-x}$ system; the Gd_5Si_4-type for Si-rich compositions, the $Gd_5Si_2Ge_2$-type for intermediate range of concentrations, and the Sm_5Ge_4-type for Ge-rich alloys. The magnetic properties of the $Sm_5Si_xGe_{4-x}$ compounds can be well described by considering the temperature-independent Van Vleck term due to small energy separation between the ground state and the first excited state of Sm^{3+} ions. All $Sm_5Si_xGe_{4-x}$ compounds have unusually high magnetic ordering temperatures. The change in both the magnetic and structural behaviors with the substitution of Ge by Si is similar to that observed in the $Gd_5Si_xGe_{4-x}$ system. The external magnetic field seems to have no effect on the magnetism of the $Sm_5Si_xGe_{4-x}$ alloys.

Europium oxides, EuO with the divalent state and Eu_3O_4 with the mixed-valence state, may exhibit a strong magnetocaloric effect (MCE) and interesting magnetism because of the unique magnetic properties of Eu. Europium has two valence states: Eu^{2+} and Eu^{3+}. The Eu^{2+} ion is similar to the Gd^{3+} ion with $4f^7$ state ($J = 7/2$), while the Eu^{3+} ion has a $4f^6$ configuration ($J = 0$). Elemental Gd and many Gd-based compounds are good magnetic refrigerant materials due to their large magnetic moments, large available magnetic entropy, and low hysteresis. Thus, we report on magnetic behavior and the MCE of EuO and Eu_3O_4 as evaluated from both the heat capacity and magnetization measurements.

EuO was synthesized through the thermal reduction of Eu_2O_3 by a stoichiometric quantity of metallic Eu. According to the heat capacity and magnetic measurements, EuO undergoes a second-order phase transformation at ~69 K from the ferromagnetic to the paramagnetic state on heating. The magnetocaloric effect of EuO, both as the isothermal magnetic entropy change (ΔS_{mag}) and the adiabatic temperature change (ΔT_{ad}), was obtained from the heat capacity data. Also, the magnetization isotherms were used to calculate ΔS_{mag}. EuO exhibits the magnetocaloric effect with a peak in the vicinity of the magnetic phase transition temperature (~69 K), the amplitude of which is comparable to other known

magnetocaloric materials. The ΔS_{mag} calculated from the heat capacity data is in excellent agreement with that calculated from the magnetization data.

Mixed-valence compound Eu_3O_4 was prepared by heating EuO and Eu_2O_3 together at 1800 °C for 30 h in a sealed W crucible under a high vacuum. It was confirmed as a single phase Eu_3O_4 using the room temperature x-ray powder diffraction method. We characterized a polycrystalline Eu_3O_4 through the heat capacity and magnetic measurements. Our results from magnetic measurements are in good agreement with the references reported previously. As far as we are aware, heat capacity of Eu_3O_4 was not studied in the past. The magnetic entropy change ($-\Delta S_{mag}$) in Eu_3O_4 near 6.5 K is around 12.7 J/kg K with the magnetic field change (ΔB) of 5 T. The adiabatic temperature change (ΔT_{ad}) in Eu_3O_4 near 7 K is around 7.0 K with the ΔB of 5 T. Also, the magnetic entropy change ($-\Delta S_{mag}$) calculated from magnetization data in Eu_3O_4 near 6.3 K is around 13.6 J/kg K with the magnetic field change (ΔB) of 5 T, which is roughly same as that from heat capacity data.

CHAPTER 1. GENERAL INTRODUCTION

Since the discovery of the giant magnetocaloric effect (GMCE) in $Gd_5Si_2Ge_2$[22], which is strongly correlated with the first-order magneto-structural transition around room temperature, $R_5Si_xGe_{4-x}$ systems (R = rare earth element) have been extensively studied to uncover the mechanism of the extraordinary magneto-responsive properties including the giant magnetoresistance (GMR) and colossal magnetostriction as well as GMCE. Until now, crystallography and phase relationships have been completely or partially investigated for more than a half of possible $R_5Si_xGe_{4-x}$ pseudobinary systems (R = La[1], Pr[2], Nd[1,3], Gd[4], Tb[5], Dy[1], Er[6], Lu[1], and Y[7]). Still, there are other $R_5Si_xGe_{4-x}$ systems (R = Ce, Sm, Eu, Ho, Tm, and Yb) that are not studied yet. The 5:4 phases (R_5Si_4 or R_5Ge_4) have not been reported for R = Pm, and they do not form for R = Eu. For other rare earth metals (R = Ce[8,9,10], Sm[18,19,20], Tm[11], and Yb[12,13,14]) they have been reported only for binary compounds, and with R = Ho they have been investigated in the binary systems[15,16] and for $Ho_5Si_2Ge_2$[17]. Phase relationships and structural, magnetic, and thermodynamic properties in the $R_5Si_xGe_{4-x}$ system with R = Yb and Sm, may be interesting because these rare earth metals may exhibit a mixed valence state. Cerny *et al*. reported that Yb_5Si_4 adopts the orthorhombic Gd_5Si_4-type crystal structure, and for Yb_5Si_4 and Sm_5Ge_4 there is a difference in the coordination of some Si (Ge) atoms because all Si atoms in Yb_5Si_4 are covalently bonded with other Si atoms in pairs while only half of Ge atoms in Sm_5Ge_4 form covalently bonded Ge_2 pairs.[12] However, Palenzona *et al*. and Pani *et al*. reported that both Yb_5Si_4 and Yb_5Ge_4 crystallize with the Sm_5Ge_4-type structure.[13,14] Thus, there is the controversy about the room temperature crystallography of Yb_5T_4 compounds (T is Si or Ge). The $Sm_5Si_xGe_{4-x}$ system has not been studied since the first report of the existence of the Sm_5Si_4 and Sm_5Ge_4 phases in 1966.

The major motivation to study $Yb_5Si_xGe_{4-x}$ and $Sm_5Si_xGe_{4-x}$ systems are: the possibility of mixed-valence behavior in these two pseudo binary systems; and the lack of knowledge of the magnetocaloric effect in mixed-valence systems. In addition this research will add new information to our understanding of the extraordinary magneto-responsive behaviors of the $R_5Si_xGe_{4-x}$ compounds.

Recently, near room-temperature magnetic refrigeration technology has received a great deal of attention because of its environmental safety and potential for considerable improvements in energy efficiency. In addition to further refinements of the existing prototype refrigerators, materials with large magnetocaloric effect (MCE) are required to take full advantage of multiple benefits such as energy savings and environmentally friendly approach offered by the magnetic refrigeration technology. Today, the development of advanced magnetocaloric materials exhibiting strong MCE between ~20 K and 300-350 K remains an important topic for basic science in order to support future magnetic refrigeration needs. Thus, EuO with Eu^{2+} ions may have a potential for application as a magnetic refrigerant material because of the unique magnetic properties of Eu. The Eu^{2+} ion is similar to the Gd^{3+} ion with a $4f^7$ state (J=7/2). Elemental Gd and many Gd-based compounds are good magnetic refrigerant materials due to their large magnetic moments, large available magnetic entropy [$S = R \ln (2J + 1)$], and low magnetic and thermal hysteresis. Divalent europium in binary compounds, such as EuO, EuS, EuSe, and EuTe, may bring about a large MCE as well as interesting magnetism. On the other hand, Eu_3O_4 is interesting because it is a heterogeneous mixed-valence compound which has two different valence sites (Eu^{2+} and Eu^{3+}) in the unit cell. This oxide can be described as $Eu^{2+}Eu^{3+}{}_2O^{2-}{}_4$ and thus the ratio of Eu^{2+} to Eu^{3+} ions is 1/2. Divalent and trivalent Eu ions occupy the Ca sites and Fe sites, respectively, of the $CaFe_2O_4$-type structure. While there have been several reports about magnetic properties of Eu_3O_4, the magneto-thermal properties of Eu_3O_4 have not been studied yet.

Thus, the motivation of my studies on EuO and Eu_3O_4 is to investigate the magneto-thermal properties, especially magnetocaloric effect, of compounds with either divalent or heterogeneous mixed-valent states of Eu ions, respectively.

Literature review

R_5Si_4-R_5Ge_4 pseudobinary system

In 1966, Smith *et al*. discovered the existence of R_5Si_4 or R_5Ge_4 phases. They reported that the germanides R_5Ge_4 (R = Nd, Sm, Gd, Tb, Er, Y) and the silicides R_5Si_4 (R = Tb, Er, Y) adopted the same orthorhombic Sm_5Ge_4-type structures while Nd_5Si_4 has a primitive tetragonal structure.[18] According to Smith *et al*.'s study, these were stoichiometric Sm_5Ge_4-type phases, which was confirmed by the x-ray diffraction method and their structure within the space group *Pnma* was described by three layers of atoms stacked along the *b*- axis.[19] Later, the same authors reported that all R_5Ge_4 (R = La, Ce, Pr, Nd, Sm, Gd, Tb, Dy, Ho, Er, Tm, Lu, Y) compounds exhibit the same Sm_5Ge_4-type structure while the structure of R_5Si_4 compounds was dependent upon the rare earth element: R_5Si_4 (R = Tb, Dy, Er, Y, Sm, Gd) adopt the Sm_5Ge_4-type structure, but R_5Si_4 (R = La, Ce, Pr, Nd) crystallize in the tetragonal Zr_5Si_4-type structure.[20] Holtzberg *et al*. reported that R_5Si_4 compounds (R = Gd, Tb, Dy, Ho, Er) order ferromagnetically at relatively high Curie temperatures, while R_5Ge_4 compounds (R = Gd, Tb, Dy, Ho, Er) are antiferromagnetic, and that the substitution of Si for Ge in Gd_5Ge_4 allows solid solutions to be ferromagnetic at low temperature.[21] In 1997, Pecharsky and Gschneidner reported the giant magnetocaloric effect (GMCE) in $Gd_5Si_2Ge_2$ compound, which was associated with a first order phase transition at 276 K.[22] Furthermore, they found that there were three crystallographically different phase regions in the $Gd_5Si_xGe_{4-x}$ pseudobinary system at room temperature: for Gd_5Si_4-based solid solution ($2 < x \leq 4$) and for the Gd_5Ge_4-based solid solution ($0 \leq x \leq 0.8$) they reported two different orthorhombic structures, and for the $Gd_5Si_2Ge_2$-type solid solution ($0.96 \leq x \leq 2$) there exists a monoclinically distorted crystal structure.[23] These authors believed that for Gd_5Si_4-Gd_5Ge_4 pseudobinary system considerable change in magnetic properties including the GMCE is related to different crystallography of three phases. The recent discovery of the GMCE in the $Gd_5Si_xGe_{4-x}$ pseudobinary system has triggered considerable interest in $R_5Si_xGe_{4-x}$ (R = rare earth metal) systems more than thirty years after Smith *et al*.'s reports.

Phase relationships and room temperature crystallography of $R_5Si_xGe_{4-x}$ systems (including the results obtained in this work for the systems with R = Sm and Yb) are shown in Fig. 1.

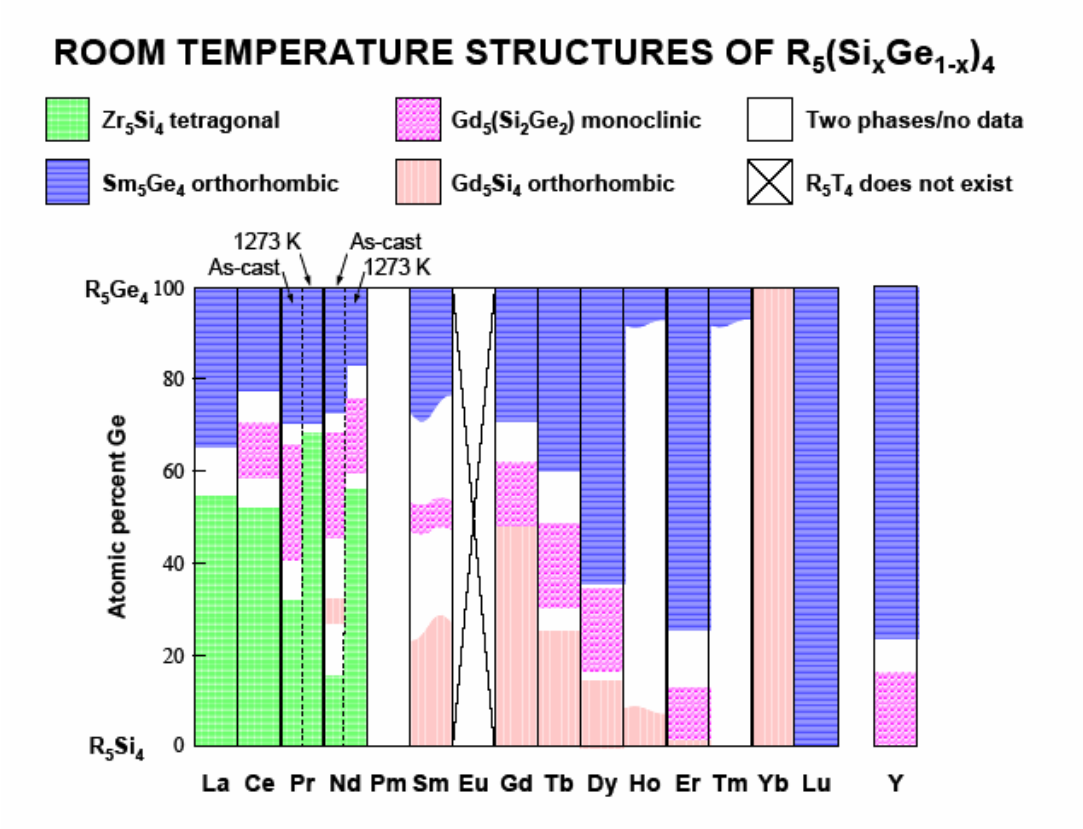

Fig. 1. Phase relationships and room temperature crystallography of $R_5Si_xGe_{4-x}$ phases. Straight phase boundaries designate terminal compositions that have been established with a few mol. % accuracy, while curved boundaries designate terminal compositions known to ~25 mol. % (usually based on examination of alloys with x = 4, 3, 2, 1, and 0).[24]

Crystallography and magnetism of the prototype Gd_5Si_4- Gd_5Ge_4 pseudobinary system

Smith *et al*. reported that both Gd_5Si_4 and Gd_5Ge_4 have the same orthorhombic Sm_5Ge_4-type structure.[20] However, according to Choe *et al*. and Pecharsky *et al*.'s studies, the structures can be described by equivalent layers (slabs), but with considerable differences in bonding arrangements between the slabs.[25,26,27] The bonding character between the slabs changes with the chemical composition in the $Gd_5Si_xGe_{4-x}$ system: for the Gd_5Si_4-type solid

solution ($2 < x \leq 4$) all slabs are interconnected via T_2 dimers (T= Si and/or Ge), for the $Gd_5Si_2Ge_2$-type solid solution ($0.96 \leq x \leq 2$), half of inter-slab T_2 bonds are broken, and for the Gd_5Ge_4-type solid solution ($0 \leq x \leq 0.8$) all inter-slab bonds are broken, Fig. 2.

The alloys show a variety of unique physical properties related to the magneto-structural transitions associated with reversible breaking and reforming of the inter-slab bonds that can be controlled by a variety of external parameters such as chemical composition, magnetic field, temperature, and pressure. When all inter-slab bonds are connected in the paramagnetic (PM) state, the alloys order ferromagnetically upon cooling without the crystallographical structural change (second order phase transformation) in Fig. 3. However, when half or all inter-slab bonds are broken, the alloys exhibit ferromagnetic ordering below the Curie temperature together with the structural change (first order phase transformation). Therefore, the existence of the GMCE and other phenomena, such as the giant magnetoresistance (GMR) and the colossal magnetostriction in the $Gd_5Si_2Ge_2$ and related alloys must be closely correlated with the combined magnetic-crystallographic transformation, Fig. 4.

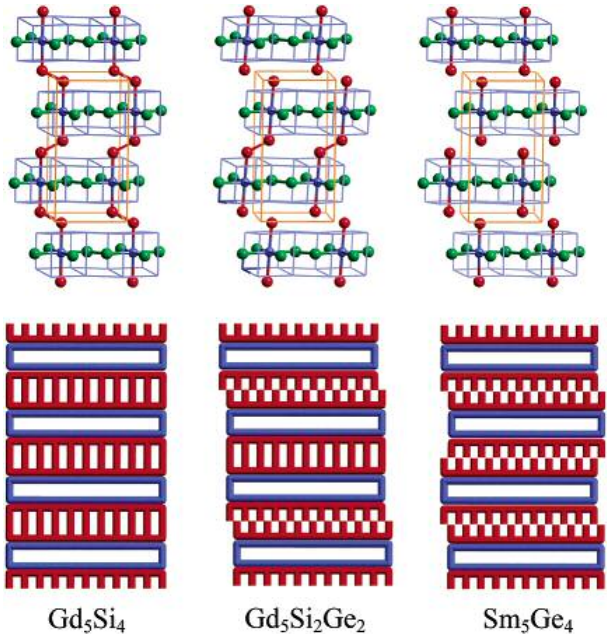

Fig. 2. Three structures in $Gd_5Si_xGe_{4-x}$ observed at room temperature: (left) orthorhombic Gd_5Si_4-type; (middle) monoclinic $Gd_5Si_2Ge_2$-type; (right) orthorhombic Sm_5Ge_4-type. The top three ball-

and-stick representations highlight the Gd3 (blue), T1 (red), T2 (green), and T3 (green) sites. The Gd1 and Gd2 network in each slab is shown as the blue "lattice". Cartoons at the bottom illustrate the "nano-zipper" relationships between the three structures as suggested by Choe *et al*.[28]

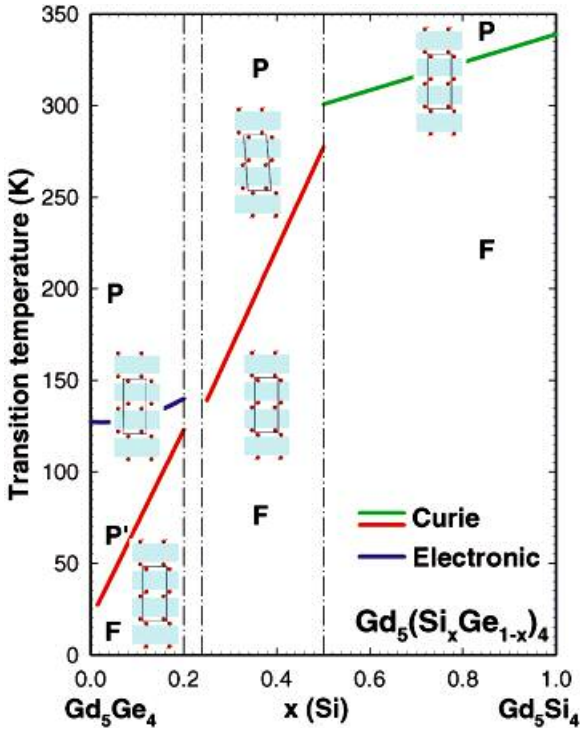

Fig. 3. Magnetic and crystallographic phases in the $Gd_5(Si_xGe_{1-x})_4$ system in zero magnetic field. The green line corresponds to a second-order paramagnetic (P) ↔ ferromagnetic (F) phase transition when $0.5 < x \leq 1$. The blue line is a second-order paramagnetic (P) ↔ electronic phase transition (P′) when $0 \leq x \leq 0.2$. The red lines are first-order ferromagnetic → paramagnetic (F → P′) and (F → P) phase transitions when $0 \leq x \leq 0.2$ and $0.24 \leq x \leq 0.5$, respectively.[26] According to most recent data, the P′ state is likely an antiferromagnetic state.[29]

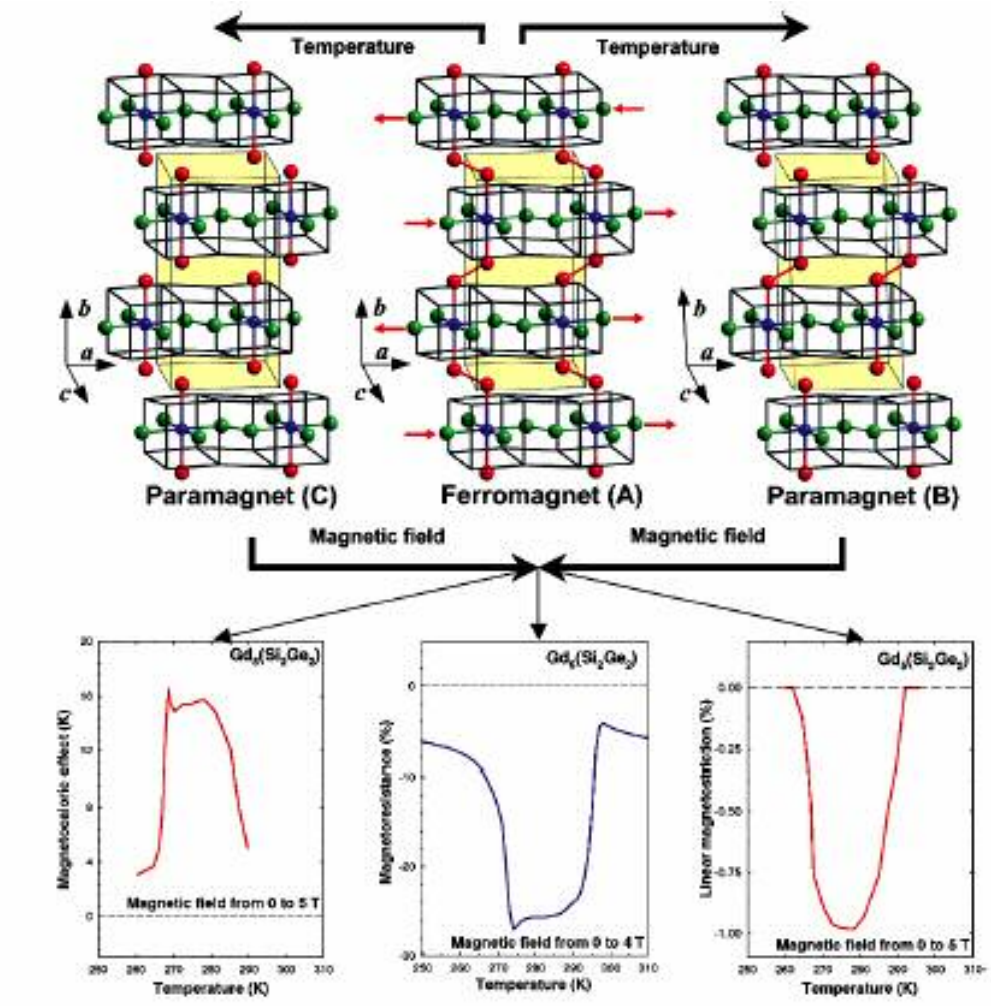

Fig. 4. Correlation between the magnetic response of the $Gd_5Si_xGe_{4-x}$ materials and their crystal structures for $0 \leq x \leq 2$. At low temperatures the compounds are ferromagnetic (A) with all slabs (light blue) connected via the Si(Ge)-Si(Ge) covalent bonds. Depending on the composition, the materials become paramagnetic with either one-half (B) or none (C) of the slabs connected above the Curie temperatures as shown by long horizontal arrows at the top of the figure. When a magnetic field is applied above Curie temperature, the reverse magnetic-martensitic transitions occur ($B \rightarrow A$ or $C \rightarrow A$, as shown by long horizontal arrows in the middle) resulting in the GMCE, GMR, and colossal magnetostriction.[26] According to Levin *et al.*'s study, the paramagnet (C) may be an antiferromagnetic state.[29]

The magnetocaloric effect (MCE)

The MCE is the magnetothermal phenomenon in which the temperature of a magnetic solid increases or decreases adiabatically with the variation of the magnetic field. It was discovered in 1881 by Warburg.[30] The MCE can be also quantified as the entropy change and it occurs due to the coupling of the magnetic moments of individual atoms with the magnetic field.[31,32]

For a magnetic solid,

$$S(T,H) = S_M(T,H) + S_L(T) + S_E(T) \qquad (1)$$

where the total entropy *S(T,H)* is the sum of the magnetic, lattice, and electronic entropies (S_M, S_L, and S_E, respectively). Normally, $S_L(T)$ and $S_E(T)$ can be considered to be independent on the magnetic field.

At constant temperature, the MCE can be expressed as the isothermal magnetic entropy change, $\Delta S_M(T)_{T,\Delta H,P}$, which considering that S_L and S_E are field independent is given as

$$\Delta S_M(T)_{T,\Delta H,P} = \left(S_M(T)_{H_2} - S_M(T)_{H_1}\right)_{T,P} = \left(S(T)_{H_2} - S(T)_{H_1}\right)_{T,P} \qquad (2)$$

where H_1 is the initial and H_2 is the final magnetic field.

When the magnetic field is applied adiabatically, the total entropy should be conserved, the lattice entropy and electronic entropy should be changed by $-\Delta S_M(T, \Delta H)$ resulting in the adiabatic temperature change ΔT_{ad}.

$$\Delta T_{ad}(T)_{T,\Delta H,P,S} = \left(T(S)_{H_2} - T(S)_{H_1}\right)_{S,P} \qquad (3)$$

The magnetic entropy change can be also calculated from magnetization, M, using the Maxwell relationship.

$$\left(\frac{\partial S}{\partial H}\right)_T = \left(\frac{\partial M}{\partial T}\right)_H,$$

which after integration yields

$$\Delta S_M(T,H)_{\Delta H,P} = \int_{H_1}^{H_2}\left(\frac{\partial M(T,H)}{\partial T}\right)_H dH \quad (4)$$

The adiabatic temperature change can be derived from the above equation and basic thermodynamics as

$$\Delta T_{ad}(T,\Delta H) = -\int_{H_1}^{H_2}\left(\frac{T}{C(T,H)}\right)_H\left(\frac{\partial M(T,H)}{\partial T}\right)_H dH \quad (5)$$

where *C(T,H)* is heat capacity measured as a function of temperature in constant field. Also, the magnetic entropy change can be calculated from the heat capacity:

$$S(T)_{H_1,P} = \int_0^T \frac{C(T)_{H_1,P}}{T} dT \quad (6)$$

$$S(T)_{H_2,P} = \int_0^T \frac{C(T)_{H_2,P}}{T} dT \quad (7)$$

$$\Delta S_M(T)_{\Delta H,P} = \Delta S(T)_{\Delta H,P} = \int_0^T \frac{\left(C(T)_{H_2} - C(T)_{H_1}\right)_P}{T} dT \quad (8)$$

Eqs. (6) and (7) are used to evaluate the total entropies needed to compute the MCE using Eqs. (2) and (3). Figure 5 shows the S-T diagram illustrating the existence of MCE.

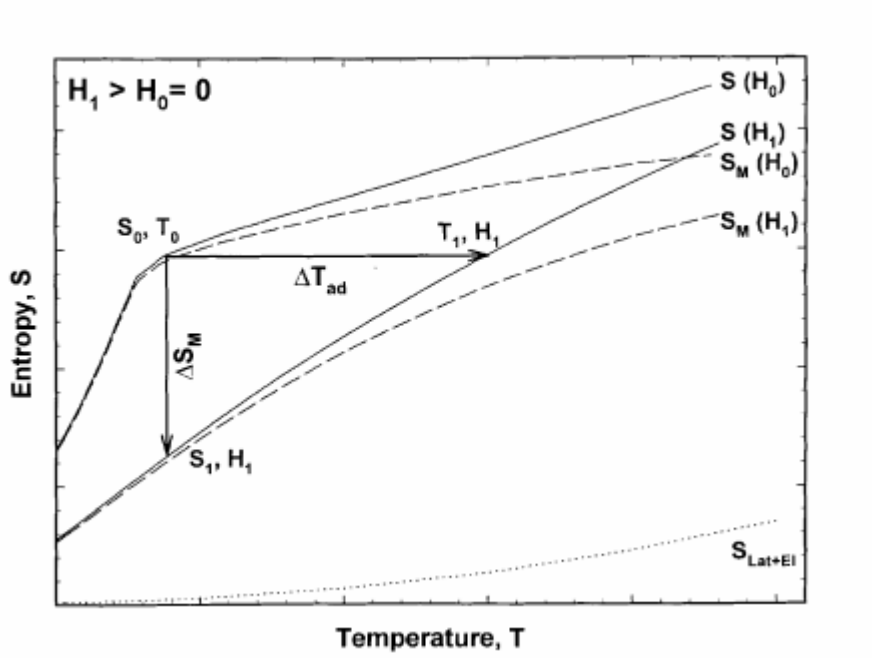

Fig. 5. The S-T diagram illustrating the existence of the magnetocaloric effect. The solid lines represent the total entropy in two different magnetic field: $H_0 = 0$ and $H_1 > 0$. The horizontal arrow shows ΔT_{ad} and the vertical arrow shows ΔS_M when the magnetic field is changed from H_0 to H_1. The dotted line shows the combined lattice and electronic (non-magnetic) entropy, and dashed lines show the magnetic entropy in the two fields. S_0 and T_0 are zero field entropy and temperature. S_1 and T_1 are entropy and temperature at the elevated magnetic field H_1.[31]

The magnetic refrigeration

After the discovery of the MCE in 1881 by Warburg[30], the effect has been successfully applied for the adiabatic demagnetization refrigeration[33] by which ultralow temperatures are often achieved today. Although several continuously operating magnetic refrigerator working at the temperature between ~1 and ~300 K have been constructed and tested, in the past most of them were inefficient because it ran for only a few days at the most.[34] The discovery of the GMCE and the construction of the proof-of-principle magnetic refrigerator in 1997 by Astronautics Corporation of America/Ames Laboratory team of scientists have generated a lot of interest about both the MCE and magnetic refrigeration.[35] Figure 6 describes the principle of magnetic refrigeration. The spins are initially random in a zero

magnetic field (Fig. 4a). Upon adiabatic magnetization (b), the material (a) heats up because of magnetic entropy decrease due to increasing magnetic order in the system and the heat is removed by a heat transfer fluid. Upon adiabatic demagnetization (c), the material cools down and it cools a load in a cold heat exchanger. Continuous refrigeration is achieved by repeating (b) and (c). The magnetic refrigeration has several advantages over the conventional gas compression/expansion cooling system. It is important for the energy savings and environmental concerns. The improvement in both the MCE and refrigeration capacity of magnetic refrigerants will lead to high performance and energy efficiency of magnetic refrigeration technology. The Astronautics/Ames Lab demonstrated the unit operating near room temperature using magnetic fields between 1.5 and 5 T. This unit has run "maintenance free" for over 1500 h. Several notable achievements were obtained with this demonstration unit: 1) a record cooling power of 600 watts (about 100 times greater than previous near room temperature magnetic refrigerators); 2) a coefficient of performance (COP), i.e. the cooling power divided by the input work, of 15 (typical gas compression cycle refrigerators have COPs between 2 and 6); 3) a maximum efficiency of 60 % of Carnot (the seal friction was subtracted off) compared to conventional vapor cycle refrigeration with a 40 % of theoretical Carnot limit; and 4) a maximum temperature span of 38 K (the difference in the temperatures of the hot and cold heat exchangers).[35,36] Beside this, the magnetic refrigeration is an environmentally friendly technology because it does not use ozone depleting chemicals (ODCs) such as chlorofluorocarbons (CFCs) [of which CF_2Cl_2 was patented under the name "Freon"], toxic chemicals such as NH_3, and greenhouse gases such as hydrochlorofluorocarbons (HCFCs) and hydrofluorocarbons (HFCs).

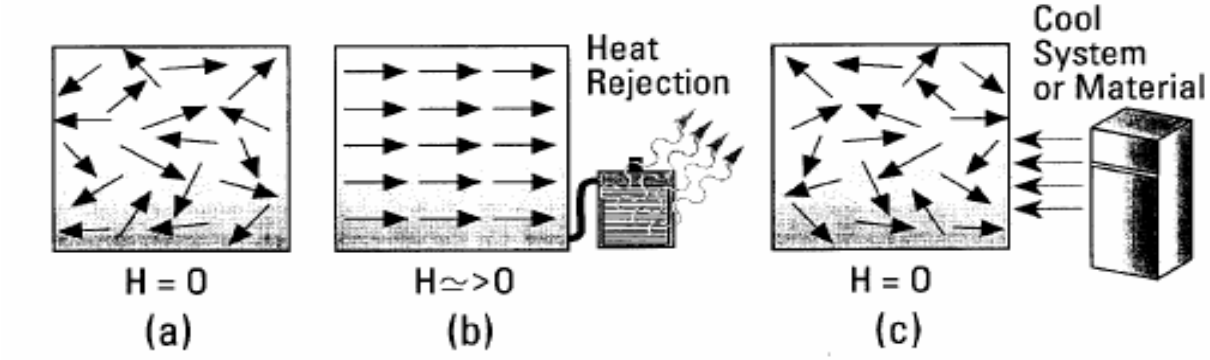

Fig. 6. A schematic representation of how magnetic refrigeration works.[37]

Mixed-valence compounds

Valence fluctuation phenomena occur in rare-earth compounds in which the proximity of the *4f* level to the Fermi energy leads to instabilities of the charge configuration (valence) and/or of the magnetic moment. Rare-earth based compounds containing Ce, Eu, Yb, and Sm may show mixed valence or valence fluctuation behavior.[38,39] In 1927, Bridgman first observed a volume change under pressure for cerium metal.[40] Bauminger reported that the Eu ions in $EuCu_2Si_2$ are in the intermediate valence state.[41] This was the first Eu-based intermetallic compound identified as a mixed valence system. A survey of available data reveals that a large number of Ce, Sm, Eu, and Yb based compounds exhibit mixed valence behavior (see Table 1).[42]

Mixed valence systems show anomalies in their physical properties compared to trivalent rare earth based compounds. Anomalies in lattice constants or unit cell volume of a compound under consideration are usually the first indication of the mixed valence behavior. The radius of R ions in the trivalent state decreases smoothly with increasing atomic number Z of the R ions (also known as lanthanide contraction). The compounds in which the R ion is in the pure divalent state show positive deviation from the lanthanide contraction. The lattice parameters of the mixed valence compounds also deviate from lanthanide contraction and they lie intermediate between integral valence states (either 2+ or 3+). Also, in the high temperature range, magnetic susceptibility $\chi(T)$ of mixed valence compounds usually follows Curie-Weiss behavior with an effective magnetic moment (p_{eff}) intermediate between the values of p_{eff} for the two integral valence states.

Table 1. List of Ce, Sm, Eu and Yb based compounds which exhibit mixed-valence behavior at ambient conditions, on application of high pressure and on alloying.[42]

Ambient conditions	High pressure	Alloying
$CePd_3$,$CeSn_3$,Ce_3Al	Ce (8 kbar)	$Ce(Rh_{1-x}Pd_x)_3$
CeN,$CeBe_{13}$,CeB_4,$CeSi_2$	SmS (6.5 kbar)	$Ce_{1-x}Y_x$
CeM_2(M = Fe,Co,Ru,Rh,Ir)	SmSe (30 kbar)	$CePt_{2-x}Ir_x$
CeNiSi,CeNiSn,CeNiIn	SmTe (50 kbar)	$CePt_{2-x}Rh_x$
CeRhIn,CeRhSb,CeIrGe	TmTe (20 kbar)	$CeLa_{1-x}Th_x$
$CeIr_2Si_2$,$CeCo_2Si_2$,$CeNi_2Si_2$	CeP (100 kbar)	$Ce_{1-x}Th_x$
$CeFe_2Si_2$,$CeOs_2Si_2$,$CePt_2Si_2$	EuO	$CePt_{1-x}Ni_xSi$
$CeNi_2Ge_2$,$CeCo_2Ge_2$	YbS,YbSe,YbTe	$Sm_{1-x}Th_xS$
$Ce_{0.5}Rh_3B_2$,$CeIr_3B_2$		$Sm_{1-x}RE_xS$
$CeOs_3B_2$,$CeRu_3B_2$,$CeRu_3Si_2$		$SmS_{1-x}As_x$
$Ce_{1-x}Y_xIn_3$(x>0.6)		$EuPd_3Si_x$
SmB_6,Sm_4Bi_3		$EuPd_3B_x$
$EuIr_2$, $EuRh_2$,$EuNiSi_2$,EuPtP		$Eu_{1-x}La_xRh_2$
$EuCu_2Si_2$,$EuPd_2Si_2$,$EuIr_2Si_2$		$YbAu_{1-x}Ag_x$
$EuNi_2P_2$,$EuFe_4Al_8$,$Eu_2Ni_3Si_5$		
Eu_4As_3		
YbB_6,YbCu,YbAg,YbAu,YbZn		
YbB_4,YbC_2,$YbAl_3$,$YbAl_2$,YbSi		
$YbCu_{3.5}$,$YbCu_{4.5}$,YbB_{12},Yb_4Bi_3		
Yb_4Sb_3,$YbIr_3$,YbCuAl,YbCuGa		
$YbAlB_4$,$YbInCu_4$,$YbAgCu_4$		
YbInAu,$YbInAu_2$,YbPdIn		

Europium oxides: EuO and Eu_3O_4

In 1961, Matthias *et al*. discovered that europium monoxide (EuO) undergoes a ferromagnetic ordering at the Curie temperature of 77 K.[43] EuO crystallizes in the NaCl-type structure with lattice parameter a = 5.143 Å.[44,45] Since EuO has a face-centered cubic structure and the pure spin magnetism of the localized Eu^{2+} ($4f^7$) with ${}^8S_{7/2}$ ground state, it has been studied actively as an example of a ferromagnetic semiconductor material (Heisenberg ferromagnet).[46] At present, EuO also receives a special interest as a candidate material for optical isolators and optomagnetic devices.[47]

On the other hand, EuO may have a potential for application as a magnetic refrigerant material because of the unique magnetic properties of Eu. There are two valence states for Eu: Eu^{2+} and Eu^{3+}. The Eu^{2+} ion is similar to the Gd^{3+} ion with $4f^7$ state (J = 7/2), while the Eu^{3+} ion is in $4f^6$ state (J = 0). Gd and many Gd-based compounds are good magnetic refrigerant materials due to their large magnetic moments. Therefore, divalent europium in binary compounds, such as EuO, EuS, EuSe, and EuTe may have large MCE as well as interesting magnetism. Experimental studies of Eu-based compounds are sluggish because of the difficulty of material preparation containing Eu^{2+} ions. Until now, only a few divalent europium binary compounds have been reported and characterized.

The Eu^{2+} ion is a stable oxidation state. However, the existence of divalent europium compounds is limited, because the Eu^{2+} ion is also a strong reducing agent and in air it may be easily converted into the Eu^{3+} state.[48] Thus, special care in handling compounds containing Eu^{2+} ions is usually required. Several researchers reported magnetic properties of EuO, yet the MCE of binary europium compounds is only known for europium sulfide, EuS.[43,44,45,46,48,49,50,51,52]

Eu_3O_4 was first reported by Achard[53] in 1960 and Barnighausen *et al*.[54], in 1962, synthesized Eu_3O_4 for the first time by heating an equimolar mixture of Eu_2O_3 and EuO at 900 ºC in an argon atmosphere. In 1966, Rau reported that Eu_3O_4 is a europium oxide

containing both divalent and trivalent europium ions.[55] It has been known that Eu_3O_4 crystallizes in the calcium ferrite ($CaFe_2O_4$-type) structure (orthorhombic system, space group *Pnam*) and its unit cell parameters are a = 10.085, b = 12.054 and c = 3.502 Å. The most interesting issue in Eu_3O_4 is that it is a mixed-valence compound which has two valence states (Eu^{2+} and Eu^{3+}). It can be described as $Eu^{2+}\,Eu^{3+}{}_2\,O^{2-}{}_4$ and thus the ratio of Eu^{2+} to Eu^{3+} ions is 1/2. Generally, divalent and trivalent Eu ions occupy the Ca sites and Fe sites, respectively. The magnetic properties of Eu_3O_4, which contains Eu^{2+} ions with the large magnetic moments, are quite interesting because the electronic configuration of Eu^{2+} is equal to that of Gd^{3+} with $4f^7$ state. The magnetic properties of Eu_3O_4 have been investigated by Holmes and Schieber.[56] They reported that Eu_3O_4 undergoes an antiferromagnetic ordering at the liquid helium temperature range (~ 5 K) and exhibits a metamagnetic behavior below T_N of ~ 5 K. Magnetothermal properties of Eu_3O_4 have not been investigated in the past.

Experimental details

The $Yb_5Si_xGe_{4-x}$ and $Sm_5Si_xGe_{4-x}$ alloys with x varying from 0 to 4, and europium oxides (EuO and Eu_3O_4) were synthesized by induction melting at ~1800°C. Prior to induction melting, stoichiometric mixtures of pure components (Yb, Sm, Eu, Si, Ge) or oxides (EuO and Eu_2O_3) were loaded into Ta or W crucibles, and then the crucibles were sealed under a pure helium atmosphere in order to avoid losses of ytterbium, samarium, and europium. For $Yb_5Si_xGe_{4-x}$ and $Sm_5Si_xGe_{4-x}$ compounds, the alloy compositions were assumed to be in the as-weighed conditions. The errors in the compositions due to the high vapor pressures of Yb and Sm at ~ 1800°C are less than 0.5 wt.% (0.1 at.%) and 0.2 wt.% (0.04 at.%) of stoichiometric Yb_5T_4 and Sm_5T_4 amounts, respectively. The calculations assumed that the empty volume of crucible is ~ 1.6 cm^3, the sample size is ~ 1 cm^3, the partial vapor pressure of them at 1800°C can be calculated from equations in Ref. 57, and that the vaporized Yb or Sm follows ideal gas equation.

The x-ray powder diffraction technique was utilized to characterize both the crystal structures and phase compositions of $Yb_5Si_xGe_{4-x}$ and $Sm_5Si_xGe_{4-x}$ alloys, EuO, and Eu_3O_4.

The x-ray powder diffraction studies were performed on an automated Scintag powder diffractometer using Cu-Kα radiation. The crystal structures were refined by the Rietveld technique using data collected at room temperature which varied between 290 K and 295 K. In order to establish the precision of lattice parameters determined from Rietveld refinements we need to take into account thermal expansion coefficients of compounds if room temperature is not precisely known and may vary during the duration of experiment. The linear thermal expansion coefficients of some R_5Si_4 compounds have been reported to be ~ 10^{-5}/K at 300 K.[58] While room temperature was not precisely known and not controlled during these x-ray powder diffraction studies, and it may vary from 290 K to 295 K, the uncertainty of lattice parameters due to thermal expansion lies within the error limits determined from Rietveld refinements.

Magnetic measurements were performed using a SQUID magnetometer (model MPMS XL). The magnetization of zero-magnetic-field cooled samples was measured as a function of temperature from 1.8 to 400 K in various dc magnetic fields. Isothermal magnetization data were collected in dc magnetic fields varying from 0 to 7 T after the samples were zero-field-cooled to the target temperatures. The heat capacity was measured using an adiabatic heat-pulse calorimeter between ~3.5 and 350 K in dc magnetic fields ranging from 0 to 10 T.

$Yb_5Si_xGe_{4-x}$ has been studied using ^{170}Yb Mössbauer spectroscopy in collaboration with C. J. Voyer and D. H. Ryan from the Center for the Physics of Materials and Physics Department at McGill Univeristy in Canada. A 20 mCi ^{170}Tm source was prepared by neutron activation of ~25 mg of Tm as a 10 wt.% alloy in aluminum. The source and sample were mounted vertically in a helium-flow cryostat and the drive was operated in sine mode. The 84.25 keV γ photons used for ^{170}Yb Mössbauer were isolated from the various x-rays emitted by the source using a high-purity Ge detector. Calibration of the spectrometer was achieved using a laser interferometer mounted on the back of the drive. Velocities were cross-checked against ^{57}Co/α-Fe at room temperature. This procedure has also been checked at higher velocities than those employed here by recording and fitting the ^{166}Er Mössbauer spectrum of $ErFe_2$ at 5 K. We observed a ^{170}Yb linewidth (half width at half maximum) of

1.33(6) mm/s with the source and a standard sample of YbB_6 at 5.0 K. A calibrated Cernox thermometer was used to monitor the sample temperature and stability of better than ±0.01 K was observed. Spectra were fitted using a nonlinear least-squares minimization routine with line positions and intensities derived from an exact solution to the full Hamiltonian.

Dissertation organization

This dissertation is written in an alternate format composed of original published papers or already drafted, preceded with a general introduction and conclusion chapters. References cited within each chapter have been placed immediately after the chapter.

The first paper, mostly presented in Chapter 2, "Phase relationships and structural, magnetic, and thermodynamic properties of the Yb_5Si_4-Yb_5Ge_4 pseudobinary system" was published in *Physical Review B* in 2005. The authors were Kyunghan Ahn (graduate student and primary researcher at the Materials Science and Engineering Department of Iowa State University and the Ames Laboratory of the U.S. Department of Energy (DOE)), A. O. Tsokol (assistant scientist at the Ames Laboratory of the U.S. DOE), Yu. Mozharivskyj (postdoctoral fellow at the Ames Laboratory of the U.S. DOE), K. A. Gschneidner, Jr. (graduate advisor at the Materials Science and Engineering Department of Iowa State University and senior metallurgist at the Ames Laboratory of the U.S. DOE), and V. K. Pecharsky (graduate advisor at the Materials Science and Engineering Department of Iowa State University and senior scientist at the Ames Laboratory of the U.S. DOE). This paper presents the results of detailed investigation of structural and magneto-thermal properties in the $Yb_5Si_xGe_{4-x}$ system. The Mössbauer work in Chapter 2 was also published in *Physical Review B* in 2006.

The second manuscript, presented in Chapter 3, "Phase relationships and structural, magnetic, and thermodynamic properties of the $Sm_5Si_xGe_{4-x}$ pseudobinary system" has been prepared for publication. The authors are Kyunghan Ahn, V. K. Pecharsky, and K. A. Gschneidner, Jr.. This manuscript presents the results of detailed investigation of structural and magneto-thermal properties in the $Sm_5Si_xGe_{4-x}$ system.

The third paper, presented in Chapter 4, "Preparation, heat capacity, magnetic properties, and the magnetocaloric effect of EuO" was published in the *Journal of Applied Physics* in 2005. The authors were Kyunghan Ahn, A. O. Pecharsky (assistant scientist at the Ames Laboratory of the U.S. DOE), K. A. Gschneidner, Jr., and V. K. Pecharsky. This paper presents the results of magnetocaloric effect of EuO.

The fourth manuscript, presented in Chapter 5, "The magnetothermal behavior of mixed valent Eu_3O_4" has been prepared for publication. The authors are Kyunghan Ahn, A. O. Tsokol, V. K. Pecharsky, and K. A. Gschneidner, Jr.. This manuscript presents the results of the magneto-thermal properties and magnetocaloric effect of mixed valent Eu_3O_4.

References

[1] K. A. Gschneidner, Jr., V. K. Pecharsky, A. O. Pecharsky, V. V. Ivtchenko, and E. M. Levin, J. Alloys Compd. **303**, 214 (2000).

[2] H. F. Yang, G. H. Rao, W. G. Chu, G. Y. Liu, Z. W. Ouyang, and J. K. Liang, J. Alloys Compd. 339, **189** (2002).

[3] H. F. Yang, G. H. Rao, G. Y. Liu, Z.W. Ouyang, W. F. Liu, X. M. Feng, W. G. Chu, and J. K. Liang, J. Alloys Compd. **346**, 190 (2002).

[4] A. O. Pecharsky, K. A. Gschneidner, Jr., V. K. Pecharsky, and C. E. Schindler, J. Alloys Compd. **338**, 126 (2002).

[5] C. Ritter, L. Morellon, P.A. Algarabel, C. Magen, and M.R. Ibarra, Phys. Rev. B **65**, 094405 (2002).

[6] A. O. Pecharsky, K. A. Gschneidner, Jr., V. K. Pecharsky, D. L. Schlagel, and T. A. Lograsso, Phys. Rev. B **70,** 144419 (2004).

[7] A. O. Pecharsky, V. K. Pecharsky, and K. A. Gschneidner, Jr., J. Alloys Compd. **379**, 127 (2004).

[8] M. V. Bulanova, P. N. Zheltov, K. A. Meleshevich, P. A. Saltykov, and G. Effenberg, J. Alloys Compd. **345**, 110 (2002).

[9] S. Bobev and E. D. Bauer, Acta Cryst. **E61**, i73 (2005).

[10] L. M. Wu, S. H. Kim, and D. K. Seo, J. Am. Chem. Soc. **127**, 15682 (2005).

[11] V. N. Eremenko, K. A. Meleshevich, Yu. I. Buyanov, and P. S. Martsenyuk, Poroshkovaya Metallurgiya (Kiev) **7**, 41 (1989).

[12] R. Cerny and K. Alami-Yadri, Acta Cryst. **E59**, i1 (2003)

[13] A. Palenzona, P. Manfrinetti, S. Brutti, and G. Balducci, J. Alloys Compd. **348**, 100 (2003).

[14] M. Pani and A. Palenzona, J. Alloys Compd. **360**, 151 (2003).

[15] P. Schobinger-Papamantellos and A. Niggli, Journal de Physique, Colloque **C5**, 156 (1979).

[16] V. N. Eremenko, V. E. Listovnichii, S. P. Luzan, Yu. I. Buyanov, and P. S. Martsenyuk, J. Alloys Compd. **219**, 181 (1995).

[17] N. P. Thuy, Y. Y. Chen, Y. D. Yao, C. R. Wang, S. H. Lin, J. C. Ho, T. P. Nguyen, P. D. Thang, J. C. P. Klaasse, N. T. Hien, and L. T. Tai, J. Magn. Magn. Mater. **262**, 432 (2003).

[18] G. S. Smith, A. G. Tharp, and Q. Johnson, Nature **210**, 1148 (1966).

[19] G. S. Smith, Q. Johnson, and A. G. Tharp, Acta Crystallogr. **22**, 269 (1967).

[20] G. S. Smith, A. G. Tharp, and Q. Johnson, Acta Crystallogr. **22**, 940 (1967).

[21] F. Holtzberg, R. J. Gambino, and R. T. McQuire, J. Phys. Chem. Solids **28**, 2283 (1967).

[22] V. K. Pecharsky and K. A. Gschneidner Jr. Phys. Rev. Lett. **78**, 4494 (1997).

[23] V. K. Pecharsky and K. A. Gschneidner Jr. J. Alloys Comp. **260**, 98 (1997).

[24] V. K. Pecharsky and K. A. Gschneidner, Jr., Unpublished results.

[25] W. Choe, V. K. Pecharsky, A. O. Pecharsky, K. A. Gschneidner, Jr., V. G. Young, Jr., and G. J. Miller, Phys. Rev. Lett. **84**, 4617 (2000).

[26] V. K. Pecharsky and K. A. Gschneidner Jr., Adv. Mater. **13**, 683 (2001).

[27] V. K. Pecharsky, A. O. Pecharsky, and K. A. Gschneidner Jr., J. Alloys Comp. **344**, 362 (2002).

[28] W. Choe, A. O. Pecharsky, M. Worle, and G. J. Miller, Inorg. Chem. **42**, 8223 (2003).

[29] E. M. Levin, V. K. Pecharsky, K. A. Gschneidner, Jr., and G. J. Miller, Phys. Rev. B **64**, 235013 (2001).

[30] E. Warburg, Ann. Phys. Chem., **13**, 141 (1881).

[31] V. K. Pecharsky and K. A. Gschneidner Jr., J. Magn. Magn. Mater. **200**, 44 (1999).

[32] V. K. Pecharsky and K. A. Gschneidner Jr., A. O. Pecharsky, A. M. Tishin, Phys. Rev. B **64**, 144406 (2001).

[33] W. F. Giaugue and D. P. Macdougall, Phys. Rev. **43**, 768 (1933).

[34] K. A. Gschneidner, Jr. and V. K. Pecharsky, p 209 in Rare Earths: Science, Technology and Applications III, R. G. Bautista, C. O. Bounds, T. W. Ellis and B. T. Kilbourn, editors, The Minerals, Metals & Materials Society, Warendale, PA (1997).

[35] C. B. Zimm, A. Jastrab, A. Sternberg, V. K. Pecharsky, K. A. Gschneidner, Jr., M. Osborne and I. E. Anderson, Adv. Cryog. Eng. **43**, 1759 (1998).

[36] C. Zimm, A. Sternberg, V. Pecharsky, and K. Gschneidner, Jr., paper presented at the Appliance Manufacturer Conference and Expo, October 12-14, Nashville, TN, 1998.

[37] K. A. Gschneidner Jr., V. K. Pecharsky, A. O. Pecharsky, and C. B. Zimm, Mater. Sci. Forum **315-317**, 69 (1999).

[38] C. M. Varma, Rev. Mod. Phys. **48**, 219 (1976).

[39] A. Jayaraman, *Handbook on the Physics and Chemistry of Rare Earths*, Chap. 20 (1979).

[40] P. W. Bridgman, Proc. Am. Acad. Arts Sci. **62**, 207 (1927).

[41] E. R. Bauminger, D. Froinlich, I. Nowick, S. Ofer, I. Felner and I. Mayer, Phys. Rev. Lett. **30**, 1053 (1973).

[42] D. T. Adroja and S. K. Malik, J. Magn. Magn. Mater. **100**, 126 (1991).

[43] B. T. Matthias, R. M. Bozorth, and J. H. Van Vleck, Phys. Rev. Lett. **7**, 160 (1961).

[44] R. A. Belayev, V. V. Bondarenko, V. P. Vyskubov, S. S. Kiparisov, V. A. Lazarevski, and V. M. Tyugin, *Properties of Europium Oxides*, ORNL-tr-2883, 1974.

[45] J. F. Dillon, Jr. and C. E. Olsen, Phys. Rev. **135**, A434 (1964).

[46] M. M. Abd-Elmeguid and R. D. Taylor, Phys. Rev. B **42**, 1048 (1990).

[47] S. Thongchant, Y. Hasegawa, Y. Wada and S. Yanagida, Chem. Lett. **30**, 1274 (2001).

[48] M. W. Shafer, J. Appl. Phys. **36**, 1145 (1965).

[49] T. Kasuya and A. Yanse, Rev. Mod. Phys. **40**, 684 (1968).

[50] W. C. Koehler, J. Appl. Phys. **36**, 1078 (1965).

[51] R. M. Bozorth and J. H. Van Vleck, Phys. Rev. **118**, 1493 (1960).

[52] P. Bredy and P. Seyfert, Cryogenics **28**, 605 (1988).

[53] Y. C. Achard, Compt. Rend. Acad. Sci. **250**, 3025 (1960).

[54] H. Barnighausen and G. Brauer, Acta. Crystallog. **15**, 1059 (1962).

[55] R. C. Rau, Acta. Crystallog. **20**, 716 (1966).

[56] L. Holmes and M. Schieber, Phys. Rev. **167**, 449 (1968).

[57] A. Desideri, V. Piacente, and S. Nobili, J. Chem. and Engr. Data, **18**, 140 (1973).

[58] Yu. V. Serdyuk and R. P. Krentsis, Deposited document (1982) 14 pp. VINITI 4230-81.

CHAPTER 2. PHASE RELATIONSHIPS AND STRUCTURAL, MAGNETIC, AND THERMODYNAMIC PROPERTIES OF THE Yb_5Si_4-Yb_5Ge_4 PSEUDOBINARY SYSTEM

A paper published in *Physical Review B*[1]

Kyunghan Ahn,[2,3] A. O. Tsokol,[3] Yu. Mozharivskyj,[3] K. A. Gschneidner, Jr.,[2,3] and V. K. Pecharsky[2,3]

Abstract

The crystallography, phase relationships, and physical properties of the $Yb_5Si_xGe_{4-x}$ alloys with $0 \leq x \leq 4$ have been examined by using single crystal and powder x-ray diffraction at room temperature, and dc magnetization and heat capacity measurements between 1.8 K and 400 K in magnetic fields ranging from 0 and 7 T. Unlike the majority of $R_5Si_xGe_{4-x}$ systems studied to date, where R is the rare earth metal, all Yb-based germanide-silicides with the 5:4 stoichiometry crystallize in the same Gd_5Si_4-type structure. The magnetic properties of $Yb_5Si_xGe_{4-x}$ materials are nearly composition-independent, reflecting the persistence of the same crystal structure over the whole range of x from 0 to 4. Both the crystallographic and magnetic property data indicate that $Yb_5Si_xGe_{4-x}$ alloys are heterogeneous mixed valence systems, in which the majority (60%) of Yb atoms is divalent, while the minority (40%) is trivalent.

---

[1] *Physical Review B* **72**, 054404-1 – 054404-11 (2005)

Physical Review B **73**, 174422-1 – 174422-6 (2006)

[2] Department of Materials Science and Engineering, Iowa State University, Ames, IA 50011-2300, USA

[3] Materials and Engineering Physics Program, Ames Laboratory of the U.S. Department of Energy, Iowa State University, Ames, IA 50011-3020, USA

Introduction

When Smith *et al.*[1] discovered a few R_5Si_4 and R_5Ge_4 phases, where R is rare earth metal, they reported that 5:4 germanides with R = Nd, Sm, Gd, Tb, Er, and Y, and the silicides with R = Tb, Er and Y adopt the same orthorhombic crystal structure, while Nd_5Si_4 crystallizes in a tetragonal lattice. In a subsequent study by the same authors,[2] the crystal structure of the orthorhombic Sm_5Ge_4 was described as the $(ABCBA)_2$ stacking of three different sheets of atoms (A, B and C) along the *b*-axis in space group symmetry *Pnma*. Within a few months, Smith, Tharp and Johnson[3] reported that R_5Ge_4 compounds, where R = La, Ce – Sm, Gd – Tm, Lu, and Y, exhibit the same Sm_5Ge_4-type structure, while the crystallography of R_5Si_4 compounds is dependent upon the rare earth metal. Thus, R_5Si_4 with R = Sm, Gd, Tb, Dy, Er, and Y adopt the Sm_5Ge_4-type structure, but R_5Si_4 crystallize in the tetragonal Zr_5Si_4-type[4] lattice when R = La, Ce, Pr, and Nd. Nearly simultaneously with the structural work, Holtzberg *et al.*[5] reported that the R_5Si_4 phases, when R = heavy lanthanide, order ferromagnetically (FM) at relatively high Curie temperatures (i.e., T_C = 336 K for R = Gd, 225 K for Tb, 140 K for Dy, 76 K for Ho, and 25 K for Er), while the R_5Ge_4 phases are antiferromagnetic (AFM) with much lower Néel temperatures, i.e., T_N = 47 K for R = Gd, 30 K for Tb, 40 K for Dy, 21 K for Ho, and 7 K for Er. Authors of Ref. 5 also showed that substitutions of Si for Ge in Gd_5Ge_4 induce low-temperature ferromagnetism in the $Gd_5Ge_{4-x}Si_x$ solid solution.

In addition to complex crystallography and unusually large differences between the magnetic properties of the apparently isostructural R_5Si_4 and R_5Ge_4 compounds (e.g., high temperature FM Gd_5Si_4 vs. low temperature AFM Gd_5Ge_4), combining magnetic Gd with just about the same amount of nonmagnetic Si increases the Curie temperature of the pure Gd metal (T_C = 293 K) by nearly 40 K, i.e., T_C = 336 K for Gd_5Si_4. Although this feature was noted by Holtzberg *et al.*[5] in 1967, and later reiterated by Elbicki *et al.*,[6] the R_5T_4 materials, where T = Si or Ge, did not attract much attention until 30 years later when Pecharsky and Gschneidner[7] reported the giant magnetocaloric effect (GMCE) in $Gd_5Si_2Ge_2$. The GMCE in this and many other members of the $Gd_5Si_xGe_{4-x}$ family of materials is due to first order

magnetic phase transitions observed between ~40 K and ~300 K.[8] Importantly, the first order nature of these transformations is preserved in magnetic fields as high as 20 T.[9] Also in 1997, Pecharsky and Gschneidner[10] reported that there are three crystallographically different phase regions in the $Gd_5Si_xGe_{4-x}$ system at room temperature. For the Gd_5Si_4-based solid solution ($2 < x \leq 4$) and for the Gd_5Ge_4-based solid solution ($0 \leq x \leq 0.8$), they reported two different orthorhombic structures, but for the $Gd_5Si_2Ge_2$-type solid solution ($0.96 \leq x \leq 2$), there exists a monoclinically distorted lattice, which may be considered a 50:50 mixture of the structural features found in the corresponding 5:4 gadolinium silicide and in the 5:4 germanide. The authors of Ref. 10 believed that in the pseudobinary Gd_5Si_4 – Gd_5Ge_4 system, the large differences in the magnetic properties, including the appearance of the GMCE, are intimately related to the crystallography of these three phases in the paramagnetic state.

Even though Smith *et al.*[1-3] reported that both Gd_5Si_4 and Gd_5Ge_4 adopt the orthorhombic Sm_5Ge_4-type structure, recent studies[11,12,13] describe them as equivalent layers of atoms assembled into slabs that are arranged in their own ways along the crystallographic *b*-direction because bonding between the slabs is distinctly different, e.g., see Fig. 1 in Ref. 12 and Ref. 14. The slabs themselves are formed by five nearly flat sheets of tightly bound atoms,[11,12] corresponding to the ABCBA sequence identified by Smith et al.[2] Hence, both the chemical and physical interactions between the slabs in the $Gd_5Si_xGe_{4-x}$ system vary with the chemical composition. For the Gd_5Si_4-type solid solution, all slabs are interconnected *via* T_2 dimers – the pairs of T-atoms from neighboring slabs at bonding distances of about 2.5 Å – and therefore, interactions between them are strong. For the $Gd_5Si_2Ge_2$-type solid solution, half of the inter-slab T_2 dimers are broken (the bonding distances increase from ~2.5 to ~3.5 Å), thus, weakening the interslab exchange. Finally, for the Gd_5Ge_4-type solid solution, all inter-slab T-T bonds are broken, and these materials exhibit the weakest interslab exchange interactions, therefore, exhibiting the lowest magnetic ordering temperatures.

The family of $Gd_5Si_xGe_{4-x}$ alloys demonstrates a variety of unique physical phenomena related to magneto-structural transitions associated with reversible breaking and reforming of

the inter-slab T_2 dimers that can be controlled by numerous external parameters such as chemical composition, magnetic field, temperature, and pressure.[12] When all inter-slab T-T bonds are present in the paramagnetic state, the alloys order ferromagnetically upon cooling without a structural change (second order phase transformation), see Fig. 2 in Ref. 12. However, when half or all of the inter-slab T_2 dimers are broken at room temperature, the alloys order ferromagnetically together with structural changes that restore all possible inter-slab T_2 dimers (first order phase transformation). The existence of the GMCE[7], large magnetoresistance[15] and colossal magnetostriction[16] in $Gd_5Si_2Ge_2$ and related alloys, is therefore, intimately related to the combined magnetic-crystallographic transformations, e.g., see Fig. 3 in Ref. 12.

As far as the *R*-component is of concern, $R_5Si_xGe_{4-x}$ systems with heavy lanthanides other than Gd have been investigated to some extent. Recently, phase diagrams of the pseudobinary systems with *R* = Tb,[17,18,19] Er[20,21] and Y[22] have been constructed. Selected $R_5Si_xGe_{4-x}$ compounds for *R* = La,[23,24] Pr,[25,26,27] Nd,[28,29,30] Tb,[31] Dy,[32] and Lu[33] have been reported as well. Nonetheless, there are several $R_5Si_xGe_{4-x}$ systems, which have not been examined to date. For example, the R_5T_4 compounds for *R* = Eu have never been reported, and those for *R* = Ce,[34] Sm,[2] Tm,[3] and Yb[35,36,37] have been examined only as binary intermetallics. Černý and Alami-Yadri[35] reported that Yb_5Si_4 adopts the orthorhombic Gd_5Si_4-type crystal structure, and noted that for Yb_5Si_4 and Sm_5Ge_4 there is a difference in the coordination of some of the T-atoms because all Si atoms in Yb_5Si_4 form covalently bonded pairs, while only a half of the Ge atoms in Sm_5Ge_4 form covalent Ge-Ge bonds. Palenzona *et al.*,[36] and Pani and Palenzona,[37] on the other hand, state that both Yb_5Si_4 and Yb_5Ge_4 crystallize with the Sm_5Ge_4-type structure, thus fueling controversy about the room temperature crystallography of Yb_5T_4 compounds.

To date, only crystallographic data for the Yb_5T_4 binary compounds (T = Si or Ge) have been reported, but neither the physical properties nor the phase relationships in the $Yb_5Si_xGe_{4-x}$ system have been explored. In this work, we report on the phase relationships, structural, magnetic, and thermodynamic properties of several alloys belonging to the

pseudobinary $Yb_5Si_xGe_{4-x}$ system. As we will show below, all binary and pseudobinary Yb_5T_4 compounds manifest characteristics of mixed valence systems. Neither of the studied alloys exhibits a structural transition concomitant with the magnetic ordering-disordering process, which is consistent with their crystallography where all of the slabs are already connected *via* the T_2 dimers in the paramagnetic state. All compounds with Yb order antiferromagnetically at low temperatures that are nearly independent of the Si:Ge ratio. This makes the $Yb_5Si_xGe_{4-x}$ system quite distinct compared to other $R_5Si_xGe_{4-x}$ systems studied to date.

Experimental details

A total of 5 alloys in the $Yb_5Si_xGe_{4-x}$ system with x varying from 0 to 4 were synthesized by induction melting at ~1800°C with the holding time of 10 min. Prior to induction melting, stoichiometric mixtures of pure components (Yb, Si and Ge) were loaded into Ta crucibles, and then the crucibles were sealed under pure helium atmosphere by arc welding in order to avoid losses of ytterbium due to the high vapor pressure of the metal. The Yb metal was prepared by the Materials Preparation Center of the Ames Laboratory and was 99.9 at.% (99.97 wt.%) pure with major impurities (in ppm atomic) as follows: Cl – 380, C – 245, Si – 140, S – 76, Al – 62, O – 49, Fe – 43, Ca – 35, and Lu – 11. The silicon and germanium, which were purchased from a commercial vendor, were better than 99.999 wt.% pure. The compositions Yb_5Ge_4, $Yb_5Si_2Ge_2$, and Yb_5Si_3Ge were investigated in the as-cast conditions, without heat treatment. Two of the alloys, i.e., Yb_5Si_4 and Yb_5SiGe_3 were examined before and after they were heat treated at 1400°C for 1 h.

The x-ray powder diffraction technique was utilized to characterize both the crystal structures and phase compositions of the $Yb_5Si_xGe_{4-x}$ alloys. The x-ray powder diffraction studies were performed on an automated Scintag powder diffractometer using Cu-Kα radiation. The crystal structures were refined by the Rietveld technique at room temperature ranging between 290 K and 295 K.[38] Upon completion of the refinements, the profile residuals (R_p) were from 4.3 % to 5.3 %, and the derived Bragg residuals (R_B) were from

2.3 % to 2.9 %, indicating excellent fits of the adopted structural models to the observed experimental data.[39] For one of the alloys (Yb_5SiGe_3), the crystal structure was determined using single crystal x-ray diffraction data collected at room temperature using a Bruker SMART Apex CCD diffractometer with Mo Kα radiation.

Magnetic measurements were performed using a SQUID magnetometer (model MPMS XL). The magnetization of zero-magnetic-field cooled samples was measured as a function of temperature from 1.8 to 400 K in various dc magnetic fields between 0.05 T and 5 T. Isothermal magnetization data were collected at 1.8, 2.5, and 10 K in dc magnetic fields varying from 0 to 7 T with 0.2 T steps after samples were zero-field-cooled to the target temperatures. The heat capacity of Yb_5Ge_4 was measured using an adiabatic heat-pulse calorimeter[40] between ~3.5 and 350 K in dc magnetic fields ranging from 0 to 7 T.

Results and discussion

Systematic research, carried out since 1997, indicates that crystallography of $R_5Si_xGe_{4-x}$ materials in the paramagnetic state is of extreme importance in order to understand and reconcile their physical, and especially, magnetic properties. Therefore, we will begin with the analysis of our room temperature diffraction data, followed by the description and relevant discussions of the basic magnetic and thermal properties of the $Yb_5Si_xGe_{4-x}$ materials.

Phase relationships and room temperature crystallography

Phase contents and room temperature crystal structures of all prepared alloys were determined using the x-ray powder diffraction technique and for one alloy using single crystal x-ray diffraction. The Rietveld refinements of the x-ray powder diffraction data resulted in precise lattice parameters (Table 1), and the coordinates of individual atoms and, in most cases, occupancies of the T-sites by the Si and Ge atoms, but occupancies of Yb-sites were not refined because of a small amount of Yb loss (Table 2). The observed and calculated (derived from the Rietveld refinements) powder diffraction patterns are shown in

Fig. 1 and Fig. 2. The refinement results illustrated in Fig. 1 confirm that Yb_5Si_4, Yb_5Si_3Ge, $Yb_5Si_2Ge_2$, and Yb_5Si_4 alloys are single phase materials within the sensitivity of the x-ray powder diffraction technique, which considering the quality of the data, was about 2 vol. % of an impurity phase.[39]

Table 1. Room temperature crystallographic data of $Yb_5Si_xGe_{4-x}$ alloys determined from the results of x-ray powder diffraction studies, unless indicated otherwise.

Composition	Structure type	Unit cell dimensions			Distance, δ_{T3-T3}, Å	Ref.
		a	*b*	*c*		
Yb_5Si_4[a]	Gd_5Si_4	7.26327(4)	14.78061(8)	7.70343(4)	2.45(2)	35
Yb_5Si_4	Sm_5Ge_4	7.262(2)	14.784(4)	7.700(2)	-	36
Yb_5Si_4	Gd_5Si_4	7.2695(3)	14.7988(6)	7.7103(3)	2.49(2)	This work
Yb_5Si_3Ge	Gd_5Si_4	7.2813(3)	14.8183(5)	7.7303(3)	2.57(1)	This work
$Yb_5Si_2Ge_2$	Gd_5Si_4	7.3035(4)	14.8711(9)	7.7661(5)	2.64(1)	This work
Yb_5SiGe_3*	Gd_5Si_4	7.326(3)	14.915(5)	7.796(3)	2.619(2)	This work
Yb_5SiGe_3	Gd_5Si_4	7.3241(2)	14.9220(3)	7.8021(2)	2.59(1)	This work
Yb_5Ge_4*	Sm_5Ge_4	7.342(2)	14.958(1)	7.828(1)	2.65(2)	37
Yb_5Ge_4	Gd_5Si_4	7.3406(5)	14.9423(9)	7.8253(5)	2.65(1)	This work

[a] T = 293 K,

* Single crystal x-ray diffraction data at T = 293(2) K

Table 2. Coordinates of atoms and T-site occupancies in $Yb_5Si_xGe_{4-x}$ alloys determined from the results of x-ray powder diffraction studies, unless indicated otherwise.

Compound	Atom/site	*x/a*	*y/b*	*z/c*	*g* (%)*
Yb_5Si_4	Yb1 in 4(c)	0.3473(3)	¼	0.0167(3)	
	Yb2 in 8(d)	0.0216(2)	0.0937(1)	0.1784(2)	
	Yb3 in 8(d)	0.3177(2)	0.8778(1)	0.1805(2)	
	Si1 in 4(c)	0.254(2)	¼	0.386(2)	100
	Si2 in 4(c)	0.989(2)	¼	0.868(2)	100
	Si3 in 8(d)	0.148(1)	0.9604(4)	0.474(1)	100
Yb_5Si_3Ge	Yb1 in 4(c)	0.3457(3)	¼	0.0159(3)	
	Yb2 in 8(d)	0.0193(2)	0.0940(1)	0.1809(2)	
	Yb3 in 8(d)	0.3191(2)	0.8778(1)	0.1745(2)	
	T1 in 4(c)	0.239(1)	¼	0.380(1)	75**
	T2 in 4(c)	0.979(1)	¼	0.886(1)	75**
	T3 in 8(d)	0.1528(9)	0.9626(3)	0.4479(9)	75**
$Yb_5Si_2Ge_2$	Yb1 in 4(c)	0.3425(3)	¼	0.0192(3)	
	Yb2 in 8(d)	0.0185(2)	0.0941(1)	0.1801(2)	
	Yb3 in 8(d)	0.3193(2)	0.8781(1)	0.1747(2)	
	T1 in 4(c)	0.2418(8)	¼	0.3848(8)	50(1)***
	T2 in 4(c)	0.980(1)	¼	0.882(1)	63(1)***
	T3 in 8(d)	0.1559(7)	0.9603(2)	0.4605(7)	45.8(7)***

Compound	Atom/site	*x*/*a*	*y*/*b*	*z*/*c*	*g* (%)*
Yb_5SiGe_3†	Yb1 in 4(c)	0.34312(6)	¼	0.01791(6)	
	Yb2 in 8(d)	0.01562(5)	0.09372(3)	0.18200(3)	
	Yb3 in 8(d)	0.32015(4)	0.87822(2)	0.17330(4)	
	T1 in 4(c)	0.2337(2)	¼	0.3856(2)	21.6(8)***
	T2 in 4(c)	0.9741(2)	¼	0.8791(2)	34.1(8)***
	T3 in 8(d)	0.1551(1)	0.96027(7)	0.4653(1)	17.4(6)***
Yb_5Ge_4	Yb1 in 4(c)	0.3398(4)	¼	0.0179(3)	
	Yb2 in 8(d)	0.0167(3)	0.0940(1)	0.1826(2)	
	Yb3 in 8(d)	0.3210(2)	0.8781(1)	0.1714(2)	
	Si1 in 4(c)	0.2299(8)	¼	0.3852(7)	100
	Si2 in 4(c)	0.9736(9)	¼	0.8780(7)	100
	Si3 in 8(d)	0.1555(6)	0.9599(2)	0.4619(6)	100

* Occupancy by the Si atoms with the remainder (100 % overall) occupied by the Ge atoms except for Yb_5Ge_4, where the value is for the site occupancies by the Ge atoms.

** The actual occupancies were not refined – they were assigned based on the as-prepared stoichiometry assuming completely random distribution of the Si and Ge atoms.

*** Occupancies of the T-sites have been refined with the only imposed constraint that each site has 100 % overall occupancy.

† Single crystal x-ray diffraction data.

One alloy, i.e., Yb_5SiGe_3, was not obtained in a single phase form. The main phase in this sample (71 wt.%, as determined from the Rietveld refinement) has the Gd_5Si_4-type structure, see Fig. 2 for the powder diffraction pattern of the two-phase alloy, Table 1 for the unit cell dimensions of the main phase, and Table 2 for the coordinates of atoms determined

from a single crystal diffraction experiment. Both the as-prepared and heat treated Yb_5SiGe_3 contained significant amounts of an impurity phase which, as follows from the analysis of the powder diffraction data (Fig. 2), is a solid solution based on $Yb_{11}Ge_{10}$. The pure germanide has a tetragonal $Ho_{11}Ge_{10}$-type[41] crystal structure with a = 10.72 Å and c = 16.53 Å.[42] The refined unit cell dimensions of the $Yb_{11}Si_xGe_{10-x}$ impurity are a = 10.6798(2) Å and c = 16.4262(6) Å, which are consistent with a solid solution where some of the larger Ge atoms are substituted by the smaller Si atoms. According to the Rietveld refinement, the chemical composition of the impurity is $Yb_{11}Si_{1.20(3)}Ge_{8.80(3)}$. This stoichiometry was obtained by refining site occupancies assuming that all five inequivalent Ge-sites in the $Ho_{11}Ge_{10}$-type lattice are occupied by the identical statistical mixtures of Ge and Si atoms.

Since Yb_5SiGe_3 was not a single phase material, a complete x-ray diffraction study of a single crystal extracted from this alloy was undertaken in order to confirm the crystal structure of the compound and achieve a high precision in determining both the chemical composition and site occupancies in the Yb_5T_4 phase with as-weighed Si to Ge atomic ratio of 1:3. As follows from Table 2, the stoichiometry of the majority phase is $Yb_5Si_{0.91(3)}Ge_{3.09(3)}$, i.e., it matches the as-weighed chemical composition to within three standard deviations. Some of the intra-slab T-sites (the T2 sites) are enriched in Si, while those that are responsible for the covalent-like inter-slab T_2 dimers (the T3 sites) accommodate more Ge compared to the 25 at.% Si and 75 at.% Ge expected for completely random occupancies of all corresponding T-sites. Similar preferences in site occupancies have been earlier observed in $Gd_5Si_xGe_{4-x}$ with x = 2,[11] and x = 0.44, 1.28 and 1.84.[14] One unit cell of the Yb_5SiGe_3 crystal structure with its nearest surroundings highlighting the slabs, their stacking along the b-axis and connectivity via the $T3_2$ dimers is shown in Fig. 3.

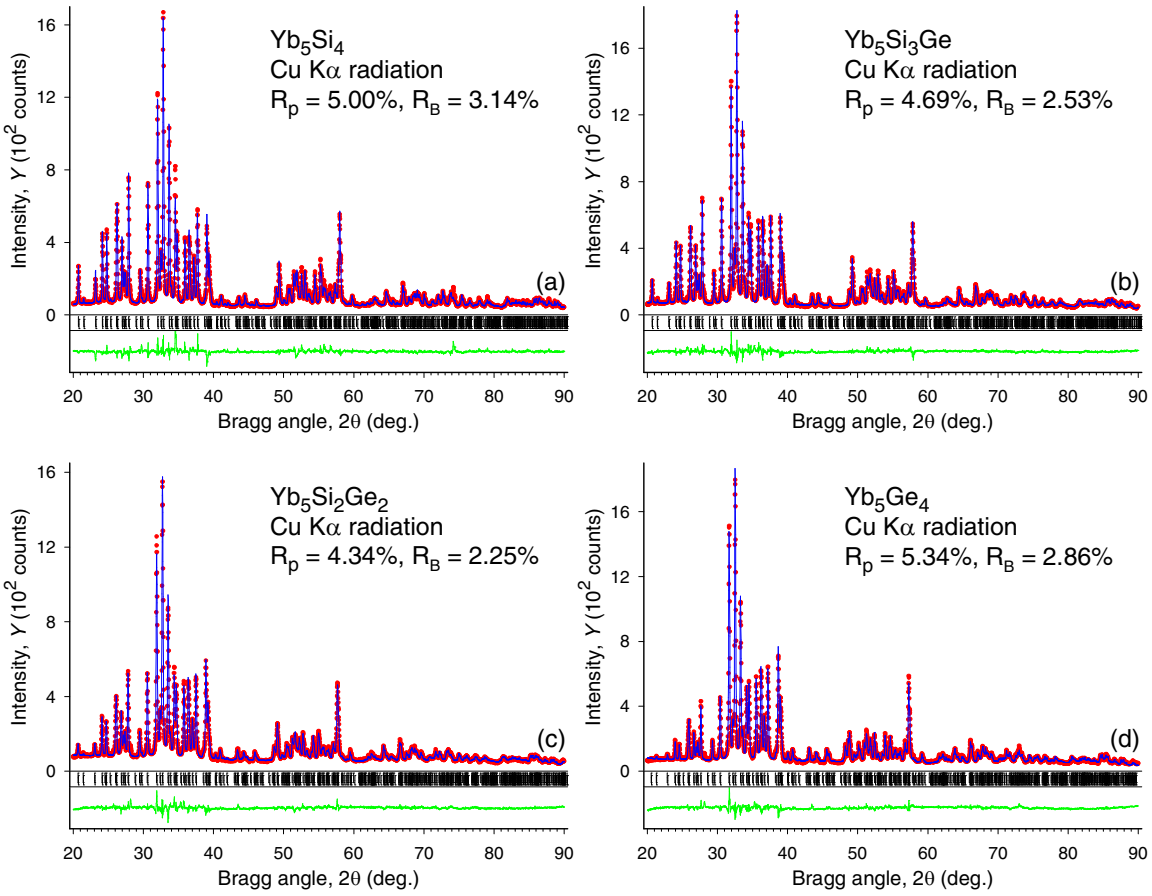

Fig. 1. (Color online) The observed (dots) and calculated (lines drawn through the data points) powder diffraction patterns of (a) - Yb_5Si_4, (b) - Yb_5Si_3Ge, (c) - $Yb_5Si_2Ge_2$, and (d) - Yb_5Ge_4 after the completion of Rietveld refinements. Calculated positions of the Bragg peaks are shown as vertical bars just below the plots of the observed and calculated intensities. The differences, $Y_{obs} - Y_{calc}$, are shown at the bottom of each plot.

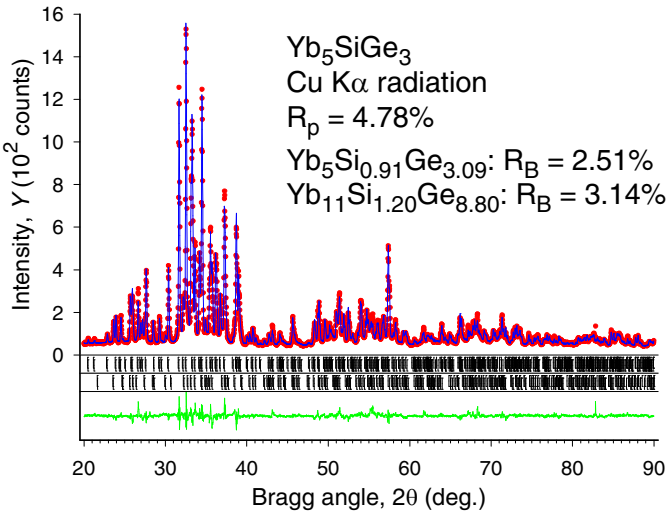

Fig. 2. (Color online) The observed (dots) and calculated (lines drawn through the data points) powder diffraction pattern of Yb_5SiGe_3 after the completion of Rietveld refinement. The upper set of vertical bars located just below the plots of the observed and calculated intensities indicates the calculated positions of the Bragg peaks of the majority $Yb_5Si_{0.91}Ge_{3.09}$ phase with the Gd_5Si_4-type structure, while the lower set of bars corresponds to the calculated positions of the Bragg peaks of the $Yb_{11}Si_{1.20}Ge_{8.80}$ impurity with the $Ho_{11}Ge_{10}$-type structure. The differences, $Y_{obs} - Y_{calc}$, are shown at the bottom of each plot.

As the rare earth component changes through the $R_5Si_xGe_{4-x}$ series, three structurally distinct phase regions have been reported to exist as a function of x for the majority of R, i.e., for R = Y,[22] Pr,[25] Nd,[29] Gd,[10] Tb,[17] Dy,[33] and Er.[20] Two or more different phase regions exist when R = La,[33] and in one reported case, i.e., when R = Lu,[33] it appears that only the Sm_5Ge_4-type crystal structure persists as the number of Si atoms per formula unit changes from 0 to 4 in the $Lu_5Si_xGe_{4-x}$ system. Considering the results of the structural analysis presented above (Fig. 1, Fig. 2, Table 1, and Table 2), all studied $Yb_5Si_xGe_{4-x}$ alloys adopt the same Gd_5Si_4-type crystal structure regardless of x, as can be judged from similar unit cell dimensions ratios and the nearly identical sets of coordinate triplets of all independent atoms. This structural identity reflects a continuous solid solubility between Yb_5Si_4 and Yb_5Ge_4 despite the fact that we were unable to prepare one of the alloys in a single phase form. The continuous solid solubility scenario is supported by the nearly linear behavior of the lattice parameters as functions of x, which is illustrated in Fig. 4. The appearance of the impurity

phase at the Yb_5SiGe_3 stoichiometry (as-weighed) is likely a result of an accidental loss of a small amount of Yb to evaporation when the components were sealed inside a Ta crucible.

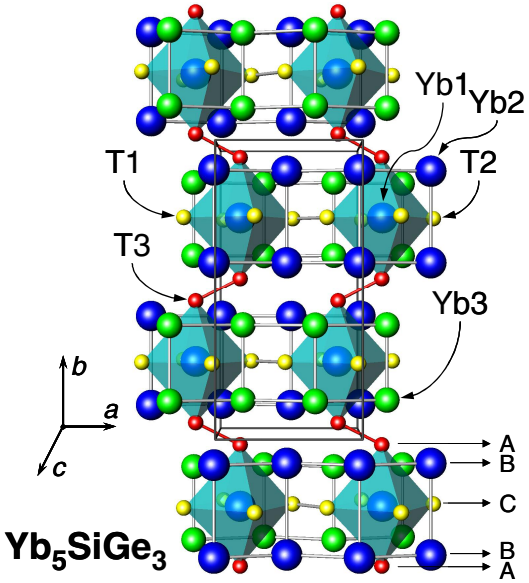

Fig. 3. (Color online) Perspective view of the crystal structure of Yb_5SiGe_3 along the *c*-axis highlighting both the slabs formed by stacking of five nearly flat atomic sheets ABCBA along the *b*-axis,[2] and the existence of short T3-T3 dimers ($\delta_{T3\text{-}T3}$ = 2.62 Å).

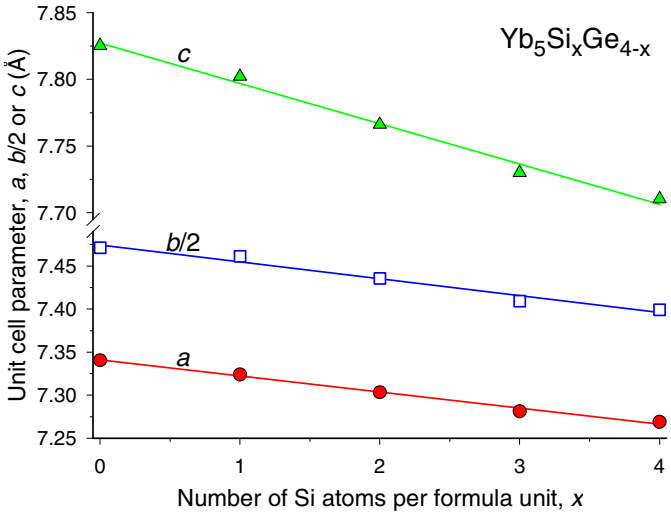

Fig. 4. (Color online) The behavior of the unit cell dimensions of $Yb_5Si_xGe_{4-x}$ as a function of *x*. Straight lines drawn through the data points are linear least squares fits.

In Fig. 5, we show the variation of the lattice parameters of the orthorhombic R_5Si_4 and R_5Ge_4 compounds with R = Gd through Lu. For the silicides, all of which have the same Gd_5Si_4-type structure (an old report[3] indicating a possibility of a monoclinic distortion in the Lu_5Si_4 lattice was not confirmed by a recent study[33]), a sharp increase in the b and c lattice parameters observed for Yb_5Si_4 is inconsistent with the normal lanthanide contraction assuming the uniform R^{3+} valence states. For the germanides, the behaviors of the b- and c-axes follow those of the silicides, but the a-axis of Yb_5Ge_4 exhibits a minimum. This minimum is in line with the differences in the crystallography of the ytterbium compound compared to the germanides with other heavy lanthanides. Similar anomalies in the lattice constants (and in the unit cell volumes) of Yb-containing compounds usually indicate that some or all of the Yb atoms in a material are either in the Yb^{2+} or in a nonintegral, mixed valence state between Yb^{3+} and Yb^{2+}. While the radii of the trivalent R ions decrease smoothly with the increasing atomic number due to the lanthanide contraction, the compounds in which Yb is in the pure 2+ state show large positive deviations from a smooth behavior. The lattice parameters of mixed valence compounds also deviate from the normal lanthanide contraction but the values of these deviations are intermediate between those observed for the two integral valence states. Thus, anomalies in the lattice constants of both Yb_5Si_4 and Yb_5Ge_4 indicate either the divalent or the mixed valence behavior of Yb in Yb_5T_4 compounds.

All things considered, the $Yb_5Si_xGe_{4-x}$ system is, therefore, quite different when compared to other $R_5Si_xGe_{4-x}$ systems studied to date. First, both the germanide and the silicide of ytterbium have the same Gd_5Si_4-type crystal structure, in which all (ABCBA) slabs are interconnected via the covalent-like T_2 dimers, whereas in the systems with other R-components, the germanide always has the Sm_5Ge_4-type structure, where all of the inter-slab dimers are broken. Second, the continuous solid solubility observed in the $Yb_5Si_xGe_{4-x}$ system is likely the result of the same crystallography of the 5:4 silicide and germanide of ytterbium. Finally, since crystallography in the paramagnetic state defines physical behaviors of the R_5T_4 compounds at low temperatures,[5-33] one might expect minimal changes

of their magnetic and thermodynamic properties as a function of x considering the structural stability within the $Yb_5Si_xGe_{4-x}$ family.

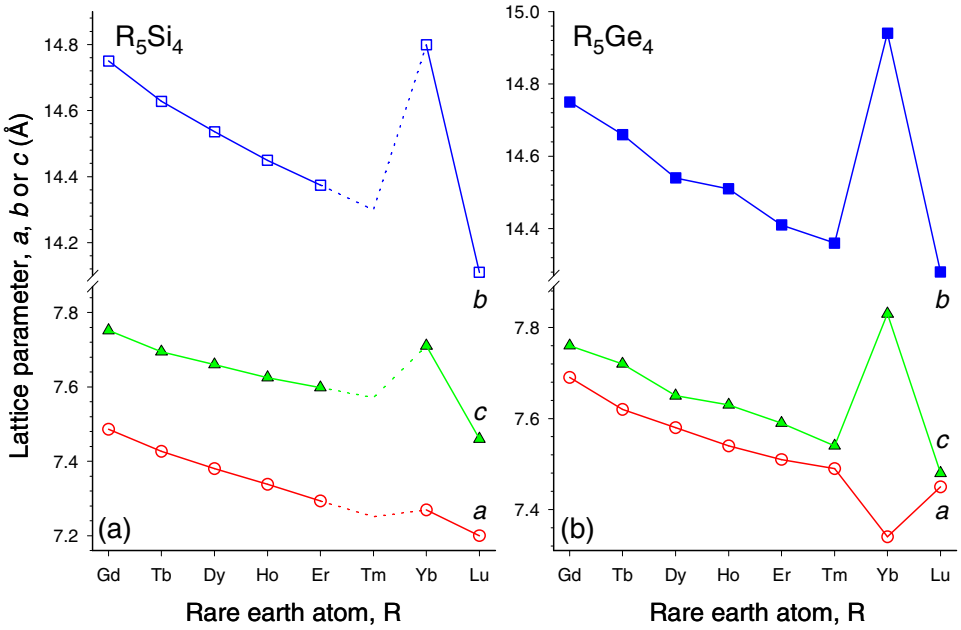

Fig. 5. (Color online) The unit cell dimensions of R_5T_4 silicides (a) and germanides (b) of heavy lanthanides as functions of the atomic number.

Magnetic properties

Considering that the amount of $Yb_{11}Si_{1.20(3)}Ge_{8.80(3)}$ impurity in the Yb_5SiGe_3 alloy was 29(1) wt.%, the physical properties of the latter were not measured. Samples extracted from all other alloys were subject to both the isofield and isothermal magnetization measurements. The low field (B = 0.05 T) magnetization data collected on warming of the zero magnetic field-cooled samples, which are shown in Fig. 6, indicate that all alloys order antiferromagnetically at low temperatures. Néel temperatures, determined from the broad maxima of $M(T)$ functions, slowly increase from T_N = 2.4 K for Yb_5Si_4 to T_N = 3.2 K for Yb_5Ge_4. This behavior is contrary to that observed in all other $R_5Si_xGe_{4-x}$ systems (R = a magnetic lanthanide) studied to date, where the magnetic ordering temperatures decrease with decreasing Si content. However, the peaks of M(T) are so broad that they do not seem to be reflective of cooperative AFM transitions. Our recent Mössbauer study of the

$Yb_5Si_xGe_{4-x}$ compounds shows that T_N values exhibit the same trend as the broad maxima of M(T), but the Mössbauer T_N values are approximately 1 K lower than the broad peaks observed in the M(T) data.[43] This discrepancy between the magnetization and Mössbauer results is likely related to anomalies in M(T) often observed above the actual magnetic ordering temperatures in low-field magnetization measurements of $R_5Si_xGe_{4-x}$ compounds.[44] Recent small angle neutron scattering work on $Tb_5Si_2Ge_2$ has linked these anomalies to a short-range magnetic clustering that occurs well above the onset of a long range magnetic order.[45] Above ~50 K, the $B/M(T)$ functions of all $Yb_5Si_xGe_{4-x}$ compounds exhibit Curie-Weiss behaviors (see inset in Fig. 6).

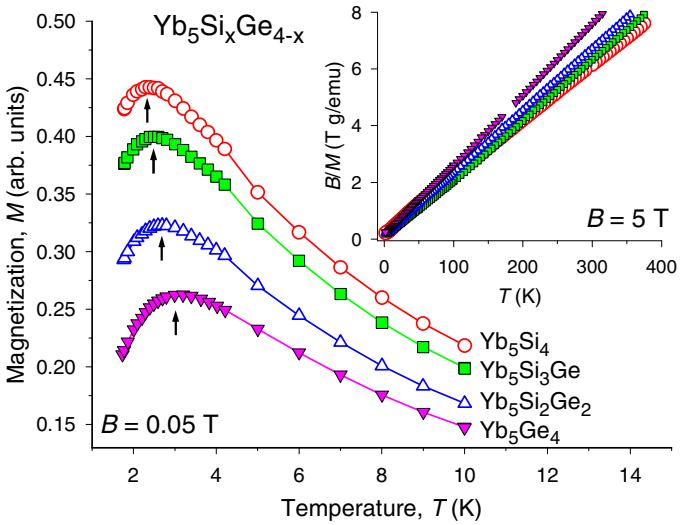

Fig. 6. (Color online) Low-magnetic field, low-temperature magnetization of zero magnetic field cooled samples of $Yb_5Si_xGe_{4-x}$ alloys measured on heating in a 0.05 T magnetic field. The arrows point to the maxima in the $M(T)$ behavior, which have been taken as Néel temperatures. The inset illustrates Curie-Weiss behavior of the inverse magnetization measured in a 5 T magnetic field.

Linear least squares fits of the data shown in the inset of Fig. 6 to $M/B = Np_{eff}^2/3k(T-\theta_p)$, where B is the magnetic induction, M is the molar magnetization, N is Avogadro's number, p_{eff} is the effective magnetic moment, k is Boltzmann's constant, T is the absolute temperature, and θ_p is the paramagnetic Curie temperature, result in a nearly identical, composition-independent effective magnetic moment of the Yb atoms, see Table 3

and, for the most part, small and negative paramagnetic Curie temperatures that are consistent with the AFM ground state of the materials. The only exception is small and positive θ_p for Yb_5Si_3Ge, yet the deviation of this value from zero is statistically insignificant considering experimental errors (±2 K). Also, we estimated that the negative temperature-independent magnetic susceptibility χ_0 is of the order of 10^{-3} to 10^{-4} cm^3/Yb-mole (i.e. the order of 10^{-2} to 10^{-3} emu/g T) due to very small deviations from the linear Curie-Weiss behavior of B/M observed for all compounds. The average p_{eff} = 2.79(5) μ_B is much smaller than the theoretical free ion effective magnetic moment of Yb^{3+} (4.54 μ_B), which is usually taken as a convincing indicator that $Yb_5Si_xGe_{4-x}$ is a mixed-valence system. Normally, Yb atoms may exist in two valence states: Yb^{2+} or Yb^{3+}. Since the electronic configuration of Yb^{2+} is $4f^{14}$, its total angular momentum is $J = 0$ resulting in $p_{eff} = 0$, while Yb^{3+} is in the $4f^{13}$ state with $J = 7/2$. Assuming that there are two distinct valence states of Yb in the lattice, one can use the following expression in order to estimate the fraction of each ion $p_{eff} = \left[z p_{eff1}^2 + (1-z) p_{eff2}^2 \right]^{1/2}$. Here, p_{eff} is the observed effective magnetic moment per Yb ion, p_{eff1} is the theoretical effective magnetic moment of the free Yb^{2+} ion ($p_{eff1} = 0$), p_{eff2} is the theoretical effective magnetic moment of the free Yb^{3+} ion (p_{eff2} = 4.54 μ_B), and z is the fraction of Yb^{2+} ions. Solving with respect to z, the fractions of Yb^{2+} ions in the unit cell vary from 0.64 for Yb_5Ge_4 to 0.61 for Yb_5Si_4 with the average z = 0.62(2), and those of Yb^{3+} ions vary from 0.36 to 0.39 with the average of 0.38(2). Considering that there are a total of 20 Yb atoms per unit cell distributed among three inequivalent lattice sites (see Table 2), it is easy to postulate that 12 out of 20 Yb atoms (60%) in each unit cell are in the Yb^{2+} state, and 8 (40%) are in the Yb^{3+} state. Although bulk magnetization measurements provide no clues with respect to which of the two 8(d) Yb sites may accommodate the Yb^{2+} ions, the crystallographic data of Table 2 may do so because of the difference in the atomic radii[46] (r_{Yb2+} = 1.939 Å, r_{Yb3+} = 1.741 Å). Analysis of the interatomic distances indicates that the Yb3 site is likely to accommodate the smaller Yb^{3+} ions. These sites are shown as the medium size spheres in Fig. 3 (the medium size green spheres in the electronic version of this paper containing the colored illustrations). Both the anomalous behaviors of the unit cell dimensions (see above), and the magnetic properties of the $Yb_5Si_xGe_{4-x}$ compounds, therefore,

indicate that the latter is a heterogeneous mixed valence family in which two crystallographically inequivalent Yb sites, i.e., Yb1 in 4(c) and Yb2 in 8(d), are occupied by the divalent Yb and one,Yb3 in 8(d), accommodates the trivalent Yb ions.

Recently, we reported the results of a ^{170}Yb Mössbauer spectroscopy study of both the valence state and magnetic ordering in the $Yb_5Si_xGe_{4-x}$ pseudobinary system.[43] Our direct, microscopic measurements complement the earlier bulk study and confirm our main conclusions. Electric field gradients and magnetic ordering make it easy to distinguish the two ytterbium valence states. Yb^{2+} is nonmagnetic with a closed-shell, spherically symmetric $4f^{14}$ electronic configuration. With no 4f contribution to the electric field gradient (efg), only the much smaller lattice contribution is present, and thus Yb^{2+} exhibits small quadrupole interactions (Δ) in a ^{170}Yb Mössbauer spectrum. By contrast, $4f^{13}$ Yb^{3+} has a large 4f contribution to the efg and also exhibits magnetic order. As can be seen in Fig. 7, the two valence states are readily distinguished. The Mössbauer study found that the Yb^{2+}:Yb^{3+} ratio is closer to 50%:50% (Figs. 7, 8, and 9), which is somewhat different from 60%:40% estimated from bulk magnetization data. This difference is reasonable because the estimated valence from the bulk magnetization data is not precise and has an error of about 10 %, while Mössbauer probe is sensitive to the valence state. Also, the onset of magnetic order occurs at temperatures about 1 K below those inferred previously from M(T) data at low magnetic fields. Finally, despite the apparent uniformity in structure and valence in this system, we find that the magnetic ordering is quite complex. For x = 1, 2, and 3, there are two distinct Yb^{3+} components that order at separate temperatures, while only one Yb^{3+} component is seen in the end-member materials (x = 0, 4). Furthermore, we observe a clear break in magnetic behavior between x = 3 and x = 3.5 that does not appear to be associated with any crystallographic changes (Fig. 10).

Table 3. Magnetic properties of $Yb_5Si_xGe_{4-x}$ alloys.

Stoichiometry	T_N (K)	θ_p (K)	p_{eff} (μ_B)	Yb^{2+} ions per unit cell	M at T = 1.8 K, B = 7T, μ_B/Yb^{3+}
Yb_5Si_4	2.4(1)*, 1.62(1)**	-16(3)	2.84(3)	12.2	2.10
Yb_5Si_3Ge	2.5(1)*	2(3)	2.78(1)	12.5	2.37
$Yb_5Si_2Ge_2$	2.7(1)*	-8(3)	2.80(5)	12.4	2.21
Yb_5Ge_4	3.2(1)*, 1.71(1)**	-4(3)	2.73(3)	12.8	2.01

* T_N determined from broad maxima of $M(T)$ in the low magnetic field
** T_N determined from Mössbauer data

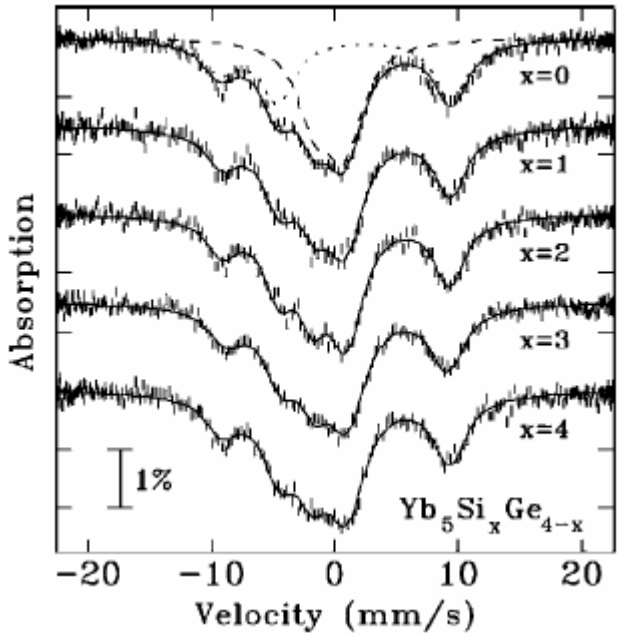

Fig. 7. ^{170}Yb Mössbauer spectra of $Yb_5Si_xGe_{4-x}$ taken at 5.0 K, above their ordering temperatures, showing the central Yb^{2+} quadrupole triplet and an approximately equal-area quadrupole triplet from Yb^{3+} giving lines to the left and right of the central feature. Solid lines are fits (see Ref. 44 for details). For x = 0 we show the form of the Yb^{2+} component (dashed line) and the Yb^{3+} component (dotted line).

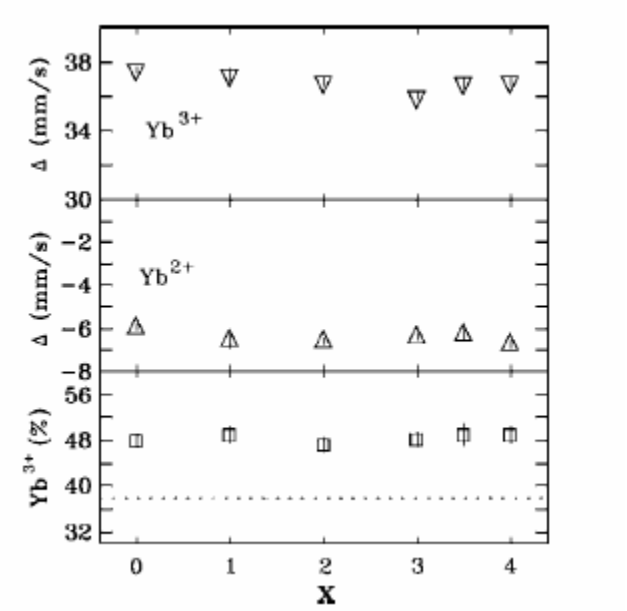

Fig. 8. Summary of fitted parameters for the spectra shown in Fig. 7. Top and middle panels: quadrupole interaction (Δ) for the Yb^{3+} and Yb^{2+} components. Note the factor of six difference in absolute values. Bottom panel: fractional area associated with Yb^{3+} for each of the compounds studied here. Dotted line in lowest panel shows Yb^{3+} fraction estimated from bulk magnetization data.

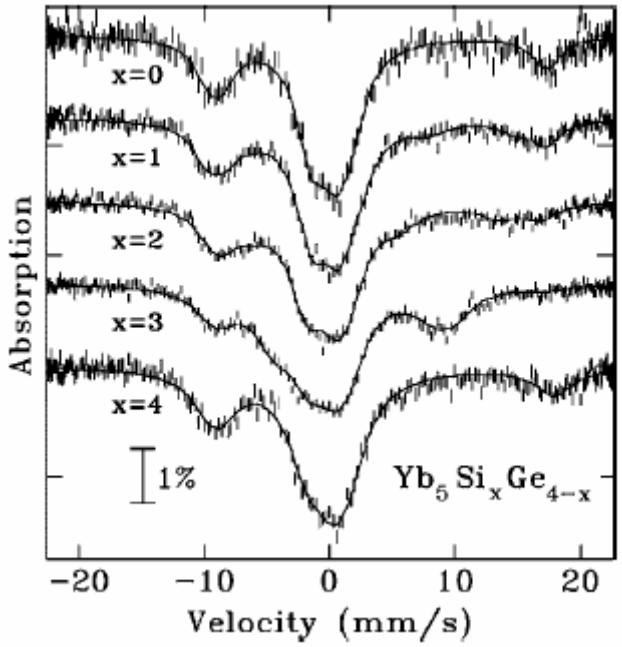

Fig. 9. ^{170}Yb Mössbauer spectra of $Yb_5Si_xGe_{4-x}$ taken at 1.5 K showing the effect of magnetic ordering on theYb^{3+}component in each compound. Note the very similar appearance of the spectra

fro the end members (x = 0, 4) and the more complex behavior evident for x = 1, 2, 3. Solid lines are fits to the full Hamiltonian as described in Ref. 44.

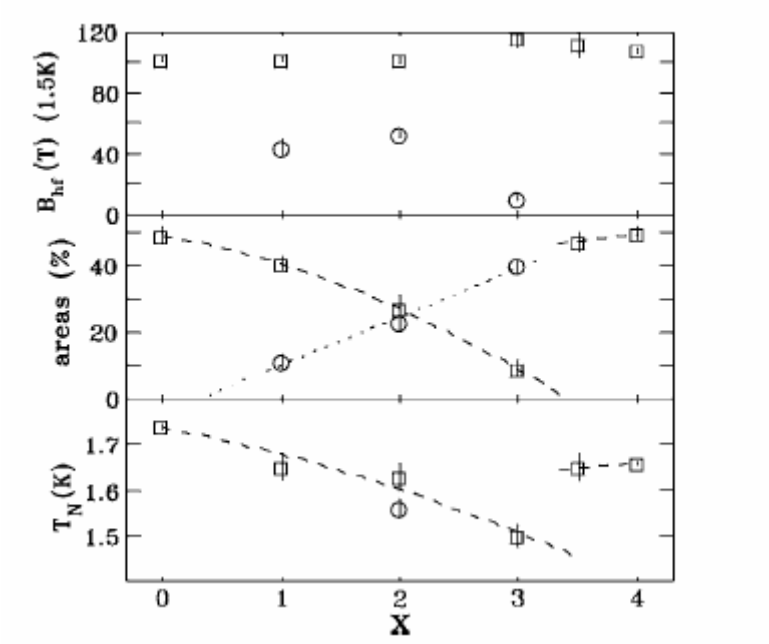

Fig. 10. Fitted values for top: B_{hf} (at 1.5 K), center: areas of the Yb^{3+} component or subcomponents, and bottom: T_N for the Yb^{3+} component or subcomponents, for $Yb_5Si_xGe_{4-x}$. In all cases, the symbols correspond between plots. Dotted and dashed lines are guides to the eye and serve to emphasize the discontinuities between x = 3 and x = 3.5.

The isothermal magnetization behaviors of $Yb_5Si_xGe_{4-x}$ are shown in Fig. 7 as a function of the magnetic field, which was varied from 0 to 7 T at T = 1.8 K and 10 K, i.e., they were measured just below and slightly above the Néel temperatures determined from M(T) data. The metamagnetic-like behavior with B_{cr} = 1.3 T (better seen as peaks in the insets displaying the derivatives of the magnetization with respect to the magnetic field), which is independent of alloy composition, is clearly visible at 1.8 K, thus indicating that the magnetic field induces spin-flip transformations in all of the alloys. Detectable, yet remanence-free hysteresis is observed both below and above T_N when x = 4 and x = 3, but as the concentration of Ge increases, the $M(B)$ curves of alloys with x = 2 and x = 0 become non-hysteretic. Most likely, the gradual change of the hysteretic behavior reflects changes in domain wall pinning, and therefore, is related to a systematic variation of the microstructural

features with x. For all $Yb_5Si_xGe_{4-x}$ alloys, the magnetization remains below 1.0 μ_B/Yb atom in the magnetic field of 7 T. In fact, as shown in Table 3, it remains below 2.4 μ_B/Yb^{3+} ion assuming that only 8 out every 20 Yb atoms are in the Yb^{3+} state, and therefore, carry a moment. Considering that the expected saturated magnetic moment of Yb^{3+} is $gJ\mu_B = 4.0$ μ_B, where g is the gyromagnetic ratio and J is the total angular momentum quantum number, the much lower values observed in the magnetically ordered state indicate that either the magnetic moments of Yb^{3+} remain undeveloped down to 1.8 K or the magnetic structures of these $Yb_5Si_xGe_{4-x}$ compounds maintain complex non-collinear arrangements of fully developed magnetic moments of Yb^{3+} even after the magnetic field-induced metamagnetic transitions. Resolution of this uncertainty will have to wait for a neutron scattering investigation of the microscopic details of the magnetic structure of a representative Yb_5T_4 compound.

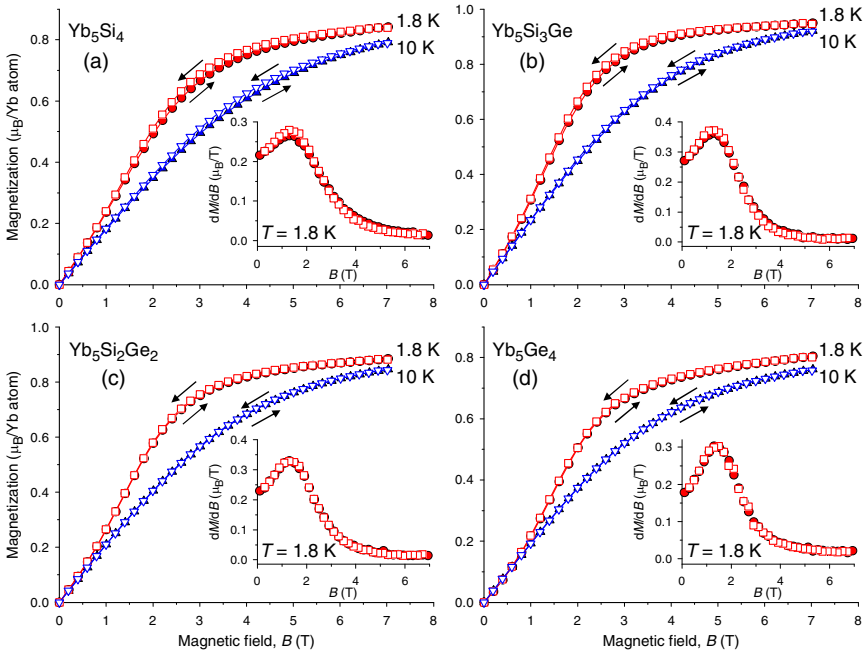

Fig. 7. (Color online) Magnetization of zero magnetic field cooled samples of $Yb_5Si_xGe_{4-x}$ alloys measured isothermally at 1.8 K and 10 K. The insets show the derivatives of the magnetization with respect to the magnetic field computed for the $T = 1.8$ K data in order to illustrate the locations of the inflection points on each $M(B)$ curve.

Heat capacity

The behavior of the heat capacity (C_P) of Yb_5Ge_4 measured on heating in various magnetic fields ranging from 0 to 7 T (Fig. 8) is consistent with the magnetization measurements. The upturn below ~9 K, observed in 0, 1 T and 2 T magnetic fields, and the enhancement of C_P over the range of temperatures exceeding 20 K in 5 T and 7 T fields, points to contributions other than normal lattice and electronic heat capacities. For comparison, we show the heat capacity of the non-magnetic Lu_5Ge_4 on the same plot, which unfortunately, may only be considered as a rough approximation of the sum of the lattice and electronic components of Yb_5Ge_4 because the crystal structure of the compound with Lu[3,33] is different from that of its ytterbium counterpart and that the valence of Lu is 3+, while it is 2.4+ for Yb. Weak magnetic fields (1 T and 2 T) have little effect on the low temperature heat capacity, which is consistent with the AFM ground state of the germanide (see Fig. 6 and Fig. 7). However, when the magnetic field is increased to 5 T and 7 T, which are considerably higher than the B_{cr} = 1.3 T observed at T = 1.8 K, the entropy of the system is shifted to high temperatures as expected for a magnetic field-induced FM-like state of Yb_5Ge_4.

The low temperature limit of our calorimeter is ~3.5 K, and therefore, we were unable to determine the shape of the zero-magnetic field heat capacity anomaly associated with the magnetic ordering of Yb_5Ge_4. Nonetheless, considerable enhancement of the heat capacity measured in a zero magnetic field at temperatures much higher than T_N = 3.2 K is indicative of a second-order phase transformation, which is in line with a conventional order $\rightarrow$ disorder transition. Combined with the absence of a reliable lattice plus electronic specific heat baseline, this makes an estimate of the total magnetic entropy [theoretically, $\Delta S = R\ln(2J + 1)$, which may have served as an additional proof that only 8 out every 20 Yb atoms in the unit cell of Yb_5Ge_4 carry a magnetic moment], nearly impossible. Considering that the magnetic contribution to the total heat capacity in a zero magnetic field has been measured incompletely due to the low-temperature limit of the apparatus, the data shown in Fig. 8 are also unsuitable for an unbiased computation of the magnetocaloric effect (MCE).[47] Yet,

taking into account the thermodynamic analysis performed by Pecharsky *et al.*,[48] it is easy to predict that the magnetocaloric effect of Yb_5Ge_4 will be negligible for magnetic field changes of 1 T and 2 T, and that the MCE will be strongly enhanced for ΔB = 5 T and ΔB = 7 T (in all cases, the magnetic field varies between 0 and the mentioned value). Furthermore, the high-field MCE of this compound should exhibit a conventional caret-like behavior with the maximum $|\Delta S_M|$ observed around 4.1 K and 4.5 K for magnetic field changes from 0 to 5 T and 0 to 7 T, respectively.

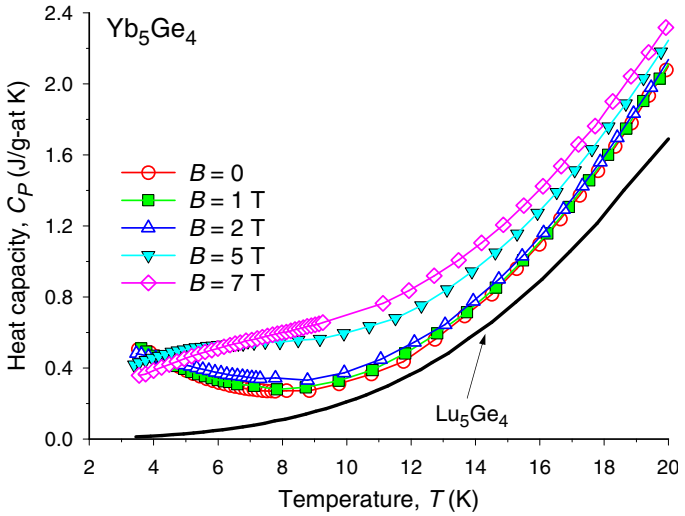

Fig. 8. (Color online) Low temperature heat capacity of Yb_5Ge_4 measured in 0, 1 T, 2 T, 5 T, and 7 T magnetic fields during heating of the zero magnetic field cooled sample. The lines drawn through the data points are guides for the eye. The thick solid line represents the heat capacity of the non-magnetic Lu_5Ge_4, which is only a rough approximation of the lattice and electronic contributions in Yb_5Ge_4 because the crystal structures of these two germanides are different.

$Yb_5Si_xGe_{4-x}$ versus other $R_5Si_xGe_{4-x}$ systems

Among the eight heavy lanthanides (i.e., when R = Gd, Tb, Dy, Ho, Er, Tm, Yb, and Lu) all of the silicides at the R_5Si_4 stoichiometry (except Tm, for which no experimental data are available) crystallize in the Gd_5Si_4-type structure at room temperature. On the other hand, all germanides at the R_5Ge_4 stoichiometry adopt the Sm_5Ge_4-type structure at room temperature except Yb, which as follows from our investigation, belongs to the Gd_5Si_4-type. The major

crystallographic difference between these two types of crystal structure is the presence of the covalent-like interslab T-T dimers connecting the slabs in the Gd_5Si_4-type lattice as highlighted in Fig. 3, and their absence in the Sm_5Ge_4-type structure. Therefore, the lengths (δ) of the interslab T3-T3 bonds are useful gauges to recognize either of these two structure types, in addition to the analysis of the *c*/*a* ratios, which are larger for the Gd_5Si_4-type with the average *c*/*a* = 1.036(5) compared to the *c*/*a* = 1.010(3) for the Sm_5Ge_4-type lattice. Following Choe *et al*.,[14] the $\delta_{T3\text{-}T3}$ of ~2.6 Å between all of the slabs may be taken as an indicator of the Gd_5Si_4-type, the alternating ~2.6 Å and ~3.5 Å interslab T3-T3 distances manifest the monoclinic $Gd_5Si_2Ge_2$-type, and all interslab $\delta_{T3\text{-}T3}$ of ~3.5 Å signal the Sm_5Ge_4-type arrangement of the slabs. The room temperature crystallographic data for the Yb_5Si_4-Yb_5Ge_4 pseudobinary system tabulated in Table 1 and Table 2, confirm that all alloys with the $Yb_5Si_xGe_{4-x}$ stoichiometry crystallize in the Gd_5Si_4-type structure at room temperature, i.e., all of the slabs are interconnected *via* short, covalent-like Si(Ge)-Si(Ge) bonds. A systematic elongation of the interslab T3-T3 bonds from ~2.5 Å to ~2.6 Å, which occurs as *x* changes from 4 to 0, is reflective of the differences in the effective radii of Si and Ge.

When divalent Yb is substituted for trivalent Gd in R_5T_4, the valence electron concentration in $Yb_5Si_xGe_{4-x}$ is lowered compared to $Gd_5Si_xGe_{4-x}$. This substitution, therefore, has a similar effect on the crystallography of R_5T_4 materials as when the tetravalent Ge is replaced by the trivalent Ga in $Gd_5Ge_{4-x}Ga_x$.[49] As the concentration of Ga increases in the latter, the Sm_5Ge_4-type structure adopted by the pure germanide (*x* = 0, valence electron concentration is 31 e^-/formula unit) is first replaced by the Pu_5Rh_4-type when *x* = 1, which corresponds to 30 valence electrons/formula unit. The Pu_5Rh_4-type lattice is intermediate between the Sm_5Ge_4- and Gd_5Si_4-types of crystal structure, as was judged by the evolution of the interslab T3-T3 distances.[49] Upon a further increase of the Ga concentration, the Gd_5Si_4-type lattice becomes stable when *x* = 2, corresponding to the formal valence electron count of 29 e^-/formula unit. Counting valence electrons in $Yb_5Si_xGe_{4-x}$ materials results in the total of 28 valence electrons per formula unit, thus explaining the stability of the Gd_5Si_4-type structure regardless of *x* when *R* = Yb. Even though the valence electron concentration argument may be considered artificial, the structural behavior exhibited by the $Yb_5Si_xGe_{4-x}$

system confirms that low valence electron count results in the stabilization of the T-T dimers. In this regard, replacing some of the Si atoms by P, Sb or As may result in weakening of the interslab interactions, thus providing additional chemical tool in tuning both the crystallography and physical properties of this particular intermetallic system, as well as of other R_5T_4 materials.

Considering the magnetic properties of R_5T_4 compounds, the silicides with R = Gd, Tb, Dy, Ho, and Er, order ferromagnetically but the germanides with the same rare earth ions, are antiferromagnets at low temperatures (see Refs. 5 through 37). Carried over into the ternary silicide-germanide $R_5Si_xGe_{4-x}$ systems with R = Gd through Er, this difference in the magnetic behaviors of the binary parent compounds results in discontinuous changes of the magnetic ground states at different R-specific concentrations, x. However, as follows from this study, the ground states of the ytterbium silicide and the germanide are nearly identical – both order antiferromagnetically at about the same low temperature of ~3 K. The low magnetic ordering temperatures in the $Yb_5Si_xGe_{4-x}$ system are likely related to the fact that the majority of Yb-atoms are the non-magnetic Yb^{2+} ions. Another peculiarity of the $Yb_5Si_xGe_{4-x}$ system is that the magnetic coupling here always remains AFM regardless of the presence of the covalent-like interslab T3-T3 bonds. Although indirectly, this result supports the notion[12] about the [-T-*R*-T-T-*R*-T-] superexchange playing a role in enhancing the FM coupling between the slabs. It is easy to see (Fig. 3, and the discussion of valence states of different Yb-sites, above) that even though the covalent-like chains [-T3-Yb1-T3-T3-Yb1-T3-] do exist in all of the $Yb_5Si_xGe_{4-x}$ alloys, their effect on the magnetic interactions is negligible because the Yb1-sites are occupied by the non-magnetic Yb^{2+} ions.

Conclusions

In summary, $Yb_5Si_xGe_{4-x}$ alloys preserve the same crystal structure as x varies from 4 to 0, which leads to a continuous solid solubility between Yb_5Si_4 and Yb_5Ge_4. As a result, replacements of Ge by Si and vise versa have little effect on the magnetic properties of materials, which is a unique feature compared to all other R_5T_4 systems formed by

lanthanides with incompletely filled *4f* shell. Three different lattice sites accommodating lanthanides in the Gd_5Si_4-type crystal structure exhibit selectivity with respect to the valence states of Yb ions. The non-magnetic Yb^{2+} ions are located in the 4(c) and one of the 8(d) sites, while the Yb^{3+} ions are located exclusively in the 8(d) sites. $Yb_5Si_xGe_{4-x}$, therefore, may be considered to be a heterogeneous mixed valence system. However, ^{170}Yb Mössbauer spectra of $Yb_5Si_xGe_{4-x}$ taken between 1.5 K and 40 K show that Yb is present as Yb^{2+} and Yb^{3+} in nearly equal amounts [51.6(3) % and 48.4(3) %, respectively] and that this balance is independent of temperature and composition. Also, intermediate compositions (x = 1, 2, 3) exhibit two distinct ordered Yb^{3+} subcomponents which appear to have separate ordering temperatures, furthermore, we observe a clear break in magnetic behavior between x = 3 and x = 3.5, that does not appear to be associated with any crystallographic changes. All $Yb_5Si_xGe_{4-x}$ alloys exhibit weak AFM correlations at temperatures between 2.4 K and 3.2 K. Final confirmation of magnetic structures will come in a future from neutron diffraction data. While neutrons are insensitive to valence, the neutron diffraction data should allow us to determine the amount and location of the Yb^{3+} ions in $Yb_5Si_xGe_{4-x}$ since only Yb^{3+} carries a magnetic moment.

Acknowledgment

This work was supported by the Office of Basic Energy Sciences, Materials Sciences Division of the U.S. Department of Energy under Contract No.W-7405-ENG-82 with Iowa State University.

References

[1] G. S. Smith, A. G. Tharp, and Q. Johnson, Nature (London) **210**, 1148 (1966).

[2] G. S. Smith, Q. Johnson, and A. G. Tharp, Acta Crystallogr. **22**, 269 (1967).

[3] G. S. Smith, A. G. Tharp, and Q. Johnson, Acta Crystallogr. **22**, 940 (1967).

[4] H.-U. Pfeifer and K. Schubert, Z. Metallk. **57**, 884 (1966).

[5] F. Holtzberg, R. J. Gambino, and T. R. McGuire, J. Phys. Chem. Solids **28**, 2283 (1967).

[6] J. M. Elbicki, L. Y. Zhang, R. T. Obermeyer, and W. E. Wallace, J. Appl. Phys. **69**, 5571 (1991).

[7] V. K. Pecharsky and K. A. Gschneidner, Jr., Phys. Rev. Lett. **78**, 4494 (1997).

[8] V. K. Pecharsky and K. A. Gschneidner, Jr., Appl. Phys. Lett. **70**, 3299 (1997).

[9] F. Casanova, A. Labarta, X. Batlle, J. Marcos, L. Mañosa, A. Planes, and S. de Brion, Phys. Rev. B **69**, 104416 (2004).

[10] V. K. Pecharsky and K. A. Gschneidner, Jr., J. Alloys Compd. **260**, 98 (1997).

[11] W. Choe, V. K. Pecharsky, A. O. Pecharsky, K. A. Gschneidner, Jr., V. G. Young, Jr., and G. J. Miller, Phys. Rev. Lett. **84**, 4617 (2000).

[12] V. K. Pecharsky and K. A. Gschneidner, Jr., Adv. Mater. **13**, 683 (2001).

[13] V. K. Pecharsky, A. O. Pecharsky, and K. A. Gschneidner, Jr., J. Alloys Compd. **344**, 362 (2002).

[14] W. Choe, A. O. Pecharsky, M. Worle, and G. J. Miller, Inorg. Chem. **42**, 8223 (2003).

[15] L. Morellon, J. Stankiewicz, B. García-Landa, P. A. Algarabel, and M. R. Ibarra, Appl. Phys. Lett. **73**, 3462 (1998).

[16] L. Morellon, P. A. Algarabel, M. R. Ibarra, J. Blasco, B. García-Landa, Z. Arnold, and F. Albertini, Phys. Rev. B **58**, R14721 (1998).

[17] C. Ritter, L. Morellon, P. A. Algarabel, C. Magen, and M. R. Ibarra, Phys. Rev. B **65**, 094405 (2002).

[18] L. Morellon, C. Ritter, C. Magen, P. A. Algarabel, and M. R. Ibarra, Phys. Rev. B **68**, 024417 (2003).

[19] L. Morellon, Z. Arnold, C. Magen, C. Ritter, O. Prokhnenko, Y. Skorokhod, P. A. Algarabel, M. R. Ibarra, and J. Kamarad, Phys. Rev. Lett. **93**, 137201 (2004).

[20] A. O. Pecharsky, K. A. Gschneidner, Jr., V. K. Pecharsky, D. L. Schlagel, and T. A. Lograsso, Phys. Rev. B **70**, 144419 (2004).

[21] J. M. Cadogan, D. H. Ryan, Z. Altounian, X. Liu, and I. P. Swainson, J. Appl. Phys. **95**, 7076 (2004).

[22] A. O. Pecharsky, V. K. Pecharsky, and K. A. Gschneidner, Jr., J. Alloys Compd. **379**, 127 (2004).

[23] H. F. Yang, G. H. Rao, W. G. Chu, G. Y. Liu, Z. W. Ouyang, and J. K. Liang, J. Alloys Compd. **334**, 131 (2002).

[24] H. F. Yang, G. H. Rao, G. Y. Liu, Z. W. Ouyang, W. F. Liu, X. M. Feng, W. G. Chu, and J. K. Liang, J. Alloys Compd. **361**, 113 (2003).

[25] H. F. Yang, G. H. Rao, W. G. Chu, G. Y. Liu, Z. W. Ouyang, and J. K. Liang, J. Alloys Compd. **339**, 189 (2002).

[26] H. F. Yang, G. H. Rao, G. Y. Liu, Z. W. Ouyang, W. F. Liu, X. M. Feng, W. G. Chu, and J. K. Liang, J. Magn. Magn. Mater. **263**, 146 (2003).

[27] G. H. Rao, Q. Huang, H. F. Yang, D. L. Ho, J. W. Lynn, and J. K. Liang, Phys. Rev. B **69**, 094430 (2004).

[28] J. M. Cadogan, D. H. Ryan, Z. Altounian, B. H. Wang, and I. P. Swainson, J. Phys.: Condens. Matter **14**, 7191 (2002).

[29] H. F. Yang, G. H. Rao, G. Y. Liu, Z. W. Ouyang, W. F. Liu, X. M. Feng, W. G. Chu, and J. K. Liang, J. Alloys Compd. **346**, 190 (2002).

[30] C. Magen, L. Morellon, P. A. Algarabel, M. R. Ibarra, C. Ritter, A. O. Pecharsky, K. A. Gschneidner, Jr., and V. K. Pecharsky, Phys. Rev. B **70**, 224429 (2004).

[31] L. Morellon, Z. Arnold, C. Magen, C. Ritter, O. Prokhnenko, Y. Skorokhod, P. A. Algarabel, M. R. Ibarra, and J. Kamarad, Phys. Rev. Lett. **93**, 137201 (2004).

[32] V. V. Ivtchenko, V. K. Pecharsky, and K. A. Gschneidner, Jr., Adv. Cryo. Eng. **46A**, 405 (2000).

[33] K. A. Gschneidner, Jr., V. K. Pecharsky, A. O. Pecharsky, V. V. Ivtchenko, and E. M. Levin, J. Alloys Compd. **303**, 214 (2000).

[34] M. V. Bulanova, P. N. Zheltov, K. A. Meleshevich, P. A. Saltykov, and G. Effenberg, J. Alloys Compd. **345**, 110 (2002).

[35] R. Černý and K. Alami-Yadri, Acta Cryst. E **59**, i1 (2003).

[36] A. Palenzona, P. Manfrinetti, S. Brutti, and G. Balducci, J. Alloys Compd. **348**, 100 (2003).

[37] M. Pani and A. Palenzona, J. Alloys Compd. **360**, 151 (2003).

[38] B. A. Hunter, Rietica – A visual Rietveld program, International Union of Crystallography Commission on Powder Diffraction, Newsletter No. 20 (Summer, 1998) http://www.rietica.org.

[39] V. K. Pecharsky and P. Y. Zavalij, *Fundamentals of Powder Diffraction and Structural Characterization of Materials* (Kluwer Academic Publishers, New York, 2003), 713 pp.

[40] V. K. Pecharsky, J. O. Moorman and K. A. Gschneidner, Jr., Rev. Sci. Instr. **68**, 4196 (1997).

[41] A. G. Tharp, G. S. Smith, and Q. Johnson, Acta Cryst. **20**, 583 (1966).

[42] V. N. Eremenko, K. A. Meleshevich, and Y. I. Buyanov, Dopov. Akad. Nauk Ukr. RSR, Ser. A No. 3, 83 (1983).

[43] C. J. Voyer, D. H. Ryan, K. Ahn, K. A. Gschneidner, Jr., and V. K. Pecharsky, Phys. Rev. B **73**, 174422 (2006).

[44] J. Szade and G. Skorek, J. Magn. Magn. Mater. **196-197**, 699 (1999).

[45] C. Magen, P. A. Algarabel, L. Morellon, J. P. Araújo, C. Ritter, M. R. Ibarra, A. M. Pereira, and J. B. Sousa, Phys. Rev. Lett. **96**, 167201 (2006).

[46] E. T. Teatum, K. A. Gschneidner, Jr. and J. T. Waber, Compilation of calculated data useful in predicting metallurgical behavior of the elements in binary alloy systems, Los Alamos Scientific Laboratory Report, LA-4003 (1968), National Technical Information Service, U.S. Department of Commerce, Springfield, VA 22161.

[47] V. K. Pecharsky and K. A. Gschneidner, Jr., J. Appl. Phys. **86**, 565 (1999).

[48] V. K. Pecharsky, K. A. Gschneidner, Jr., A. O. Pecharsky, and A. M. Tishin, Phys. Rev. B **64**, 144406 (2001).

[49] Yu. Mozharivskyj, W. Choe, A. O. Pecharsky, and G. J. Miller, J. Am. Chem. Soc. **125**, 15183 (2003).

CHAPTER 3. PHASE RELATIONSHIPS AND STRUCTURAL, MAGNETIC, AND THERMODYNAMIC PROPERTIES IN THE $Sm_5Si_xGe_{4-x}$ PSEUDOBINARY SYSTEM

This is a manuscript prepared for publication.

Kyunghan Ahn,[4,5] V. K. Pecharsky,[4,5] and K. A. Gschneidner, Jr.[4,5]

Abstract

The crystallography, phase relationships, and physical properties of the $Sm_5Si_xGe_{4-x}$ alloys with $0 \leq x \leq 4$ have been investigated by using a x-ray powder diffraction, dc magnetization and heat capacity measurements between 3.5 K and 350 K in magnetic fields ranging from 0 and 10 T. Similar to the $Gd_5Si_xGe_{4-x}$ system, there are three distinct phase regions in the $Sm_5Si_xGe_{4-x}$ system; the Gd_5Si_4-type for Si-rich compositions, the $Gd_5Si_2Ge_2$-type for intermediate range of concentrations, and the Sm_5Ge_4-type for Ge-rich alloys. The magnetic properties of the $Sm_5Si_xGe_{4-x}$ compounds can be well described by considering the temperature-independent Van Vleck term due to small energy separation between the ground state and the first excited state of Sm^{3+} ions. All $Sm_5Si_xGe_{4-x}$ compounds have unusually high magnetic ordering temperatures. The change in the magnetic and structural behaviors with the substitution of Ge by Si is similar to that observed in the $Gd_5Si_xGe_{4-x}$ system. The external magnetic field seems to have no effect on the magnetism of the $Sm_5Si_xGe_{4-x}$ alloys.

[4] Ames Laboratory of US DOE, Materials and Engineering Physics Program, Iowa State University, Ames, IA 50011-3020, USA

[5] Department of Materials Science and Engineering, Iowa State University, Ames, IA 50011-2300, USA

Introduction

The first R_5Si_4 and R_5Ge_4 compounds were discovered by Smith *et al.* in 1966 who reported an orthorhombic Sm_5Ge_4-type structure for all the germanides studied (R = Nd, Sm, Gd, Tb, Er, and Y) and for the silicides with the heavy lanthanides (R = Tb and Er) and R = Y except for tetragonal Nd_5Si_4.[1] The crystal structure of Sm_5Ge_4 adopts the space group symmetry *Pnma* and, according to Smith *et al.*, is well described by three distinct layers of atoms, which are the layer G (only Ge atoms), the layer S (only Sm atoms), and the layer C (combination of Sm and Ge atoms), stacked along the *b* axis in a (GSCSG) sequence.[2] Later, Smith *et al.* found that the orthorhombic 5:4 phase is stable for all of the lanthanide germanides R_5Ge_4 except for R = Pm, Eu and Yb, but for silicides there are two different crystal structures depending on the rare earth element: the Zr_5Si_4-type tetragonal structure for light rare earth elements (R = La, Ce, Pr, and Nd) and the Sm_5Ge_4-type orthorhombic structure for R = Sm and heavy lanthanides (R = Gd, Tb, Dy, Er) and R = Y except for the monoclinically distorted orthorhombic structure of Lu_5Si_4.[3] According to Holtzberg *et al.* [4], both R_5Si_4 and R_5Ge_4 with the heavy lanthanides (R = Gd, Tb, Dy, Ho, and Er) have the orthorhombic crystal structure and relatively high ferromagnetic (FM) ordering temperatures (T_C) for silicides, i.e., the respective T_Cs are 336, 225, 140, 76, and 25 K, but the germanides are antiferromagnetic (AFM) with the much lower Néel temperatures (T_N) of 47, 30, 40, 21, and 7 K, respectively. Furthermore, they found that substituting Si for Ge in Gd_5Ge_4 triggers ferromagnetism at low temperatures in the $Gd_5Si_xGe_{4-x}$ solid solution.[4]

Since the discovery of the giant magnetocaloric effect (GMCE) in $Gd_5Si_2Ge_2$, which is strongly correlated with a first-order magneto-structural transition around room temperature[5], the $R_5Si_xGe_{4-x}$ systems (R = rare earth element) have been extensively studied to uncover the mechanism of the extraordinary magneto-responsive properties including the giant magnetoresistance (GMR) and colossal magnetostriction (CMR) as well as GMCE.[6,7,8] The phase relationships and crystallography in the $Gd_5Si_xGe_{4-x}$ system were reported by Pecharsky and Gschneidner[9] who identified three structurally distinct phase regions: Gd_5Si_4-type orthorhombic ($2 < x \leq 4$), Sm_5Ge_4-type orthorhombic ($0 < x \leq 0.8$), and $Gd_5Si_2Ge_2$-

type monoclinically distorted derivative of the orthorhombic structures ($0.96 \leq x \leq 2$). Subsequent studies show that these three solid solution alloys exhibit quite different magnetic behaviors.[8,10] In contrast to the crystallographic description reported by Smith *et al.*[3], Gd_5Si_4 and Gd_5Ge_4 can be better described as formed by pseudo two-dimensional ~7 Å thick slabs that are arranged differently in terms of bonding between the slabs rather than stacking of monolayers.[11,12] All of the slabs, half of them, or none of the slabs are interconnected via short T_2 dimers (T= Si and/or Ge) for the Gd_5Si_4-type, the $Gd_5Si_2Ge_2$-type, and the Gd_5Ge_4-type structures, respectively, e.g. see Fig. 1 in Refs. 8 and 13. Interesting physical properties of $Gd_5Si_xGe_{4-x}$ are strongly correlated with the magneto-structural transitions that are characterized by reversible breaking and reforming of the inter-slab T_2 bonds, which can be controlled by chemical composition, magnetic field, temperature, and pressure. While the inter-slab bonding differences are preserved in the paramagnetic or antiferromagnetic states depending on the crystal structure type, all of the slabs are always interconnected via the T_2 dimers in the ferromagnetic state, see Fig. 2 in Ref. 8.

Until now, the crystallography and phase relationships have been investigated for more than a half of possible $R_5Si_xGe_{4-x}$ pseudobinary systems (R = La[14], Pr[15], Nd[14,16], Gd[17], Tb[18], Dy[14], Er[19], Yb[20], Lu[14], and Y[21]). Still, there are other $R_5Si_xGe_{4-x}$ systems (R = Ce, Sm, Eu, Ho, and Tm) that have not been studied. The 5:4 phases (R_5Si_4 or R_5Ge_4) have not been reported for R = Pm since it is radioactive with the longest half-life of 14 years, and they do not form for R = Eu. For other rare earth metals (R = Ce[3,22,23,24], Sm[1,2,3], Ho[3,25,26], and Tm[3,27]) only the binary compounds have been reported with the exception of the ternary $Ho_5Si_2Ge_2$ compound[28]. Here, we report on the phase relationships, the crystal structures, and the magnetic and thermodynamic properties of several pseudobinary alloys in the $Sm_5Si_xGe_{4-x}$ system.

Experiment

A total of five alloys in the $Sm_5Si_xGe_{4-x}$ system with x varying from 0 to 4 were synthesized by induction melting at ~1800 °C for 10 min in sealed Ta crucibles. Prior to

induction melting, stoichiometric mixtures of the pure components (Sm, Si, and Ge) were loaded into Ta crucibles, and then the crucibles were sealed under a pure helium atmosphere by arc welding in order to avoid the loss of samarium due to its low boiling temperature (~ 1800 °C). The Sm metal was prepared by the Materials Preparation Center of the Ames Laboratory[29] and it was 99.5 at.% pure with major impurities in ppm atomic as follows: F – 1040, Ca – 900, O – 864, C – 125, Cl – 110, Mg – 77, N – 32, Zn – 30, Fe – 27, and Yb – 20. The silicon and germanium, which were purchased from a commercial vendor, were 99.999 wt. % pure. All alloys were investigated in the as-cast condition without additional heat treatment.

The room temperature x-ray powder diffraction was utilized to characterize the crystal structures and phase compositions of the $Sm_5Si_xGe_{4-x}$ alloys. The room temperature x-ray powder diffraction studies were performed on an automated Scintag powder diffractometer using Cu-K_α radiation. The crystal structures were refined by using full profile Rietveld refinement technique at room temperature.[30] Moreover, *in-situ* x-ray powder diffraction measurements of $Sm_5Si_2Ge_2$ were carried out as a function of temperature between 8 and 300 K both on cooling and on heating in a zero magnetic field on a Rigaku TTRAX rotating anode powder diffractometer employing Mo-K_α radiation. The sample preparation, instrument setup, and the refinement method employed to process the *in-situ* x-ray powder diffraction data were the same as in Refs. 31, 32, and 33. The profile residuals were between 7 and 9 %, and derived Bragg residuals were between 3 and 5 %.

Magnetic measurements were performed on a SQUID magnetometer (model MPMS XL). The magnetization was measured as a function of temperature from 1.8 to 300 K in 0.05 T, 0.5 T, and 5 T dc magnetic fields. Isothermal magnetization data were collected only around the magnetic ordering temperatures of the alloys in dc magnetic fields varying from 0 to 7 T with 0.2 T steps. The heat capacity of the $Sm_5Si_xGe_{4-x}$ alloys was measured using an adiabatic heat-pulse calorimeter [34] from ~3.5 to 350 K in dc magnetic fields ranging from 0 to 10 T.

Results and discussion

Phase relationships and crystallography

As mentioned above, the crystal structure in the paramagnetic (PM) state in the $R_5Si_xGe_{4-x}$ systems is a critical parameter that usually defines physical properties of individual alloys, especially their magnetism. When non-bonded slabs are present in the PM state, these generally become interconnected via short T_2 dimers at or below the magnetic ordering temperature that may occur as first-order magnetic - structural phase transformations. The magnetic phase transitions, if any, are normally second-order when all slabs are connected in the PM state.

The room temperature x-ray powder diffraction measurements were performed for all five alloys in the $Sm_5Si_xGe_{4-x}$ systems in order to investigate their crystallography and phase purity in the PM state. The room temperature crystallographic data including the structure type and lattice parameters are given in Table 1 and the coordinates of atoms in Table 2. Figures 1 and 2 show the observed and calculated powder diffraction patterns of the five alloys. $Sm_5Si_2Ge_2$ and Sm_5Ge_4 are nearly single phase materials (~98 at. % pure or greater) , but there were small amounts of the 5:3 impurity phase in Sm_5Si_4, Sm_5Si_3Ge, and Sm_5SiGe_3; the concentration levels were 5.7, 7.6, and 4.6 wt. %, respectively, as determined from the Rietveld refinements. The lattice parameters as a function of Si content, x(Si), are shown in Fig. 3. In the $R_5Si_xGe_{4-x}$ systems, all lattice parameters generally decrease with the replacement of Ge by Si because of the smaller atomic radius of Si. In the $Sm_5Si_xGe_{4-x}$ system, there are small discontinuous changes in the *b* and *c* lattice parameters coinciding with the structural changes from the Sm_5Ge_4-type to the $Gd_5Si_2Ge_2$-type and the Gd_5Si_4-type structures, but the greatest change occurs in the lattice parameter *a*. This is similar to the $Gd_5Si_xGe_{4-x}$ system, which exhibits the same phase sequence when Si is substituted for Ge.

Table 1. Room temperature crystallographic data of $Sm_5Si_xGe_{4-x}$ alloys.

Composition	Structure type	Unit cell dimensions			Distance d_{T3-T3}, Å	Reference
		a, Å	b, Å	c, Å		
Sm_5Si_4	Gd_5Si_4	7.5738(7)	14.890(1)	7.8156(7)	2.745(2)	This work
Sm_5Si_4	Sm_5Ge_4	7.57	14.88	7.78	-	3
Sm_5Si_3Ge	Gd_5Si_4	7.5858(6)	14.911(1)	7.8440(6)	2.722(2)	This work
$Sm_5Si_2Ge_2$[a]	$Gd_5Si_2Ge_2$	7.6716(7)	14.945(2)	7.8543(8)	3.821(4)[b] 2.831(3)[b]	This work
Sm_5SiGe_3	Sm_5Ge_4	7.7492(5)	14.927(1)	7.8414(6)	3.733(2)	This work
Sm_5Ge_4	Sm_5Ge_4	7.7726(6)	14.947(1)	7.8611(6)	3.754(3)	This work
Sm_5Ge_4	Sm_5Ge_4	7.75	14.94	7.84	3.71(2)	2

[a] γ is 93.344(5)° in the monoclinic structure (space group $P112_1/a$).

[b] There are two kinds of T3-T3 distances in the monoclinic structure; long T3a-T3a and short T3b-T3b distances.

Lattice parameters in the known binary 5:4 rare earth silicides, germanides, and ternary $R_5Si_xGe_{4-x}$ compounds with the same crystal structure (except for Yb_5Ge_4) are plotted as a function of the atomic number of the rare earth element in Fig. 4. The Sm ions in some compounds may have divalent, or trivalent, or mixed valent state, but in the $Sm_5Si_xGe_{4-x}$ system the Sm ion appears to be trivalent because their lattice parameters follow the normal lanthanide contraction with the increasing atomic number.

Table 2. Atomic coordinates and T-site occupancies of $Sm_5Si_xGe_{4-x}$ compounds.

Compound	Atom/site	x/a	y/b	z/c	g (%)[a]
Sm_5Si_4	Sm1 in 4(c)	0.3574(9)	1/4	0.0104(6)	
	Sm2 in 8(d)	0.0311(5)	0.0972(2)	0.1750(6)	
	Sm3 in 8(d)	0.3151(4)	0.8766(2)	0.1866(5)	
	Si1 in 4(c)	0.225(1)	1/4	0.342(3)	100
	Si2 in 4(c)	0.001(3)	1/4	0.926(3)	100
	Si3 in 8(d)	0.146(3)	0.947(1)	0.479(3)	100
Sm_5Si_3Ge	Sm1 in 4(c)	0.3507(8)	1/4	0.0096(7)	
	Sm2 in 8(d)	0.0258(5)	0.0967(2)	0.1792(5)	
	Sm3 in 8(d)	0.3161(4)	0.8781(2)	0.1828(5)	
	T1 in 4(c)	0.223(2)	1/4	0.339(2)	41.2[b]
	T2 in 4(c)	0.997(3)	1/4	0.925(3)	82[b]
	T3 in 8(d)	0.187(2)	0.962(1)	0.484(2)	66.4[b]
$Sm_5Si_2Ge_2$	Sm1 in 4(e)	0.3211(1)	0.2544(6)	-0.0066(9)	
	Sm2a in 4(e)	-0.0117(9)	0.0986(5)	0.1729(1)	
	Sm2b in 4(e)	0.0116(1)	0.4009(5)	0.1935(1)	
	Sm3a in 4(e)	0.3645(1)	0.8850(5)	0.1630(1)	
	Sm3b in 4(e)	0.3320(1)	0.6221(5)	0.1788(1)	
	T1 in 4(e)	0.198(3)	0.247(2)	0.366(3)	50[c]
	T2 in 4(e)	0.943(3)	0.256(2)	0.908(2)	50[c]
	T3a in 4(e)	0.228(3)	0.956(1)	0.479(3)	50[c]

	T3b in 4(e)	0.150(3)	0.558(1)	0.475(3)	50[b]
Sm_5SiGe_3	Sm1 in 4(c)	0.2883(7)	1/4	0.0002(7)	
	Sm2 in 8(d)	-0.0215(4)	0.0998(2)	0.1817(5)	
	Sm3 in 8(d)	0.3803(4)	0.8841(2)	0.1633(4)	
	T1 in 4(c)	0.173(1)	1/4	0.370(2)	25[c]
	T2 in 4(c)	0.915(2)	1/4	0.898(1)	25[c]
	T3 in 8(d)	0.221(1)	0.953(4)	0.469(1)	25[c]
Sm_5Ge_4	Sm1 in 4(c)	0.2909(7)	1/4	0.0011(6)	
	Sm2 in 8(d)	-0.0187(4)	0.1000(2)	0.1862(5)	
	Sm3 in 8(d)	0.3808(4)	0.8853(2)	0.1647(4)	
	Ge1 in 4(c)	0.178(1)	1/4	0.362(1)	100
	Ge2 in 4(c)	0.929(2)	1/4	0.905(1)	100
	Ge3 in 8(d)	0.222(1)	0.952(1)	0.474(1)	100

[a] Occupancy by the Si atoms with the remainder occupied by the Ge atoms except for Sm_5Ge_4, where the value is for the site occupancies by the Ge atoms.

[b] Occupancies of the T sites have been refined with the only imposed constraint that each site has 100 % overall occupancy.

[c] The actual occupancies were not refined – they were assigned based on the as-prepared stoichiometry assuming completely random distribution of the Si and Ge atoms.

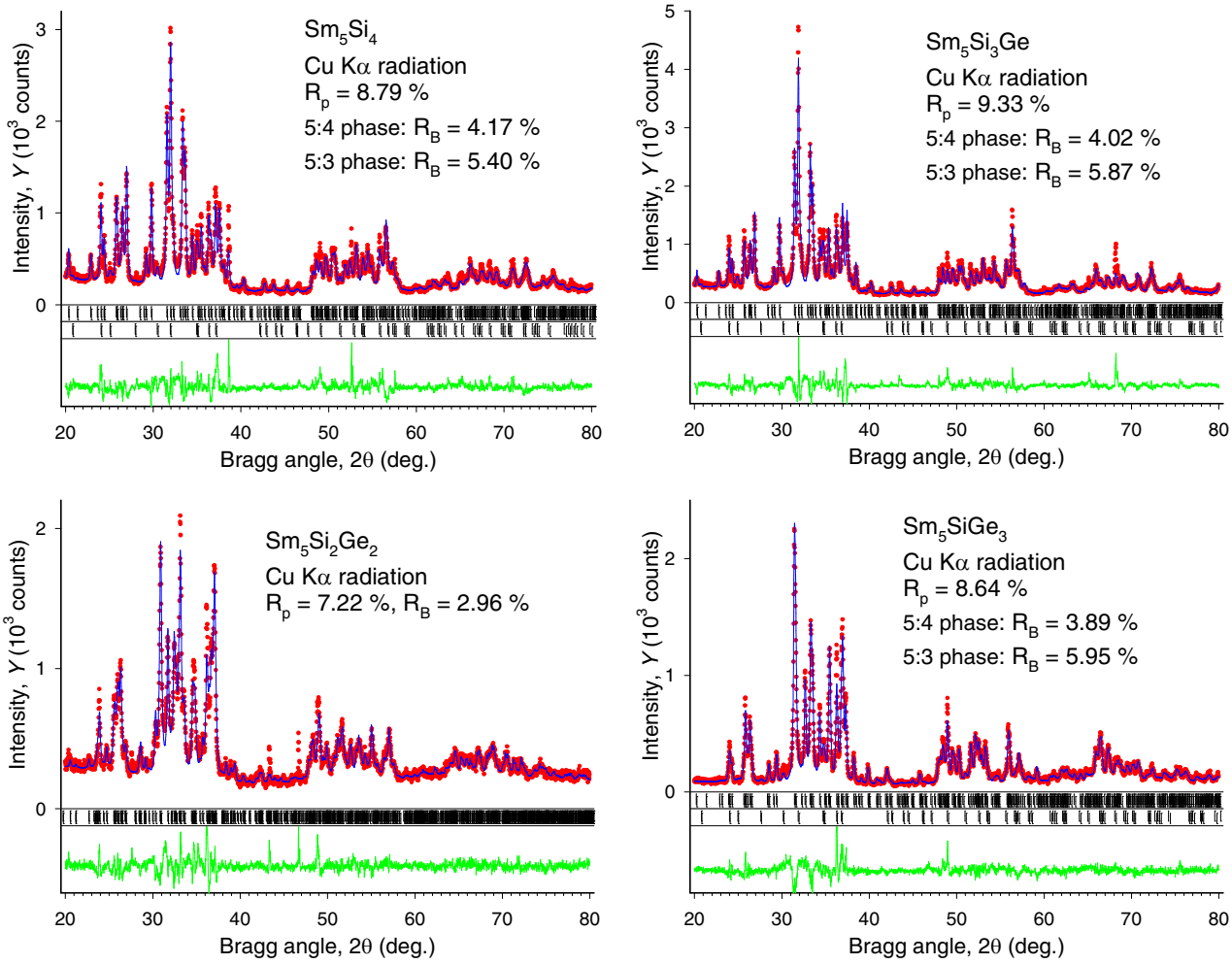

Fig. 1. The observed (dots) and calculated (lines drawn through the data points) powder diffraction patterns of Sm_5Si_4, Sm_5Si_3Ge, $Sm_5Si_2Ge_2$, and Sm_5SiGe_3 after the completion of Rietveld refinements. The upper sets of vertical bars located just below the plots of the observed and calculated intensities indicate the calculated positions of the Bragg peaks of the majority 5:4 phase, while the lower sets of bars correspond to the calculated positions of the Bragg peaks of the 5:3 impurity. The differences, $Y_{obs} - Y_{calc}$, are shown at the bottom of the plot.

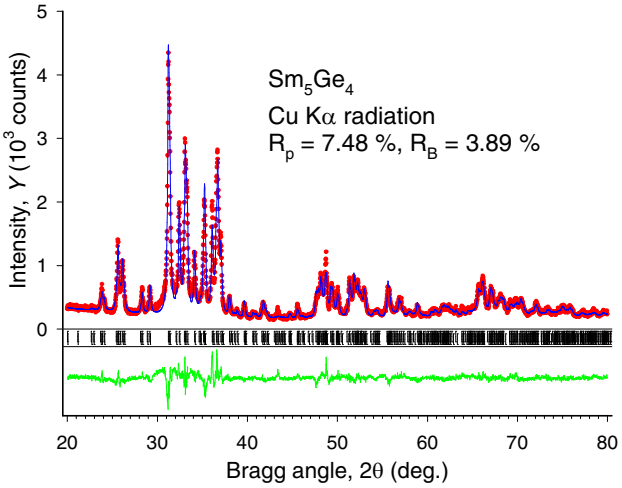

Fig. 2. The observed (dots) and calculated (lines drawn through the data points) powder diffraction pattern of Sm_5Ge_4 after the completion of Rietveld refinements. The calculated positions of the Bragg peaks are shown as vertical bars just below the plots of the observed and calculated intensities. The differences, $Y_{obs} - Y_{calc}$, are shown at the bottom of the plot.

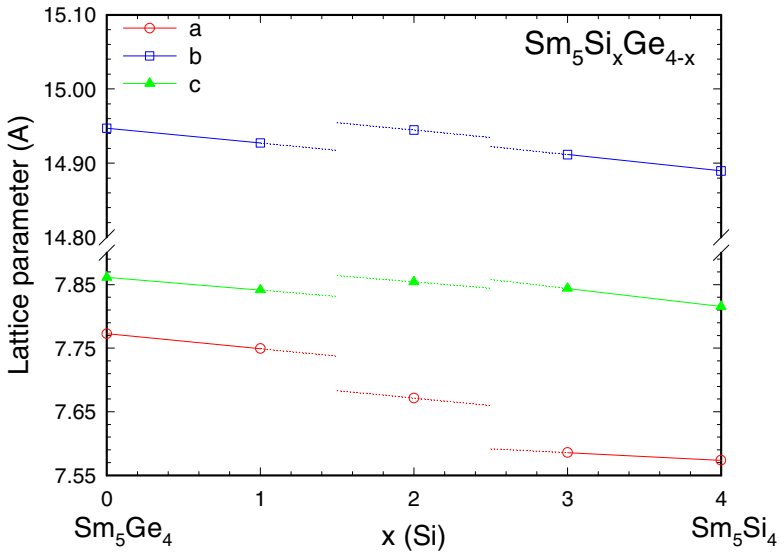

Fig. 3. Lattice parameters as a function of x in the $Sm_5Si_xGe_{4-x}$ system. Sm_5Ge_4 and Sm_5SiGe_3 have the Sm_5Ge_4-type structure; $Sm_5Si_2Ge_2$ has the $Gd_5Si_2Ge_2$-type structure; and Sm_5Si_3Ge and Sm_5Si_4 have the Gd_5Si_4-type structure.

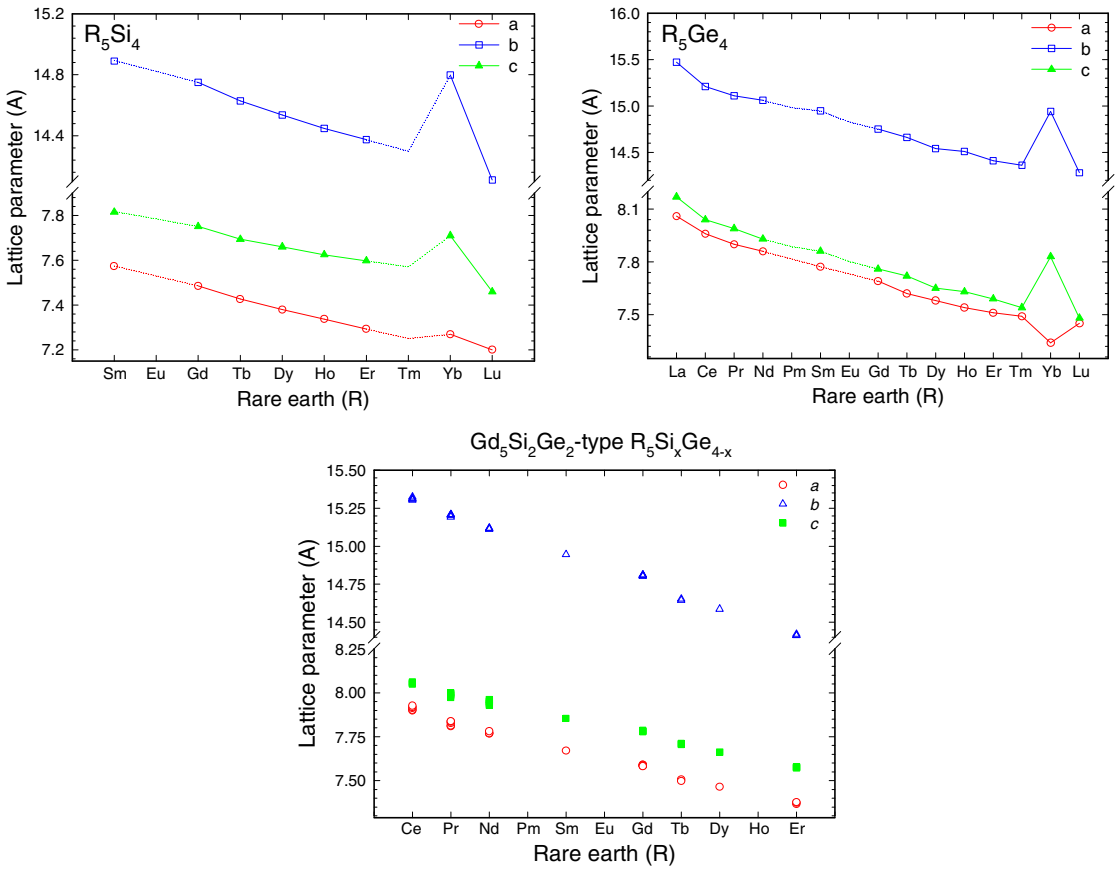

Fig. 4. The unit cell parameters of the isostructural R_5Si_4 (Gd_5Si_4-type structure), R_5Ge_4 (Sm_5Ge_4-type structure), and $R_5Si_xGe_{4-x}$ ($Gd_5Si_2Ge_2$-type structure), except for Yb_5Ge_4 which has the Gd_5Si_4-type structure, are plotted as a function of the atomic number.

Magnetic properties

The isofield magnetization as a function of temperature and the isothermal magnetization as a function of magnetic field were measured to characterize the type of magnetic ordering and to derive the magnetic ordering transition temperatures, the effective magnetic moments, and the ordered magnetic moments.

The free-trivalent Sm ion has five *4f* electrons ($L = 5$ and $S = 5/2$) and in a solid the ^6H levels are split by the spin-orbit interaction into the ground state $^6H_{5/2}$, the excited states $^6H_{7/2}$,

$^6H_{9/2}$ ... $^6H_{15/2}$ J multiplets.[35] The consecutive multiplet energy interval between the ground state ($^6H_{5/2}$) and the first excited state ($^6H_{7/2}$) is only ~ 930 cm^{-1}, so that temperature-independent term of the Van Vleck type are expected to contribute and thus the Van Vleck theory includes a second term (Van Vleck term) which is especially important for Sm and Eu ions but is negligible for the last half of the rare earth group.[36] Therefore, in contrast to other lanthanide compounds apart from Eu, the temperature-independent Van Vleck term of Sm compounds plays a major role in the magnetic susceptibility because of the varying population of the excited levels and second-order Zeeman splitting. Normally, the Curie part of the susceptibility in Sm compounds is considerably smaller compared to other lanthanide compounds because the g_J (Landé splitting factor) of the ground state ($J = 5/2$) is only 2/7. Thus, in principle, in the calculation of the susceptibility of the metallic compounds containing Sm^{3+} ions, there are various factors to be considered: the crystalline electric field (CEF) splitting of a ground state and the low level exicted states of the *J* multiplet, Ruderman-Kittel-Kasuya-Yosida (RKKY) interaction, the Van Vleck transition between different *J* multiplets which are caused both by the applied magnetic field and by the exchange fields, the effect of conduction-electron polarization due to *4f* moments, and the thermal population of higher-lying *J* multiplets. With the consideration of these factors, the susceptibility calculation of metallic tri-positive Sm compounds has been reported by several groups.[36,37,38,39,40] Stewart[39] reported that when only the conduction-electron polarization, interionic Heisenberg exchange interaction, and the thermally populated admixture of the $^6H_{7/2}$ into the $^6H_{5/2}$ state are taken into account, the susceptibility $\chi(T)$ can be well described by a simple form $\chi(T) = \chi_0 + C/(T - \theta_p)$ without considering the CEF splitting, where χ_0 is the temperature-independent Van Vleck term, *C* is the Curie-Weiss constant, *T* is the absolute temperature, and θ_p is the paramagnetic Curie temperature.

The dc magnetic susceptibilities of $Sm_5Si_xGe_{4-x}$ alloys are shown in Figs. 5 and 6. Irrespective of the dc magnetic fields, including 0.5 T and 5 T data, the magnetic susceptibilities of Sm_5Si_4, Sm_5Si_3Ge, and $Sm_5Si_2Ge_2$ shown in Fig. 5 exhibit a broad maximum around the magnetic ordering temperature, and then decrease with the decreasing temperature showing nearly constant dc magnetic susceptibilities below ~ 50 K. This

behavior mimics ferrimagnetic arrangements of spins, but different temperature dependencies of spin and orbital magnetic moments arising from ferromagnetically aligned Sm^{3+} ions may also induce such behavior.[41,42,43,44] On the other hand, both Sm_5SiGe_3 and Sm_5Ge_4 seem to order antiferromagnetically around 90 K, but there are upturns in dc magnetic susceptibilities below ~ 50 K, which are uncommon for a conventional AFM, see Fig. 6.

The isothermal magnetization data measured just below the magnetic ordering temperatures that are shown in Figs. 7 b), d), and f) confirm that Sm_5Si_4, Sm_5Si_3Ge, and $Sm_5Si_2Ge_2$ order ferromagnetically with low saturation magnetization (M_S) value, but with a substantial coercivity (H_C), and hysteresis. At 1.8 K, none of the compounds approaches saturation and exhibits narrower hystereses. On the other hand, the isothermal magnetizations of the Ge-rich compounds measured at 80 K and seen in Fig. 7 h) and j) are nearly linear functions of the magnetic field between 0 and 7 T; this behavior changes little at 1.8 K. The magnetic behavior in the $Sm_5Si_xGe_{4-x}$ system is consistent with other $R_5Si_xGe_{4-x}$ systems where the ferromagnetic or ferromagnetic-like ground state is found in Si-rich alloys changing over to the AFM state for Ge-rich alloys. The dc magnetic susceptibility of $Sm_5Si_2Ge_2$ in the field-cooled (FC) cooling regime does not match that in the zero-field-cooled (ZFC) heating regime around the magnetic ordering temperature exhibiting a Curie temperature difference of ~ 10 K between the heating and cooling branches, which is consistent with a first-order magnetic phase transition. There is no measurable hysteresis of T_C in Sm_5Si_4 and Sm_5Si_3Ge nor is there a hysteretic behavior around T_N in Sm_5SiGe_3 and Sm_5Ge_4, which is consistent with second-order magnetic phase transitions. Moreover, the Sm_5Ge_4-type compounds show no magneto-structural features despite the absence of the interslab T_2 bonds in the PM state.

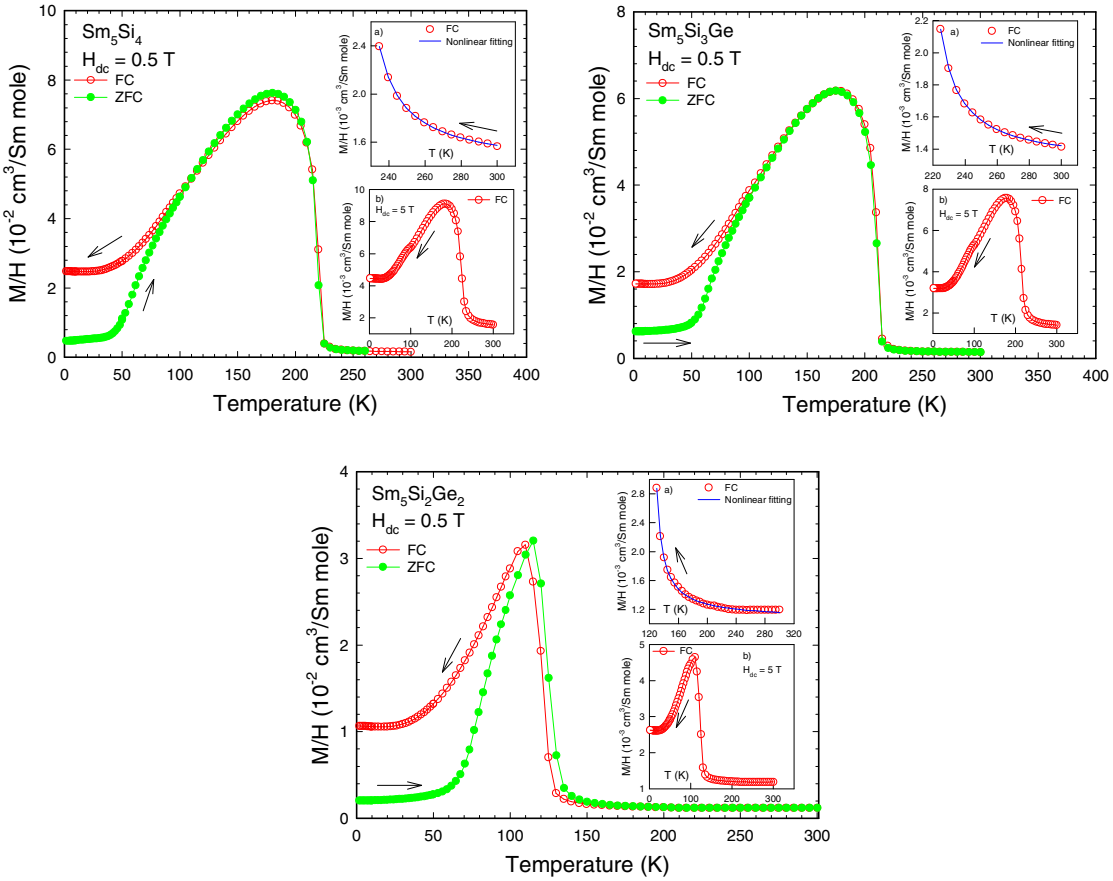

Fig. 5. The dc magnetic susceptibilities of Sm_5Si_4, Sm_5Si_3Ge, and $Sm_5Si_2Ge_2$ measured in dc magnetic field of 0.5 T. Insets a) and b) show the nonlinear fittings in the paramagnetic regime above the Curie temperature, and the dc magnetic susceptibilities in a 5 T magnetic field, respectively.

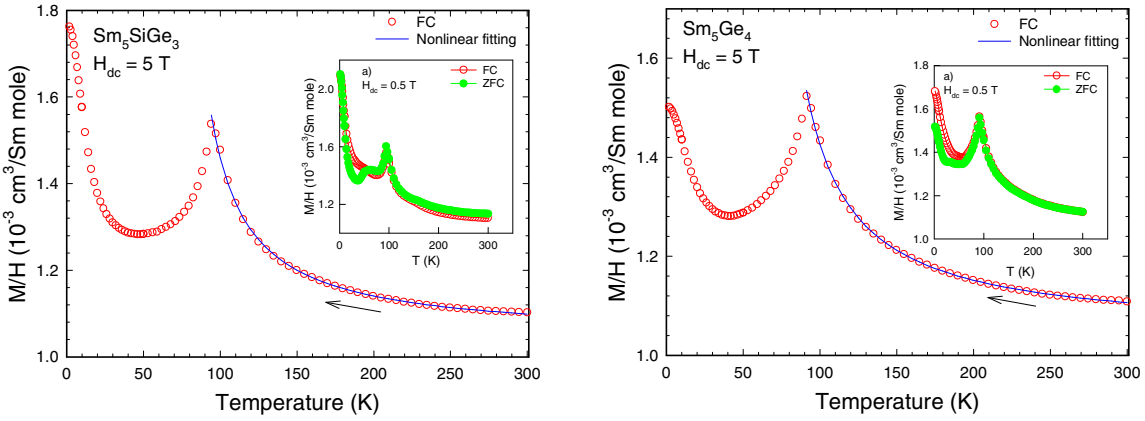

Fig. 6. The dc magnetic susceptibilities of Sm_5SiGe_3 and Sm_5Ge_4 measured in a dc magnetic field of 5 T. Inset a) shows the dc magnetic susceptibilities measured in a 0.5 T magnetic field.

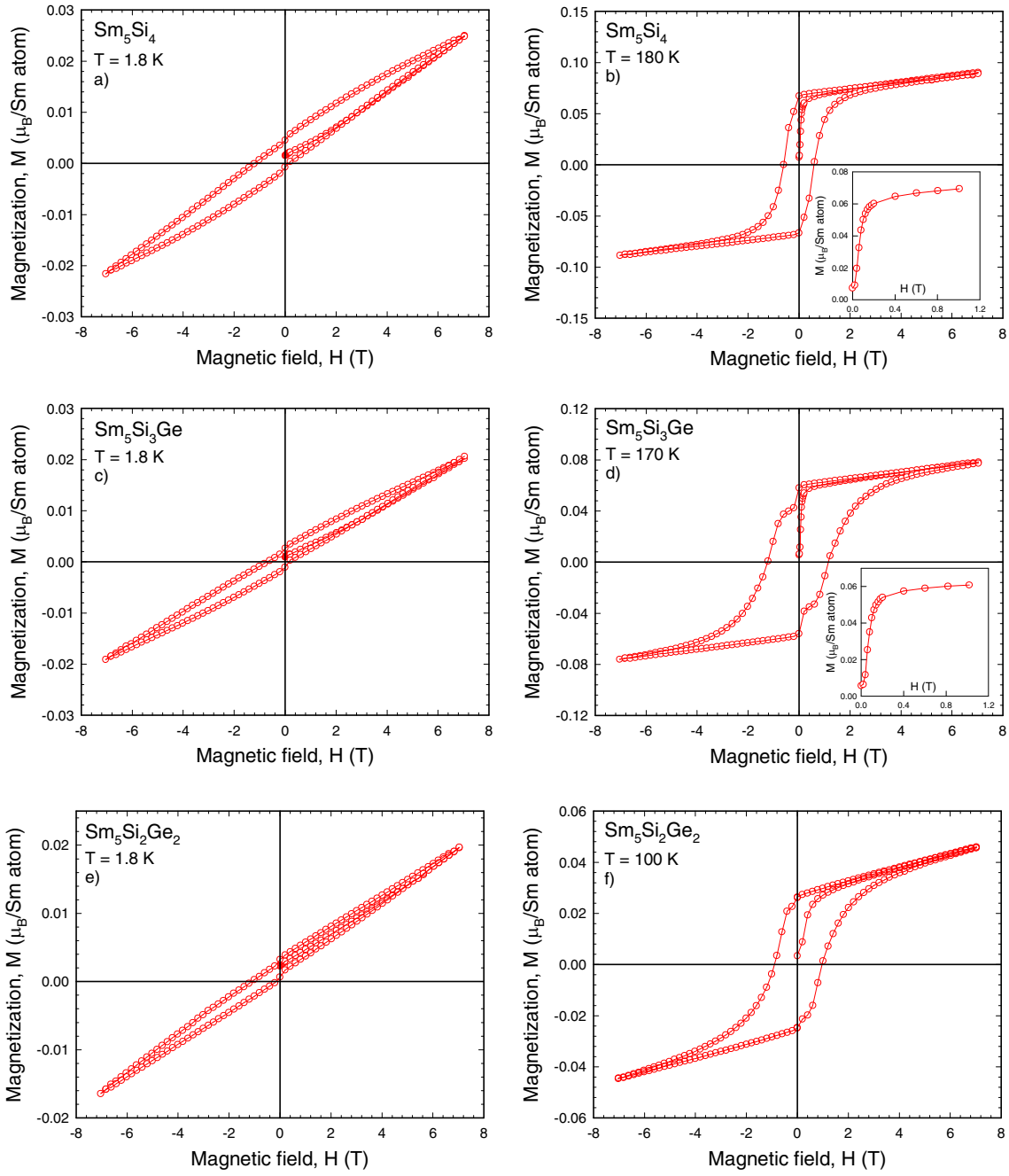

Fig. 7. Magnetization as a function of magnetic field measured at 1.8 K and a few Kelvin below the magnetic phase transition temperatures for a) and b) Sm_5Si_4, c) and d) Sm_5Si_3Ge, e) and f) $Sm_5Si_2Ge_2$. Insets in b) and d) show initial magnetizations in magnetic fields between 0 and 1 T.

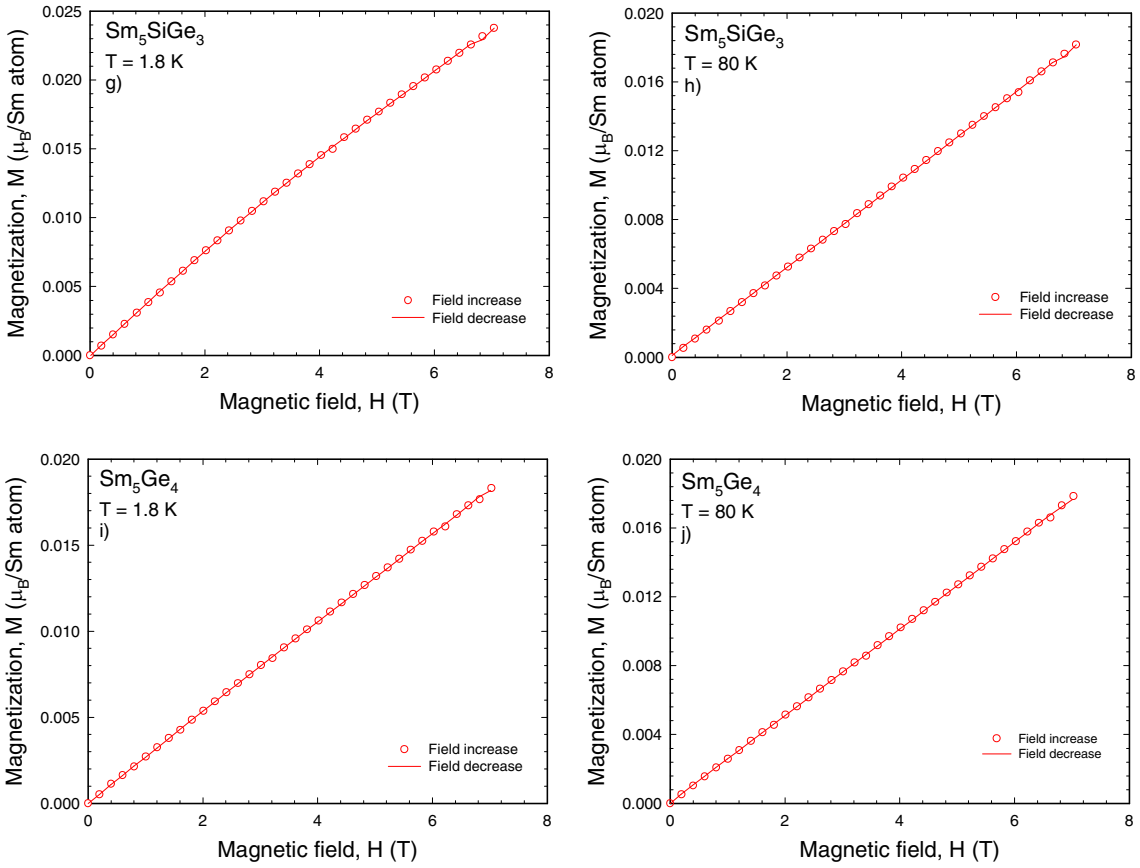

Fig. 7. Magnetization as a function of magnetic field measured at 1.8 K and a few Kelvin below the magnetic phase transition temperatures for g) and h) Sm_5SiGe_3, i) and j) Sm_5Ge_4.

As mentioned above, the dc magnetic susceptibilities of these compounds in paramagnetic states cannot be described by a simple Curie-Weiss law because of the nonlinearity of $1/\chi$ above the magnetic ordering temperature, but they can be well fitted by the modified Curie-Weiss law $\chi(T) = \chi_0 + C/(T-\theta_p)$ without considering CEF splitting, where χ_0 is the temperature-independent Van Vleck term due to the admixture of the first excited angular momentum state (J = 7/2) to the unperturbed ground state (J = 5/2) when either a magnetic field is applied or a temperature is high enough to allow thermal population, and $C/(T-\theta_p)$ is the Curie-Weiss term arising from the ground state (J = 5/2). Especially, in the case of tri-positive Sm compounds,

$\chi(T) = \chi_0 + C/(T-\theta_p) = \left(\frac{N_A}{k_B}\right)\left[\alpha_J \mu_B^2 + \frac{\mu_{eff}^2}{3(T-\theta_p)}\right]$ can be derived, where N_A is Avogadro's number, k_B is Boltzmann constant, μ_B is the Bohr magneton, μ_{eff} is the effective magnetic moment, θ_p is the paramagnetic Curie temperature, and α_J =

$$k_B\left\{\frac{(J^2-(L-S)^2)((L+S+1)^2-J^2)}{6J(2J+1)(E_{J-1}-E_J)} + \frac{((J+1)^2-(L-S)^2)((L+S+1)^2-(J+1)^2)}{6(J+1)(2J+1)(E_{J+1}-E_J)}\right\}$$ is

$20/7\Delta$, where Δ is the energy separation (expressed in units of K) between J = 7/2 and J = 5/2 states.[45] Thus, the best fitting parameters Δ, μ_{eff}, and θ_p extracted from the nonlinear least square fits of the dc magnetic susceptibilities are listed in Table 3 along with other basic magnetic quantities. The root mean square (rms) errors for nonlinear fittings were less than 0.7 % except for $Sm_5Si_2Ge_2$ where they were 3 %. The Van Vleck terms χ_0 in the $Sm_5Si_xGe_{4-x}$ system range between 1.04 x 10^{-3} cm^3/Sm mole for Sm_5Ge_4 and 1.38 x 10^{-3} cm^3/Sm mole for Sm_5Si_4, which compares well with the value of 1.18 x 10^{-3} cm^3/mole obtained in Ref. 39 for the rhombohedral Sm metal.

Even though both Sm_5SiGe_3 and Sm_5Ge_4 are likely to have an AFM ground state, their paramagnetic Curie temperatures, θ_P, are positive (70 and 60 K, respectively), which is one of the most unusual features of all of the other AFM R_5Ge_4 compounds studied to date (i.e., θ_P=94 K for R=Gd, 80 K for Tb, 43 K for Dy, 16 K for Ho, and 10 K for Er).[4] The effective magnetic moments of the $Sm_5Si_xGe_{4-x}$ alloys range between 0.29 and 0.36 μ_B/Sm atom, which is considerably smaller than the theoretical effective magnetic moment of the free Sm^{3+} ion (0.85 μ_B/Sm atom), while Δ ranges between 776 K and 1030 K; all are lower than ~ 1350 K estimated for free Sm^{3+} ions.[36] The reduced effective magnetic moments in the $Sm_5Si_xGe_{4-x}$ alloys are probably due to the effect of CEF splittings of the Hund's rule ground

state because crystal fields can also admix the ground and excited levels and thus affect the magnetic susceptibility. The low Δ values have been reported for other Sm-based compounds.[46,47]

Table 3. The magnetic properties of $Sm_5Si_xGe_{4-x}$ compounds.

Composition	T_C (K)[a]	Θ_P (K)	μ_{eff} (μ_B)	$\mu_{at\ 1.8\ K}$ (μ_B)[c]	$\mu_{at\ \sim\ Tc}$ (μ_B)[d]	χ_0 (10^{-3} cm^3/Sm mole)	Δ (K)
Sm_5Si_4	220	220(2)	0.34(2)	0.025	0.1	1.38	776
Sm_5Si_3Ge	210	212(3)	0.29(1)	0.02	0.08	1.30	824
$Sm_5Si_2Ge_2$	125	120(2)	0.36(3)	0.02	0.05	1.07	1000
Sm_5SiGe_3	90[b]	70(1)	0.31(2)	0.024	0.018	1.04	1030
Sm_5Ge_4	90[b]	60(2)	0.35(3)	0.018	0.018	1.04	1030

[a] T_C or T_N from the C_P measurement

[b] Néel temperature (T_N).

[c] The magnetic moment per Sm atom in the magnetic field of 7 T at T = 1.8 K.

[d] The magnetic moment per Sm atom in the magnetic field of 7 T between 10 and 40 K below the magnetic transition temperature.

The magnetization values around the Curie temperatures for Sm_5Si_4, Sm_5Si_3Ge, and $Sm_5Si_2Ge_2$ are ~ 0.091, 0.076, and 0.046 μ_B/Sm atom, respectively, obtained in the maximum field of our apparatus (7 T), which are only ~12.8, 10.7, and 6.5 % of the theoretical value of the saturation magnetization $M_{sat} = g_J J \mu_B = 0.71\ \mu_B$/Sm atom. The possible causes for the low saturation magnetization values at high magnetic fields are the magnetic anisotropy, second-order Zeeman effects, and CEF. Interestingly, high coercive fields H_C of ~ 0.7, 1.4, and 1 T are observed in the close proximity of T_C for Sm_5Si_4, Sm_5Si_3Ge, and $Sm_5Si_2Ge_2$, respectively, see Fig. 7. Moreover, the paramagnetic Curie temperature of Sm_5Si_4 is approximately two times higher than the expected temperature estimated from the de Gennes scaling (Fig. 8).

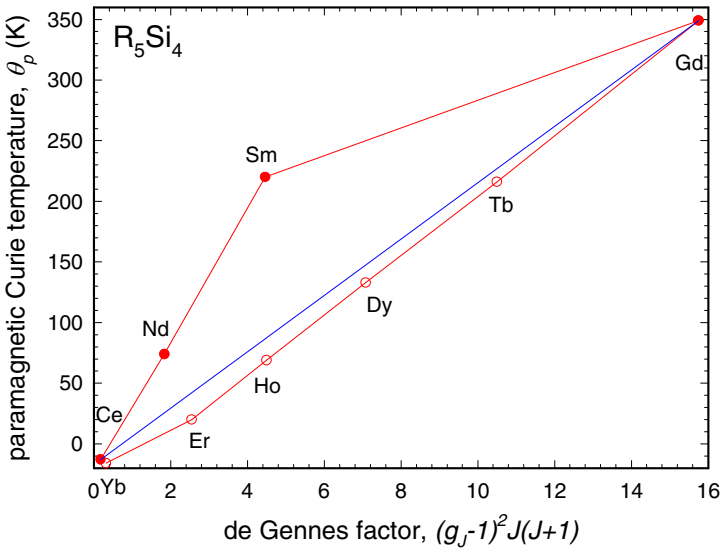

Fig. 8. The paramagnetic Curie temperatures, θ_p, as a function of de Gennes factor for R_5Si_4 compounds. Blue solid line is θ_ps estimated from the de Gennes scaling for light rare earth metals.

Heat capacity

The heat capacity (C_P) data of all alloys in the $Sm_5Si_xGe_{4-x}$ system are shown as a function of temperature between ~ 3.5 K and 350 K in magnetic fields of 0 and 10 T in Figs. 9. The peak shapes of C_P for Sm_5Si_4, Sm_5Si_3Ge, Sm_5SiGe_3, and Sm_5Ge_4 at either T_C or T_N have the typical lamda shape of a material which exhibits a second-order magnetic transformation, but that for $Sm_5Si_2Ge_2$ is indicative of a first-order magnetic phase transition at T_C = 125 K. The magnetic ordering temperatures from C_P data are in good agreement with those from the dc susceptibilities. Interestingly, the C_P data for 10 T (the highest magnetic field available in our calorimeter) are nearly superimposed on those for zero magnetic field in all the alloys, that is, the external magnetic field has little to no effect on the magnetic entropy. In general, the magnetocaloric effect (MCE) as the isothermal magnetic entropy change, ΔS_{mag}, and the adiabatic temperature change, ΔT_{ad}, can be calculated from the C_P data as described by Pecharsky and Gschneidner.[48]

Since $\Delta S_{mag} = S(B,T) - S(0,T) = \int_0^T \frac{C(B,T) - C(0,T)}{T} dT$, the MCE in the $Sm_5Si_xGe_{4-x}$ system

is expected to be negligibly small because of roughly overlapping C_P data, i.e., $C(B,T) \approx C(0,T)$.

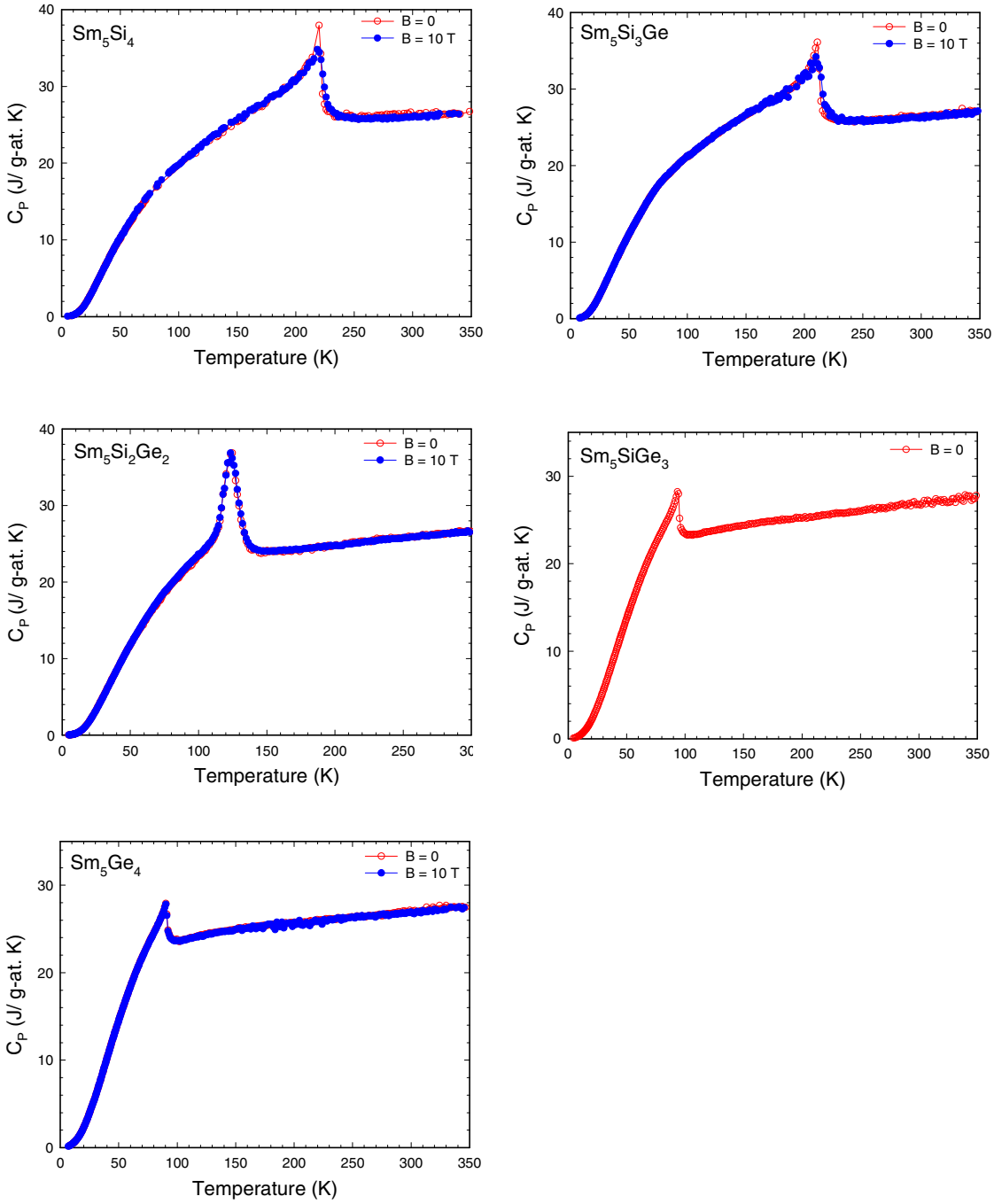

Fig. 9. The heat capacities of Sm_5Si_4, Sm_5Si_3Ge, $Sm_5Si_2Ge_2$, Sm_5SiGe_3,and Sm_5Ge_4 measured in 0 and 10 T magnetic fields during heating.

The heat capacities of non-magnetic analogs R_5Si_4, R_5Ge_4, and $R_5Si_2Ge_2$ for R = La and Lu were used to estimate the electronic and lattice contributions to the heat capacities of magnetic Sm_5Si_4, Sm_5Ge_4, and $Sm_5Si_2Ge_2$. The purely magnetic contribution to the heat capacities of Sm_5Si_4, Sm_5Ge_4, and $Sm_5Si_2Ge_2$ were obtained by subtracting the estimated electronic and lattice heat capacities of Sm phases. The molar magnetic entropies of Sm_5Si_4, Sm_5Ge_4, and $Sm_5Si_2Ge_2$ are plotted in Fig. 10. The molar magnetic entropies of Sm_5Si_4, Sm_5Ge_4, and $Sm_5Si_2Ge_2$ at ~ 350 K are 71 %, 74 %, and 71 % of the theoretical maximum molar magnetic entropy of the Sm^{3+} ion (J = 5/2) of 5Rln6, i.e., $S_{mag} = R\ln(2J+1)$ J/mol K, respectively (where R = 8.31 J/mol K is the molar gas constant). In any case the magnetic entropy should attain its full $R\ln(2J+1)$ value for 1 mole of *4f* ions at high temperature. With all the rare earths except Gd, the entropy does not reach this maximum value because of CEF splittings. Furthermore, there is a clear indication of first-order magnetostructural transition in the molar magnetic entropy of $Sm_5Si_2Ge_2$ in Fig. 10 and thus the change of entropy during the structural transformation (ΔS_{str}) can be easily estimated for $Sm_5Si_2Ge_2$. It is approximately equal to that of $Gd_5Si_2Ge_2$ (ΔS_{str} = 1.08 J/g-at. K).[49]

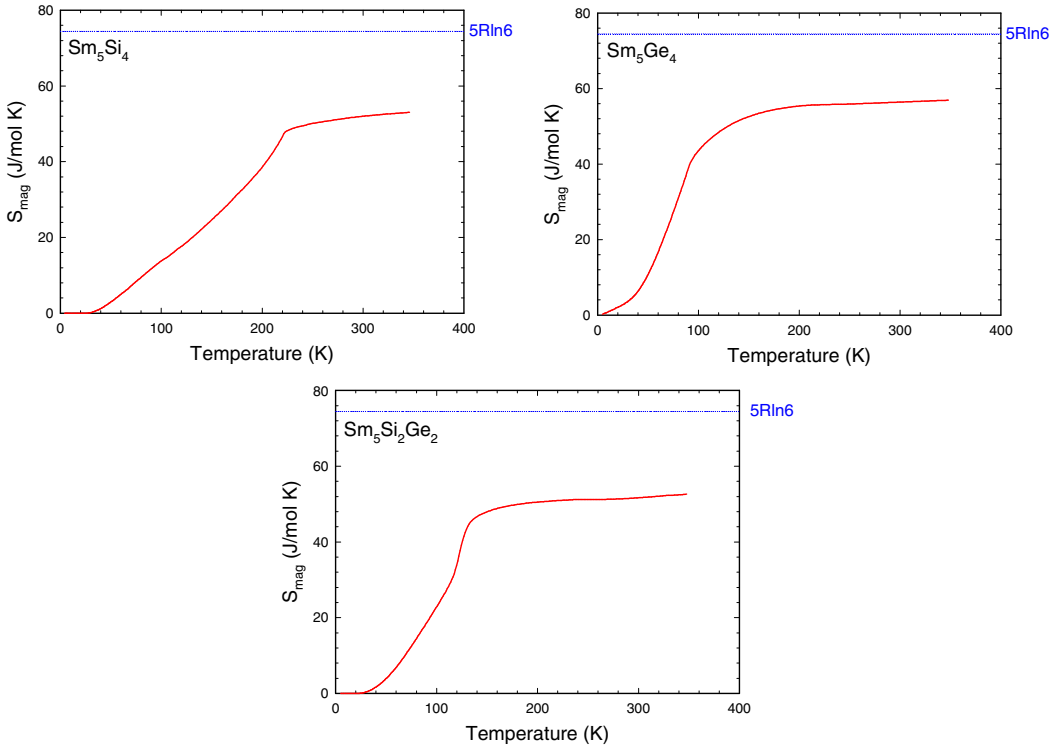

Fig. 10. The molar magnetic entropies of Sm_5Si_4, Sm_5Ge_4, and $Sm_5Si_2Ge_2$ at the zero magnetic field.

Low temperature crystallography

Since both the heat capacity and magnetization of $Sm_5Si_2Ge_2$ point to a first-order transformation, we studied the temperature dependence of the crystal structure of this compound. The crystallographic data and coordinates of atoms of low-temperature (LT) $Sm_5Si_2Ge_2$ at 8 K in a zero magnetic field, which has the Gd_5Si_4-type structure, are tabulated in Table 4. The observed x-ray powder diffraction patterns of $Sm_5Si_2Ge_2$, which were collected in a zero magnetic field during cooling from 300 K to 8 K, is shown in Fig. 11. There are distinguishable differences in the positions and intensities of Bragg peaks between the low-temperature (Gd_5Si_4-type orthorhombic structure) and high-temperature ($Gd_5Si_2Ge_2$-type monoclinic structure) patterns, which indicate that a structural phase transformation begins around ~ 115 K on cooling. These crystallographic changes are similar to those observed in $Gd_5Si_2Ge_2$[11] and $Tb_5Si_2Ge_2$[18]. The temperature dependencies of the unit cell parameters observed during the temperature-induced structural transformations are illustrated in Fig. 12 for heating and cooling in a zero magnetic field. As the temperature induces the $Gd_5Si_2Ge_2$-type to the Gd_5Si_4-type transformation around 115 K on cooling in the zero magnetic field, the unit cell volume decreases by $\Delta V/V$ = -0.48 % and the lattice parameters change by -0.63 %, -0.02 %, and -0.01 % along the *a*-, *b*-, and *c*-axes, respectively. Reverse structural transformation is completed around 125 K on heating and the unit cell volume increases by $\Delta V/V$ = +0.55 % and the lattice parameters change by +0.66 %, +0.01 %, and +0.08 % along the *a*-, *b*-, and *c*-axis, respectively. The temperature dependencies of the molar concentrations of the Gd_5Si_4-type $Sm_5Si_2Ge_2$ phase derived from the Rietveld refinement of the x-ray patterns are shown in Fig. 13. The structural transformation from the Gd_5Si_4-type to the $Gd_5Si_2Ge_2$-type on heating is nearly complete, but the transformation on cooling is incomplete. Even at 8 K, the concentration of the monoclinic $Gd_5Si_2Ge_2$-type phase amounts to ~ 40 %. A similar phenomenon was also reported in *in-situ* x-ray powder diffraction studies of Gd_5Ge_4, with ~ 6.5 % of the high temperature phase retained at low temperatures, which was explained by existence of microstructure imperfections, such as impurity and defects.[32] The $Gd_5Si_2Ge_2$-type to Gd_5Si_4-type phase transformation begins at T_{st} = ~ 115 K on cooling in a zero field, while the reverse transformation is completed at T_{st} =

~ 125 K on heating. There is a difference of ~ 10 K between the structural phase transformation on cooling and on heating in a zero magnetic field, which is consistent with that observed in the dc magnetic susceptibility in both ZFC and FC conditions for $Sm_5Si_2Ge_2$ (see Fig. 5). Moreover, T_{st} = ~ 125 K on heating is nearly equal to the Curie temperature (125 K) determined from the heat capacity peak on heating in a zero magnetic field, which confirms that there is the coupling of the magnetic and crystallographic phase transitions in $Sm_5Si_2Ge_2$.

Table 4. The Gd_5Si_4-type crystal structure of the low-temperature (LT) $Sm_5Si_2Ge_2$ at 8 K in a zero magnetic field. The space group symmetry is *Pnma*.

T = 8 K, H = 0 kOe			
LT-$Sm_5Si_2Ge_2$, a = 7.594(2), b = 14.898(3), c = 7.846(1) Å			
Atom	*x/a*	*y/b*	*z/c*
Sm1	0.3542(2)	1/4	0.0132(1)
Sm2	0.0229(9)	0.0981(3)	0.1780(1)
Sm3	0.3236(8)	0.8787(4)	0.1741(1)
T1	0.221(3)	1/4	0.349(4)
T2	0.966(4)	1/4	0.930(3)
T3	0.171(3)	0.955(1)	0.484(3)

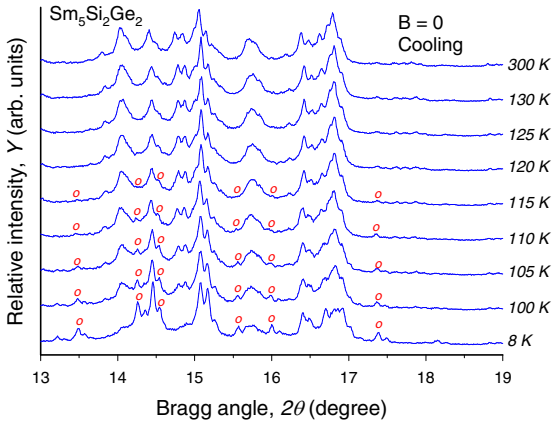

Fig. 11. The observed x-ray powder diffraction patterns of $Sm_5Si_2Ge_2$ collected in a zero magnetic field during cooling from 300 K to 8 K. All patterns were collected using Mo Kα radiation. Only the

range from 13 to 19° 2θ is shown for clarity. The letter *O* indicates selected characteristic Bragg peaks of the Gd_5Si_4-type orthorhombic phase.

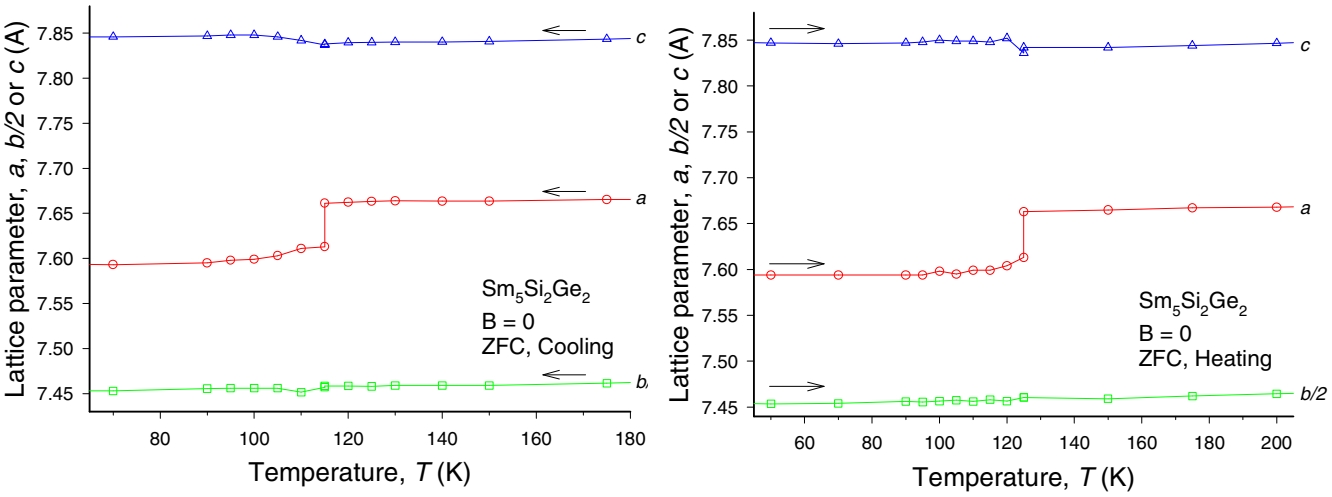

Fig. 12. Temperature dependencies of the unit cell dimensions of the major component during cooling of $Sm_5Si_2Ge_2$ (left) and during heating (right) in a zero magnetic field. The error bars are smaller than the size of symbols.

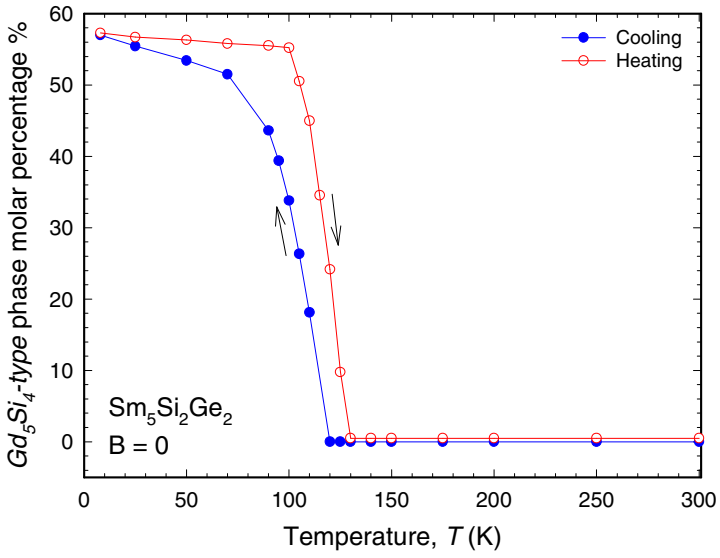

Fig. 13. The concentration of the Gd_5Si_4-type phase as a function of temperature determined from Rietveld refinement of the patterns collected during cooling and heating of $Sm_5Si_2Ge_2$ sample in a zero magnetic field.

Conclusions

In summary, there are three distinct phase regions for $Sm_5Si_xGe_{4-x}$ alloys as x varies from 0 to 4, which are the Gd_5Si_4-type, the $Gd_5Si_2Ge_2$-type, and the Sm_5Ge_4-type structure which is consistent with the $Gd_5Si_xGe_{4-x}$ system. The samarium ions in both Sm_5Si_4 and Sm_5Ge_4 compounds follow the normal lanthanide contraction rule, thus indicating that Sm ions are in the trivalent state. The dc magnetic susceptibilities for $Sm_5Si_xGe_{4-x}$ alloys can be well described with the consideration of the temperature-independent Van Vleck term because of the narrow energy separation between $J = 5/2$ and $J = 7/2$ multiplet states of Sm^{3+} ions. The reduced effective magnetic moment and saturated magnetic moment of $Sm_5Si_xGe_{4-x}$ alloys are likely due to CEF splittings. The magnetic behaviors with the replacement of Ge by Si in $Sm_5Si_xGe_{4-x}$ alloys are similar to those observed in $Gd_5Si_xGe_{4-x}$ alloys (FM for Si-rich regions, first-order FM for intermediate regions, and AFM for Ge-rich regions). Interestingly, the magnetic transition temperatures of Sm_5Si_4 (T_C = 220 K) and Sm_5Ge_4 (T_N = 90 K) are quite high. An external magnetic field of 10 T does not suppress the specific heat peaks, which are clearly of magnetic origin in the $Sm_5Si_xGe_{4-x}$ system, which is in contrast to the behaviors observed in other $R_5Si_xGe_{4-x}$ systems which are significantly affected (either reduced and broadened or shifted) by high magnetic fields. Thus, the magnetocaloric effect values are negligible in the $Sm_5Si_xGe_{4-x}$ system. *In-situ* x-ray powder diffraction measurements as a function of temperature indicate that there is a coupling of the magnetic and structural phase transitions for $Sm_5Si_2Ge_2$.

Acknowledgement

This work was supported by the Office of Basic Energy Sciences, Materials Sciences Division of the U.S. Department of Energy under contract No.DE-AC02-07CH11358 with Iowa State University.

References

[1] G. S. Smith, A. G. Tharp, and Q. Johnson, Nature **210**, 1148 (1966).

[2] G. S. Smith, Q. Johnson, and A. G. Tharp, Acta Crystallogr. **22**, 269 (1967).

[3] G. S. Smith, A. G. Tharp, and Q. Johnson, Acta Crystallogr. **22**, 940 (1967).

[4] F. Holtzberg, R. J. Gambino, and R. T. McQuire, J. Phys. Chem. Solids **28**, 2283 (1967).

[5] V. K. Pecharsky and K. A. Gschneidner, Jr., Phys. Rev. Lett. **78**, 4494 (1997).

[6] L. Morellon, P. A. Algarabel, M. R. Ibarra, J. Blasco, and B. García-Landa, Phys. Rev. B **58**, R14721 (1998).

[7] L. Morellon, J. Stankiewicz, B. García-Landa, P. A. Algarabel, and M. R. Ibarra, Appl. Phys. Lett. **73**, 3462 (1998).

[8] V. K. Pecharsky and K. A. Gschneidner, Jr., Adv. Mater. **13**, 683 (2001).

[9] V. K. Pecharsky and K. A. Gschneidner, Jr., J. Alloys Compd. **260**, 98 (1997).

[10] V. K. Pecharsky and K. A. Gschneidner, Jr., Appl. Phys. Lett. **70**, 3299 (1997).

[11] W. Choe, V. K. Pecharsky, A. O. Pecharsky, K. A. Gschneidner, Jr., V. G. Young, Jr., and G. J. Miller, Phys. Rev. Lett. **84**, 4617 (2000).

[12] V. K. Pecharsky, A. O. Pecharsky, and K. A. Gschneidner, Jr., J. Alloys Compd. **344**, 362 (2002).

[13] W. Choe, A. O. Pecharsky, M. Worle, and G. J. Miller, Inorg. Chem. **42**, 8223 (2003).

[14] K. A. Gschneidner, Jr., V. K. Pecharsky, A. O. Pecharsky, V. V. Ivtchenko, and E. M. Levin, J. Alloys Compd. **303**, 214 (2000).

[15] H. F. Yang, G. H. Rao, W. G. Chu, G. Y. Liu, Z. W. Ouyang, and J. K. Liang, J. Alloys Compd. 339, **189** (2002).

[16] H. F. Yang, G. H. Rao, G. Y. Liu, Z.W. Ouyang, W. F. Liu, X. M. Feng, W. G. Chu, and J. K. Liang, J. Alloys Compd. **346**, 190 (2002).

[17] A. O. Pecharsky, K. A. Gschneidner, Jr., V. K. Pecharsky, and C. E. Schindler, J. Alloys Compd. **338**, 126 (2002).

[18] C. Ritter, L. Morellon, P.A. Algarabel, C. Magen, and M.R. Ibarra, Phys. Rev. B **65**, 094405 (2002).

[19] A. O. Pecharsky, K. A. Gschneidner, Jr., V. K. Pecharsky, D. L. Schlagel, and T. A. Lograsso, Phys. Rev. B **70,** 144419 (2004).

[20] K. Ahn, A. O. Tsokol, Yu. Mozharivskyj, K. A. Gschneidner, Jr., and V. K. Pecharsky, Phys. Rev. B **72**, 054404 (2005).

[21] A. O. Pecharsky, V. K. Pecharsky, and K. A. Gschneidner, Jr., J. Alloys Compd. **379**, 127 (2004).

[22] M. V. Bulanova, P. N. Zheltov, K. A. Meleshevich, P. A. Saltykov, and G. Effenberg, J. Alloys Compd. **345**, 110 (2002).

[23] S. Bobev and E. D. Bauer, Acta Cryst. **E61**, i73 (2005).

[24] L. M. Wu, S. H. Kim, and D. K. Seo, J. Am. Chem. Soc. **127**, 15682 (2005).

[25] P. Schobinger-Papamantellos and A. Niggli, Journal de Physique, Colloque **C5**, 156 (1979).

[26] V. N. Eremenko, V. E. Listovnichii, S. P. Luzan, Yu. I. Buyanov, and P. S. Martsenyuk, J. Alloys Compd. **219**, 181 (1995).

[27] V. N. Eremenko, K. A. Meleshevich, Yu. I. Buyanov, and P. S. Martsenyuk, Poroshkovaya Metallurgiya (Kiev) **7**, 41 (1989).

[28] N. P. Thuy, Y. Y. Chen, Y. D. Yao, C. R. Wang, S. H. Lin, J. C. Ho, T. P. Nguyen, P. D. Thang, J. C. P. Klaasse, N. T. Hien, and L. T. Tai, J. Magn. Magn. Mater. **262**, 432 (2003).

[29] Materials Preparation Center, Ames Laboratory US-DOE, Ames, IA USA, www.mpc.ameslab.gov

[30] B. A. Hunter, Rietica – A visual Rietveld program, International Union of Crystallography Commission on Powder Diffraction, Newsletter No. 20 (Summer, 1998) http://www.rietica.org.

[31] V. K. Pecharsky, A. P. Holm, K. A. Gschneidner, Jr., and R. Rink, Phys. Rev. Lett. **91**, 197204 (2003).

[32] Ya. Mudryk, A. P. Holm, K. A. Gschneidner, Jr., and V. K. Pecharsky, Phys. Rev. B **72**, 064442 (2005).

[33] A. P. Holm, V. K. Pecharsky, K. A. Gschneidner, Jr., R. Rink, and M. Jirmanus, Rev. Sci. Instr. **75**, 1081 (2004).

[34] V. K. Pecharsky, J. O. Moorman and K. A. Gschneidner, Jr., Rev. Sci. Instr. **68**, 4196 (1997).

[35] N. W. Ashcroft and N. D. Mermin, *Solid State Physics* (New York, Holt, Rinehart and Winston, 1976).

[36] J. H. Van Vleck, *The Theory of Electric and Magnetic Susceptibilities* (Oxford University Press, London, 1932).

[37] A. Frank, Phys. Rev. **48**, 765 (1935).

[38] H. W. De Wijn, A. M. Van Diepen, and K. H. J. Buschow, Phys. Rev. **161**, 253 (1967).

[39] A. M. Stewart, Phys. Rev. B **6**, 1985 (1972).

[40] Z. Liu, Phys. Rev. B **64**, 144407 (2001).

[41] H. Adachi, H. Ino, and H. Miwa, Phys. Rev. B **56**, 349 (1997).

[42] H. Adachi, H. Ino, and H. Miwa, Phys. Rev. B **59**, 11445 (1999).

[43] H. Adachi and H. Ino, Nature **401**, 148 (1999).

[44] H. Adachi, H. Kawata, H. Hashimoto, Y. Sato, I. Matsumoto, and Y. Tanaka, Phys. Rev. Lett. **87**, 127202 (2001).

[45] D. Wagner, *Introduction to the theory of magnetism* (Pergamon Press, 1972).

[46] H. C. Hamaker, L. D. Woolf, H. B. MacKay, Z. Fisk, and M. B. Maple, Solid State Comm. **32**, 289 (1979).

[47] W. M. Yuhasz, N. A. Frederick, P.-C. Ho, N. P. Butch, B. J. Taylor, T. A. Sayles, M. B. Maple, J. B. Betts, A. H. Lacerda, P. Rogl, and G. Giester, Phys. Rev. B **71**, 104402 (2005).

[48] V. K. Pecharsky and K. A. Gschneidner, Jr., J. Appl. Phys. **86**, 565 (1999).

[49] V. K. Pecharsky, K. A. Gschneidner, Jr. In *Magnetism and Structure in Functional Materials* (A. Planes, L. Mañosa, A. Saxena, eds.), pp. 199-222. Springer-Verlag, Berlin (2005).

CHAPTER 4. PREPARATION, HEAT CAPACITY, MAGNETIC PROPERTIES, AND THE MAGNETOCALORIC EFFECT OF EuO

The paper is published in *Journal of Applied Physics*[6]

Kyunghan Ahn,[7,8] A. O. Pecharsky,[7] K. A. Gschneidner, Jr.,[7,8] and V. K. Pecharsky[7,8]

Abstract

EuO was synthesized through the thermal reduction of Eu_2O_3 by a stoichiometric quantity of metallic Eu. According to the heat capacity and magnetic measurements, EuO undergoes a second-order phase transformation at ~69 K from the ferromagnetic to the paramagnetic state on heating. The magnetocaloric effect of EuO, both as the isothermal magnetic entropy change (ΔS_{mag}) and the adiabatic temperature change (ΔT_{ad}), was obtained from the heat capacity data. Also, the magnetization isotherms were used to calculate ΔS_{mag}. EuO exhibits the magnetocaloric effect with a peak in the vicinity of the magnetic phase transition temperature (~69 K), the amplitude of which is comparable to other known magnetocaloric material $DyAl_2$. The ΔS_{mag} calculated from the heat capacity data is in excellent agreement with that calculated from the magnetization data.

---

[6] *Journal of Applied Physics* **97**, 063901-1 - 063901-5 (2005)

[7] Ames Laboratory, Materials and Engineering Physics Program, Iowa State University, Ames, IA 50011-3020, USA

[8] Department of Materials Science and Engineering, Iowa State University, Ames, IA 50011-2300, USA

Introduction

Recently, near room temperature magnetic refrigeration (MR) technology has received a great deal of attention because of its environmental safety and potential for considerable improvements in energy efficiency.[1, 2] In addition to further refinements of the existing prototype refrigerators, materials with large magnetocaloric effect (MCE) are required to take full advantage of multiple benefits offered by MR technology. In 1997, Pecharsky and Gschneidner discovered that $Gd_5Si_2Ge_2$ exhibits the giant MCE around its Curie temperature, $T_C \cong 270$ K, which set a new standard for near room temperature magnetocaloric materials.[3] The discovery of the giant MCE in $Gd_5Si_2Ge_2$ intensified the quest for new compounds with similar properties.[4, 5] Today, the development of advanced magnetocaloric materials exhibiting strong MCE between ~20 K and 300 – 350 K remains an important topic for basic science in order to support future MR needs.[6]

In 1961, Matthias *et al.*[7] discovered that europium monoxide (EuO) orders ferromagnetically at 77 K; it was the first rare-earth metal oxide ferromagnet. EuO crystallizes in the NaCl-type structure with a room temperature lattice parameter $a = 5.143$ Å.[8, 9] Since EuO has a purely spin magnetism due to the localized Eu^{2+} $4f^7$ electrons with $^8S_{7/2}$ ground state, it has been studied extensively as an example of a ferromagnetic semiconductor material (Heisenberg ferromagnet).[10] At present, EuO also receives a special attention as a candidate material for optical isolators and optomagnetic devices.[11]

On the other hand, EuO may have a potential for application as a magnetic refrigerant material because of the unique magnetic properties of Eu. Europium has two valence states: Eu^{2+} and Eu^{3+}. The Eu^{2+} ion is similar to the Gd^{3+} ion with a $4f^7$ state ($J = 7/2$), while the Eu^{3+} ion has a $4f^6$ configuration ($J = 0$). Elemental Gd and many Gd-based compounds are good magnetic refrigerant materials due to their large magnetic moments. Therefore, divalent europium in binary compounds, such as EuO, EuS, EuSe, and EuTe, may bring about a large MCE, as well as interesting magnetism. Experimental studies of Eu^{2+}-based compounds have been limited because of difficulties in preparation of materials containing

Eu^{2+} ions. Until now, only a few divalent europium compounds (both binary and ternary) have been reported and characterized.

The Eu^{2+} ion is a stable oxidation state for this element. However, the existence of divalent europium compounds at ambient conditions is limited, because the Eu^{2+} ion is also a strong reducing agent: in air, it may be easily oxidized to the Eu^{3+} state.[12] Thus, special care in handling compounds containing Eu^{2+} ions is usually required. Several researchers reported on the magnetic properties of EuO,[7-10, 12, 13, 14, 15] yet among the europium compounds, the MCE is only known for europium sulfide, EuS – it was measured by Bredy and Seyfert [16] and theoretically calculated by Hashimoto *et al.*[17]

In this paper, we report on the preparation, magnetic behavior, and the MCE of EuO as evaluated from both the heat capacity and magnetization measurements. The results are compared with those of EuS and a well-known low-temperature magnetic refrigerant material $DyAl_2$, which orders magnetically at nearly the same temperature as EuO.

Experimental details

EuO was prepared via the thermal reduction of Eu_2O_3 by using the stoichiometric amount of Eu. High purity Eu (99.99 wt.%) was prepared by the Materials Preparation Center of the Ames Laboratory, and Eu_2O_3 with 99.99 wt.% purity was purchased from a commercial vendor. Both a piece of Eu metal and Eu_2O_3 powder, which weighed together around 10 g, were loaded into a Ta crucible in a glove box with He atmosphere. The crucible was sealed by arc-welding also in helium atmosphere. The synthesis reaction was carried out for 30 min at 1800 ºC in a high vacuum (~ 10^{-5} torr) induction furnace. After the reaction, the induction furnace was switched off to cool down the crucible and sample. The cooling from 1800 ºC to room temperature takes about two hours.

X-ray powder diffraction was used to establish the phase purity and to verify the crystal structure of EuO at room temperature. The diffraction data were collected at room

temperature on a Rigaku TTRAX rotating anode powder diffractometer equipped with a wide angle goniometer using Mo Kα radiation. The crystal structure was refined by a full profile Rietveld refinement technique using LHPM-Rietica program.[18]

Magnetic measurements were performed on a LakeShore ac/dc magnetometer (model 7225) from ~5 K to ~320 K at various magnetic fields between 0 and 50 kOe. The magnetization isotherms were measured from 5 K to 110 K at 5 K intervals and with the magnetic field changing from 0 to 50 kOe in 2 kOe steps. The heat capacity was measured in a semiadiabatic heat pulse calorimeter[19] from ~3.5 K to ~350 K in various magnetic fields ranging from 0 to 100 kOe. The magnetocaloric effect as the isothermal magnetic entropy change, ΔS_{mag}, and the adiabatic temperature change, $\Delta T_{ad,}$ was calculated from both magnetization and heat capacity data as described by Pecharsky and Gschneidner.[20]

Results and discussion

The results of Rietveld refinement for EuO are shown in Fig. 1. A small amount of Eu_3O_4 impurity (1.3 mol.%, see inset in Fig. 1) has been detected, while the majority of the sample (98.7 mol.%) is the cubic europium monoxide. The concentrations of other possible phases (e.g., Eu_2O_3) were below the limits of detection for this technique, which considering the quality of the powder diffraction data, is on the order of 1 vol.% of an impurity. The purity of the europium monoxide, therefore, is 96.2 wt.%. Our results confirm that EuO crystallizes in the NaCl-type structure, space group $Fm\bar{3}m$, with a lattice parameter a = 5.1468(7) Å and an x-ray density of 8.185 g/cm^3. These results are in good agreement with the crystallographic data reported by other researchers.[8, 9]

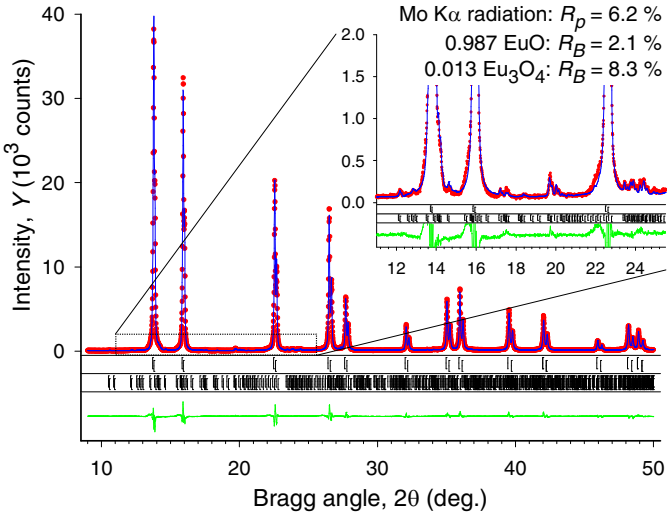

Fig. 1. The observed (dots) and calculated (line) powder diffraction patterns of EuO. The difference, Y_{obs}-Y_{calc}, is shown at the bottom of the plot. The upper set of vertical bars below the main plot indicates calculated positions of Bragg peaks (for both $K\alpha_1$ and $K\alpha_2$ wavelengths) for EuO and the lower set of bars is the same for Eu_3O_4. The inset shows low intensity details in order to visualize the contribution from the small amount of the Eu_3O_4 impurity.

The temperature dependencies of the magnetization of EuO in 10, 20 and 50 kOe are shown from ~ 5 to 200 K in Fig. 2. The observed *M(T)* behaviors are typical for a temperature induced magnetic phase transition from a ferromagnetic (FM) to a paramagnetic (PM) state on heating. Inset in Fig. 2 shows the temperature dependence of the inverse dc magnetic susceptibility of EuO measured in a 50 kOe dc magnetic field. Above ~125 K, the dc magnetic susceptibility follows the Curie-Weiss law $\chi(T) = Np_{eff}^2 / 3k(T - \theta_p)$ with the paramagnetic Curie temperature (θ_p) of 70.6(3) K and the effective magnetic moment (p_{eff}) of 8.15(3) μ_B. The observed effective magnetic moment is consistent with that expected for divalent Eu; the theoretical free ion effective magnetic moment for Eu^{2+} is 7.94 μ_B. The Curie temperature determined from the ac susceptibility (Fig. 3) is 69 K. The nearly constant magnetic susceptibility below T_C indicates negligible coercivity which is consistent with the spherical symmetry of the *4f* electron wave functions of Eu^{2+}. The upturn below ~ 20 K is likely associated with the proximity of the Neėl temperature of the Eu_3O_4 impurity (according to Holmes and Schieber[21] Eu_3O_4 orders antiferromagnetically at 5 K).

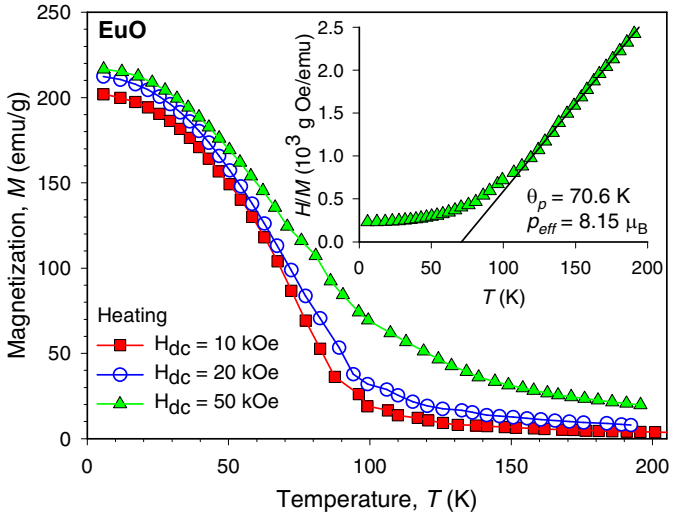

Fig. 2. Temperature dependencies of the magnetization of EuO measured on heating in dc magnetic fields of 10 kOe, 20 kOe and 50 kOe. The insert shows the inverse magnetic susceptibility (*H/M*) of EuO measured in a 50 kOe magnetic field with the straight line indicating the Curie-Weiss behavior above ~125 K. The sample was cooled from room temperature to ~5 K in a zero magnetic field before each measurement.

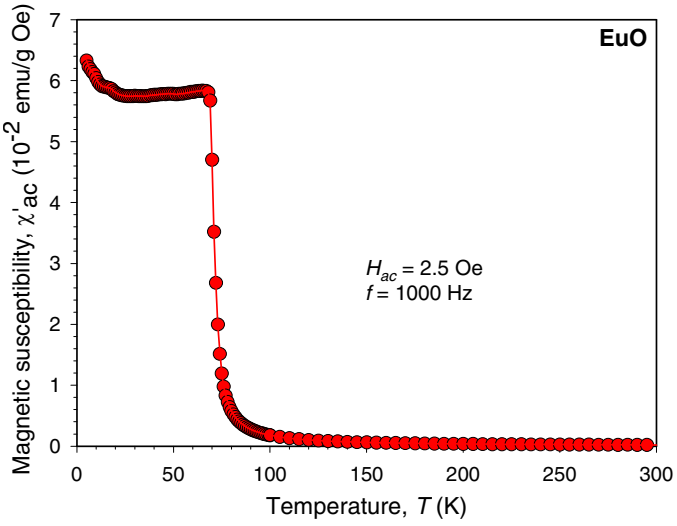

Fig. 3. The ac magnetic susceptibility of EuO measured in ac magnetic field with the amplitude of 2.5 Oe and frequency of 1000 Hz.

Figure 4 shows selected magnetization isotherms of EuO between 5 K and 110 K. The behavior of the magnetization as a function of magnetic field in EuO is also consistent with conventional ferromagnetic ordering. The non-linearity of the *M* vs. *H* behavior well above the T_C = 69 K indicates that short range magnetic ordering and/or ferromagnetic clustering persist to 30 K – 40 K above the zero magnetic field Curie temperature. The Curie temperature estimated from Arrott plot (M^3 vs H) lies between 80 K and 85 K, which is about 10 K higher than that from both C_P data and ac susceptibility data because of the persistence of short range magnetic ordering above T_C. The ordered magnetic moment calculated by extrapolating the nearly linear behavior of *M(H)* at *T* = 5 K observed above ~20 kOe to zero magnetic field is 6.4 μ_B (6.7 μ_B after correcting for the Eu_3O_4 impurity), which is slightly lower than the theoretically expected value of 7 μ_B, and it is slightly lower than 6.9 μ_B reported by Matthias *et al.*[7] Still, this value is consistent with a nearly collinear ferromagnetism of the oxide at this temperature.

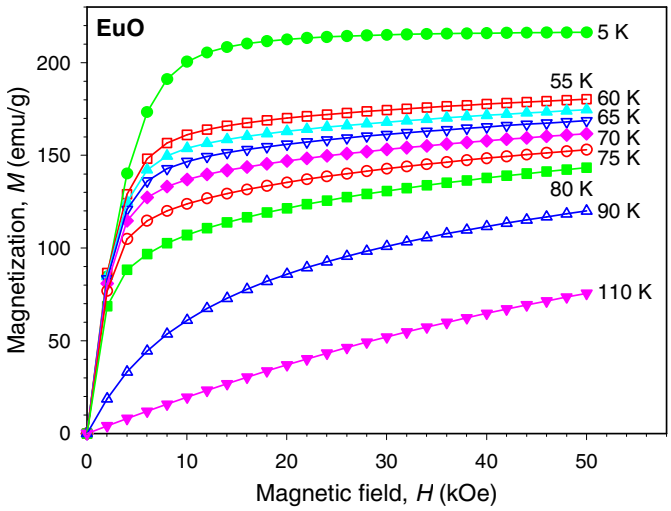

Fig. 4. Selected magnetization isotherms of EuO measured during increasing magnetic field.

The heat capacity of EuO as a function of temperature and magnetic field is shown in Fig. 5. For EuO, a λ-like peak is observed in a zero magnetic field, and with increasing magnetic field, the peak becomes broader, rounded and shifts to higher temperatures. Finally, the peak disappears in magnetic field of 75 kOe. This type of behavior confirms that EuO undergoes a second-order phase transition between the paramagnetic and ferromagnetic

states at ~69 K. Because the low temperature limit of our calorimeter is relatively high (~3.5 K) and because the magnetic ordering temperature of EuO is relatively low (~69 K), we were unable to obtain reasonable fits of the lowest temperature data and determine the electronic heat capacity and the Debye temperature of the compound.

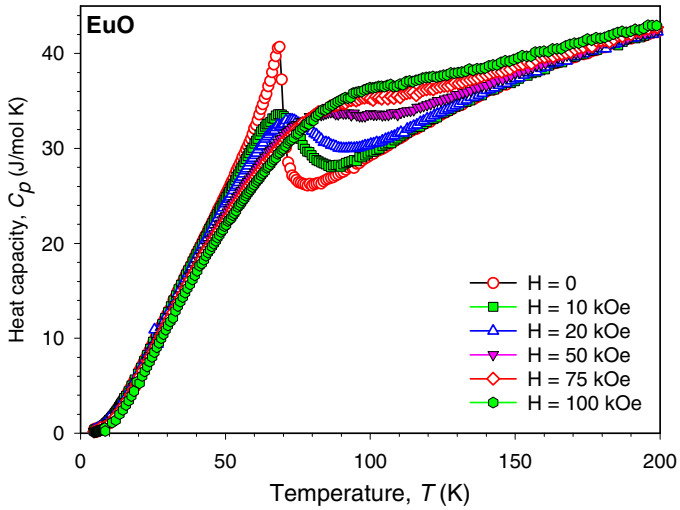

Fig. 5. The heat capacity of EuO measured during heating in constant magnetic fields of 0, 10 kOe, 20 kOe, 50 kOe, 75 kOe and 100 kOe.

The isothermal magnetic entropy change calculated from the heat capacity data is shown in Fig. 6. The maximum $|\Delta S_{mag}|$ values of EuO near T_C = 69 K are about 5, 8.5, 17.5, 22, and 28 J/kg K for magnetic field changes of 10, 20, 50, 75, and 100 kOe, respectively. For EuO, the adiabatic temperature rise (ΔT_{ad}) is shown in Fig. 7. The maximum ΔT_{ad} of EuO near T_C are about 1.6, 3.2, 6.8, 8.8, and 11.2 K for magnetic field changes of 10, 20, 50, 75, and 100 kOe, respectively. For comparison, the ΔS_{mag} and ΔT_{ad} values for $DyAl_2$ (T_C = 64 K) [22, 23] are also plotted in Fig. 6 and Fig. 7, respectively. In general, the MCE values are about the same for the two compounds. The ΔS_{mag} calculated from both the magnetization and heat capacity data are nearly the same (Fig. 8), thus indicating that the two techniques yield consistent results. The typical caret-like behavior of the magnetocaloric effect (Figs. 6 – 8) is consistent with the second order nature of the magnetic ordering in EuO. The weak anomaly in ΔT_{ad} around 5 K (see Fig. 7) is consistent with a small amount of Eu_3O_4, which is metamagnetic in fields higher than 2 – 3 kOe.[21]

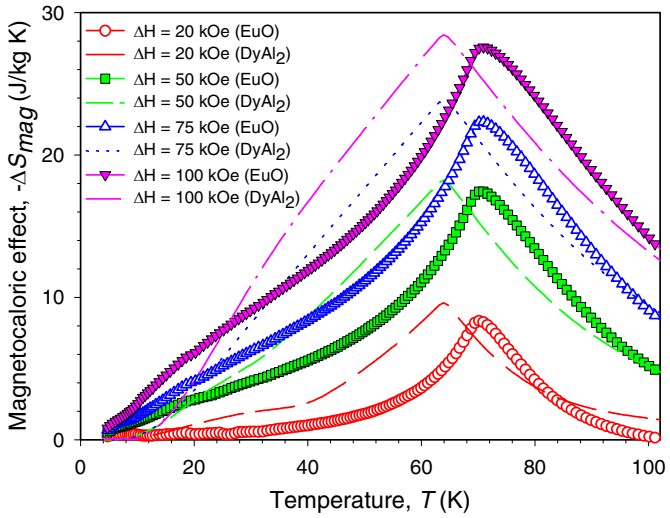

Fig. 6. The magnetocaloric effect of EuO and $DyAl_2$ as the magnetic entropy change (ΔS_{mag}) calculated from the heat capacity data. The data for $DyAl_2$ are taken from Refs. 22 and 23.

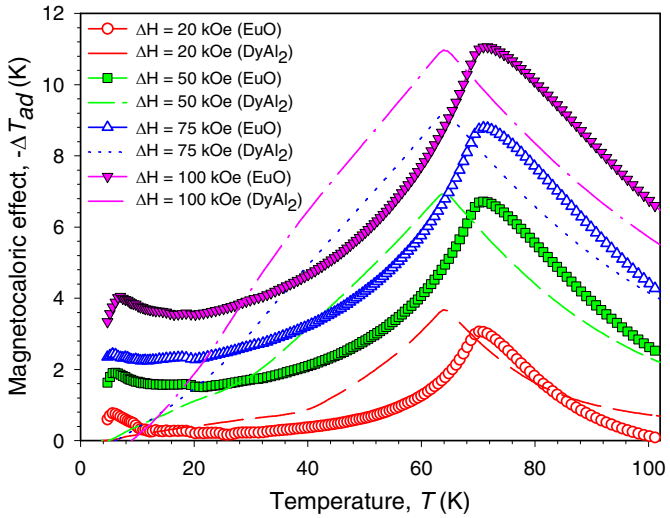

Fig. 7. The magnetocaloric effect of EuO and $DyAl_2$ as the adiabatic temperature change (ΔT_{ad}) calculated from the heat capacity data. The data for $DyAl_2$ are taken from Refs. 22 and 23.

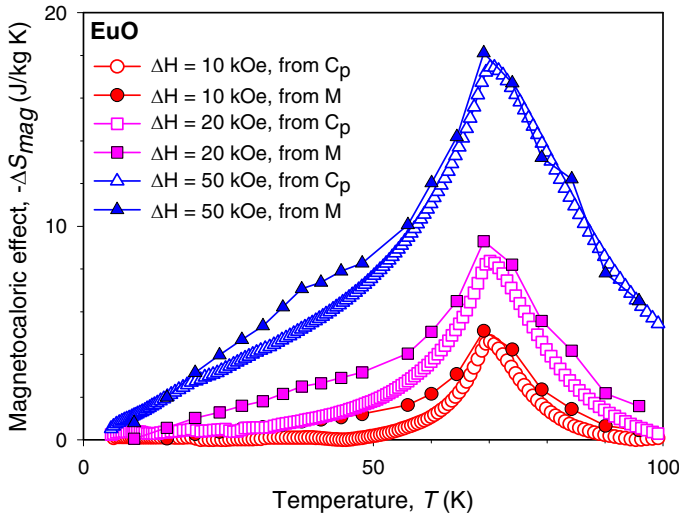

Fig. 8. The magnetocaloric effect of EuO as the magnetic entropy change (ΔS_{mag}) calculated from both heat capacity and magnetization data.

Some of the better active magnetic refrigerant materials, which order between ~ 60 K and 80 K, are $DyAl_2$ (T_C = 64 K) and $GdNi_2$ (T_C = 72 K). Both have been suggested as regenerator materials for magnetic refrigeration.[24] Although the ΔS_{mag} values in mass units of EuO and $DyAl_2$ are nearly identical, for magnetic refrigeration applications the critical property for the magnetic entropy change is the volumetric ΔS_{mag}.[24, 25] For a magnetic field change of 50 kOe, ΔS_{mag} = -143 mJ/cm^3 K for EuO, which is ~ 30 % larger than that of $DyAl_2$ (ΔS_{mag} = -110 mJ/cm^3 K), and ~ 40 % larger than that of $GdNi_2$ (ΔS_{mag} of the latter was estimated to be -100 mJ/cm^3 K from the only reported value, -137 mJ/cm^3 K for a ΔH = 70 kOe). Thus, EuO is best potential magnetic refrigerant material of those compounds which undergo a second order magnetic transition around 70 K. There are, however, some first order magnetic transition compounds which have significantly better MCE values, i.e. $HoCo_2$ and Dy_5Si_3Ge.[24] The $|\Delta S_{mag}|$ maximum of EuS for ΔH of 20 kOe near T_C (~17 K) is 15 J/kg K.[16] Thus, the $|\Delta S_{mag}|$ of EuS is approximately two times larger than the ΔS_{mag} in EuO near its T_C of 69 K for the same magnetic field change, 8.4 J/kg K, see Fig. 6. However, in volumetric units, the difference is much smaller (-88 mJ/cm^3 K for EuS vs. -69 mJ/cm^3 K for EuO). In general, such comparisons are not recommended for materials with

significantly different T_C because of the additional internal entropy losses due to the larger lattice heat capacity of the material with the higher *Tc*.[25] But in this case, the large density difference dominates (5.75 g/cm^3 for EuS vs. 8.185 g/cm^3 for EuO) as seen for the nearly identical volumetric $|\Delta S_{mag}|$ of EuO compared to that of EuS.

Conclusions

Polycrystalline EuO was successfully synthesized by the thermal reduction of Eu_2O_3 with Eu. The room temperature crystal structure of the material and its ferromagnetism below ~69 K were confirmed. The MCE of the polycrystalline EuO was calculated from both heat capacity and magnetization data. The $|\Delta S_{mag}|$ maximum in EuO near T_C (69 K) are 4.6, 8.4, 17.5, 22.3, and 27.6 J/kg K for ΔH of 10, 20, 50, 75, and 100 kOe, respectively. The ΔT_{ad} maximum of EuO are 1.6, 3.2, 6.8, 8.8, and 11.2 K for the same magnetic field changes, respectively.

Acknowledgement

This work was supported by the Office of Basic Energy Sciences, Materials Sciences Division of the U.S. Department of Energy under contract No.W-7405-ENG-82.

References

[1] V. K. Pecharsky and K. A. Gschneidner, Jr., J. Magn. Magn. Mater. **200**, 44 (1999).

[2] V. K. Pecharsky, K. A. Gschneidner, Jr., A. O. Pecharsky, and A. M. Tishin, Phys. Rev. B **64**,144406 (2001).

[3] V. K. Pecharsky and K. A. Gschneidner, Jr., Phys. Rev. Lett. **78**, 4494 (1997).

[4] F. X. Hu, B. G. Shen, J. R. Sun, Z. H. Cheng, G. H. Rao, and X. X. Zhang, Appl. Phys. Lett. **78**, 3675 (2001).

[5] O. Tegus, E. Brück, K. H. J. Buschow, and F. R. deBoer, Nature (London) **415**, 150 (2002).

[6] A. M. Tishin and Yu. S. Spichkin, The magnetocaloric effect and its applications, IOP Publishing Ltd., Bristol (2003).

[7] B. T. Matthias, R. M. Bozorth, and J. H. Van Vleck, Phys. Rev. Lett. **7**, 160 (1961).

[8] R. A. Belayev, V. V. Bondarenko, V. P. Vyskubov, S. S. Kiparisov, V. A. Lazarevski, and V. M. Tyugin, *Properties of Europium Oxides*, ORNL-tr-2883, 1974.

[9] J. F. Dillon, Jr. and C. E. Olsen, Phys. Rev. **135**, A434 (1964).

[10] M. M. Abd-Elmeguid and R. D. Taylor, Phys. Rev. B **42**, 1048 (1990).

[11] S. Thongchant, Y. Hasegawa, Y. Wada and S. Yanagida, Chem. Lett. 1274 (2001).

[12] M. W. Shafer, J. App. Phys. **36**, 1145 (1965).

[13] T. Kasuya and A. Yanse, Rev. Mod. Phys. **40**, 684 (1968).

[14] W. C. Koeiler, J. App. Phys. **36**, 1078 (1965).

[15] R. M. Bozorth and J. H. Van Vleck, Phys. Rev. **118**, 1493 (1960).

[16] P. Bredy and P. Seyfert, Cryogenics **28**, 605 (1988).

[17] T. Hashimoto, T. Numasawa, M. Shino and T. Okada, Cryogenics **21**, 647 (1981).

[18] B. A. Hunter, Rietica – A visual Rietveld program, International Union of Crystallography Commission on Powder Diffraction, Newsletter No. 20 (Summer, 1998) http://www.rietica.org.

[19] V. K. Pecharsky, J. O. Moorman, and K. A. Gschneidner, Jr., Rev. Sci. Instr. **68**, 4196 (1997).

[20] V. K. Pecharsky and K. A. Gschneidner, Jr., J. Appl. Phys. **86**, 565 (1999).

[21] L. Holmes and M. Schieber, J. Appl. Phys. **37**, 968 (1966).

[22] K. A. Gschneidner, Jr., V. K. Pecharsky, and S. K. Malik, Adv. Cryog. Eng. **42A**, 475 (1996).

[23] P. J. Von Ranke, V. K. Pecharsky, and K. A. Gschneidner, Jr., Phys. Rev. B **58**, 12110 (1998).

[24] K. A. Gschneidner, Jr. and V. K. Pecharsky, p. 519, Chap. 25 in Intermetallic Compounds: Vol. 3, Principles and Practice. J. H. Westbrook and R. L. Fleischer, eds., John Willey & Sons, Ltd., New York (2002).

[25] V. K. Pecharsky and K. A. Gschneidner, Jr., J. Appl. Phys. **90**, 4612 (2001).

CHAPTER 5. THE MAGNETOTHERMAL BEHAVIOR OF MIXED VALENT Eu_3O_4

This is a manuscript prepared for publication

Kyunghan Ahn,[9,10] A. O. Tsokol,[9] V. K. Pecharsky,[9,10] and K. A. Gschneidner, Jr.[9,10]

Abstract

Mixed-valence compound Eu_3O_4 was prepared by heating EuO and Eu_2O_3 together at 1800 °C for 30 h in a sealed W crucible under a high vacuum. It was confirmed as single phase Eu_3O_4 by the room temperature x-ray powder diffraction method. We characterized polycrystalline Eu_3O_4 through the heat capacity and magnetic measurements. Our results from magnetic measurements are in good agreement with the results reported previously. As far as we are aware, heat capacity of Eu_3O_4 was not studied before. The magnetocaloric effect (MCE) in Eu_3O_4, both the magnetic entropy change (ΔS_{mag}) and the adiabatic temperature change (ΔT_{ad}), were measured for different applied magnetic fields. The magnetic entropy change ($-\Delta S_{mag}$) from heat capacity data in Eu_3O_4 near 6.5 K is approximately 12.7 J/kg K for a magnetic field change (ΔB) of 5 T. The adiabatic temperature change (ΔT_{ad}) in Eu_3O_4 near 7 K is about 7.0 K for a ΔB of 5 T. Also, the magnetic entropy change ($-\Delta S_{mag}$) calculated from magnetization data in Eu_3O_4 near 6.3 K is approximately 13.6 J/kg K for a magnetic field change (ΔB) of 5 T, which is roughly the same as that from the heat capacity data.

[9] Ames Laboratory, Materials and Engineering Physics Program, Iowa State University, Ames, IA 50011-3020, USA

[10] Department of Materials Science and Engineering, Iowa State University, Ames, IA 50011-2300, USA

Introduction

A mixed-valence compound is one in which some ions have more than one valence state. Mixed-valence or valence-fluctuation phenomena occur in rare earth-based compounds in which the localized *4f* level is near the Fermi energy level and such proximity leads to unstable valence states. Rare earth (R)-based compounds containing Ce, Sm, Eu, Tm, and Yb may show mixed-valence or valence-fluctuation behavior. The R ions in rare earth based compounds are normally in the trivalent state. However, Ce compounds may have valences of 3 and 4 while Sm, Eu, Tm, and Yb compounds may have valences of 2 and 3. Anomalies in electronic transport, magnetic, thermal, and structural properties for mixed-valence compounds may be caused by the mixing of *4f* electrons with conduction electrons.[1,2,3,4]

The magnetocaloric effect (MCE) is the magneto-thermal phenomenon in which the temperature of magnetic solids increases (decreases) adiabatically with the application (removal) of the magnetic field. Magnetic refrigeration is an application of MCE and the magnetic refrigeration has several advantages over the conventional gas compression/ expansion cooling system because of the energy savings and environmental concerns.[5] The near room temperature giant magnetocaloric effect (GMCE) was discovered in $Gd_5Si_2Ge_2$ compound nine years ago by Pecharsky and Gschneidner and it was caused by a first order magneto-structural phase transition at 276 K under a magnetic field.[6] After the discovery of GMCE in the $Gd_5Si_2Ge_2$ compound, there have been broad studies of MCE and magnetic refrigeration as an alternative technology of conventional cooling system.

There are three different europium oxides: EuO, Eu_2O_3, and Eu_3O_4. Generally, there are two integral valence states such as Eu^{2+} and Eu^{3+} for Eu. According to Hund's rule Eu^{2+} is in the $4f^7$ state (the total angular momentum $J = 7/2$), but Eu^{3+} is in the $4f^6$ state ($J = 0$). The existence of Eu_3O_4 was first reported in 1960 by Achard.[7] Barnighausen *et al*. reported the synthesis method of Eu_3O_4 by heating the same molar quantities of Eu_2O_3 and EuO at 900 ºC in an argon atmosphere.[8] Rau reported the crystal structure of Eu_3O_4 from single crystal x-ray diffraction data.[9] According to Rau's study, Eu_3O_4 shows mixed valent states containing

both divalent and trivalent europium ions [9] while EuO and Eu_2O_3 exhibit divalent and trivalent europium ion character, respectively. Eu_3O_4 crystallizes in the calcium ferrite-type ($CaFe_2O_4$-type) structure (orthorhombic structure, space group *Pnam*) and its unit cell parameters are a = 10.085, b = 12.054 and c = 3.502 Å.[9] Eu_3O_4 is a heterogeneous mixed-valence compound which has two different valence sites (Eu^{2+} and Eu^{3+}) in the unit cell. It can be described as $Eu^{2+}Eu^{3+}{}_2O^{2-}{}_4$ and thus the ratio of Eu^{2+} to Eu^{3+} ions is 1 to 2 and the Eu ions occupy nonequivalent sites, where divalent and trivalent Eu ions occupy the Ca sites and Fe sites, respectively.[9, 10]

The magnetic properties of Eu_3O_4, which contains both Eu^{2+} ions with the large magnetic moments and Eu^{3+} ions with much smaller magnetic moment, are interesting because of its mixed-valence character. The magnetic properties of Eu_3O_4 were first investigated by Holmes and Schieber.[11,12] They reported that Eu_3O_4 undergoes an antiferromagnetic ordering at the liquid helium temperature range (~ 5 K) and exhibits a metamagnetic behavior below T_N of ~ 5 K which occurs in a low magnetic field.[11] Recently, intermetallic compounds with metamagnetism have been extensively studied as potential magnetic refrigerant materials because the giant MCE has been observed in $Gd_5Si_2Ge_2$[6], $MnFeP_{0.45}As_{0.55}$[13], and $LaFe_{11.4}Si_{1.6}$[14]. The study of metamagnetism in Eu_3O_4 may also give information about interactions in magnetic compounds of ferrite-type AB_2O_4 form.[11] However, up to date, although there have been several papers about the investigation of magnetic properties of Eu_3O_4, there is no information about magneto-thermal properties of Eu_3O_4. Especially, among the europium compounds, the MCE is only known for EuS which was measured by Bredy and Seyfert[15] and theoretically calculated by Hashimoto *et al.*[16], and EuO which was recently studied by Ahn *et al.*[17]

Here, we report structural, magnetic, and magneto-thermal properties of the mixed-valence compound Eu_3O_4.

Experimental methods

The mixed valent compound Eu_3O_4 was prepared by heating a stoichiometric equimolar mixture of EuO and Eu_2O_3 in a sealed tungsten crucible at 1800 °C for 30 hrs under a high vacuum (~10^{-5} torr). First, EuO was prepared by the thermal reduction of Eu_2O_3 with the stoichiometric amount of Eu with 99.99 wt.% purity (the preparation of EuO is described in Ref. 17). The Eu_2O_3 with 99.99 wt.% purity was purchased from a commercial vendor. For the Eu_3O_4 synthesis a tungsten crucible, which is durable at high temperature, was used. Both EuO and Eu_2O_3 powder, which weighed together around 10 g, were loaded in a tungsten crucible in a glove box with the helium atmosphere. The crucible was sealed by electron beam welding under inert atmosphere. After the reaction, the induction furnace was switched off to cool down the crucible. The cooling from 1800 ºC to room temperature takes about two hours.

Room temperature x-ray powder diffraction measurement was used to establish both phase purity and crystal structure of Eu_3O_4. The x-ray powder diffraction studies were performed on an automated Scintag powder diffractometer using Cu-Kα radiation. The crystal structure was refined by full profile Rietveld refinement technique using LHPM-Rietica program.[18]

Magnetic measurements were performed on a SQUID magnetometer (model MPMS XL) from 1.8 to 400 K at various magnetic fields between 0 and 70 kOe. The magnetization isotherms were measured from 1.8 K to 30 K with 2.5 K intervals and with magnetic field changing from 0 to 70 kOe with 2 kOe steps.

The heat capacity was measured in a semiadiabatic heat pulse calorimeter from ~2 K to 350 K in various magnetic fields (0, 0.5, 0.75, 1, 2, and 5 T).[19] The magnetocaloric effect as the isothermal magnetic entropy change, ΔS_{mag}, and the adiabatic temperature change, $\Delta T_{ad,}$ was calculated from both magnetization and heat capacity data as described by Pecharsky and Gschneidner.[20]

Results and discussion

The Rietveld refinement of x-ray powder diffraction data in Eu_3O_4 is illustrated in Fig. 1. Room temperature x-ray powder diffraction confirms that Eu_3O_4 is a single phase material. From the refinement results, unit cell parameters in the orthorhombic system (space group *Pnma*) are a = 10.1026(8), b = 3.5032(3), and c = 12.0796(9) Å.

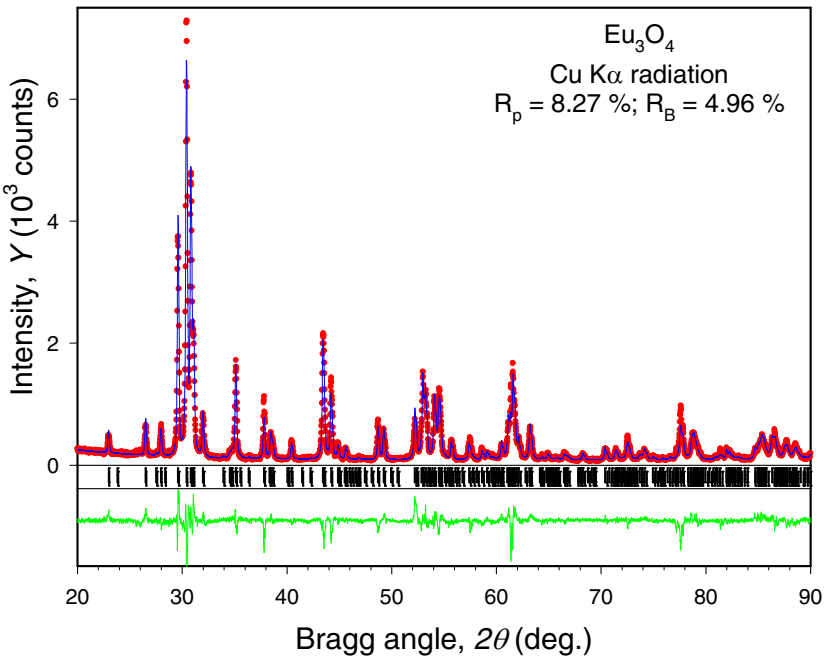

Fig. 1. The observed (dots) and calculated (line) powder diffraction patterns of Eu_3O_4. The difference, Y_{obs}-Y_{calc}, is shown at the bottom of the plot. The set of vertical bars below the main plot indicates calculated positions of Bragg peaks for both $K\alpha_1$ and $K\alpha_2$ components.

Figure 2 shows the heat capacity as a function of temperature in Eu_3O_4 under various magnetic fields (0, 0.5, 0.75, 1, 2, and 5 T). A heat capacity peak is observed at 5.3 K in a zero magnetic field, decreases and becomes rounded with increasing magnetic field. The peak moves toward lower temperatures with increasing magnetic field (4.7 K for 0.5 T and 4.3 K for 0.75 T) and at about 1 T the peak shifts to higher temperature and tends to broaden, indicating the FM state for B $\geq$ 1 T. This behavior for heat capacity data confirms that there

is a second-order antiferromagnetic transition near 5.3 K in Eu_3O_4, which is in agreement with the results of previous magnetic studies by other researchers.[11,12]

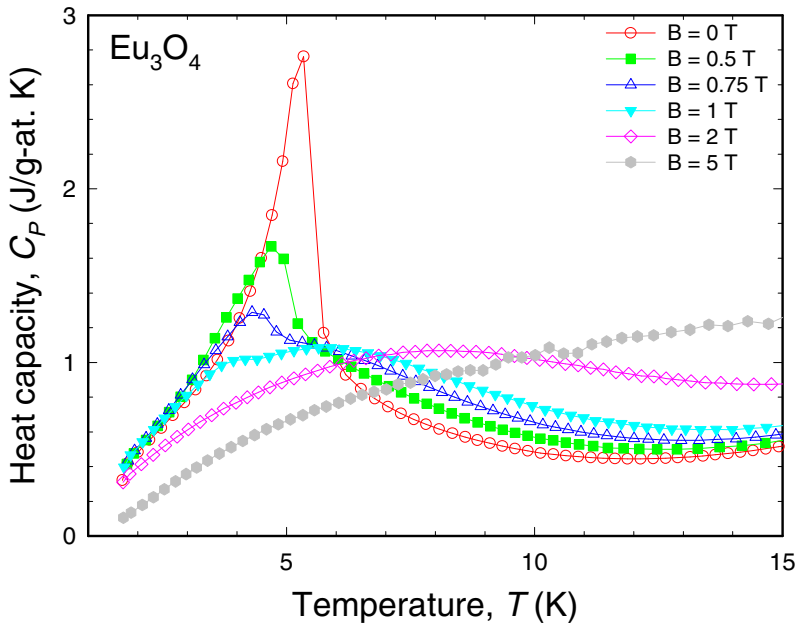

Fig. 2. The heat capacity (C_P) of Eu_3O_4 as a function of temperature and magnetic field

The isothermal magnetic entropy change ($-\Delta S_{mag}$) calculated from the heat capacity data for various magnetic field changes (ΔB = 0.5, 0.75, 1, 2, and 5 T) for Eu_3O_4 are shown in Fig. 3. The ΔS_{mag} is calculated from $\Delta S_{mag} = S(B,T) - S(0,T) = \int_0^T \frac{C(B,T) - C(0,T)}{T} dT$. The ΔS_{mag} is positive for a small temperature range at ΔB of 0.75 and 1 T because the zero field heat capacity value is lower than the non-zero field (0.75 and 1 T) heat capacity value below ~ 5 K. A peak is observed at 6.5 K for ΔB of 5 T and its magnitude is 12.7 J/kg K. The peak position slightly decreases toward lower temperature with decreasing ΔB (6.2 and 5.8 K for ΔB of 2 and 1 T, respectively) and the magnitude of maximum $|\Delta S_{mag}|$ also decreases (i.e. 7.1, 3.7, and 2.5 J/kg K for ΔB of 2, 1, and 0.75 T, respectively).

Figure 4 shows the adiabatic temperature change (ΔT_{ad}) from the heat capacity data for Eu_3O_4 with the magnetic field change (ΔB). Consistent with the behavior of ΔS_{mag}, the ΔT_{ad}

is negative below ~ 5 K for ΔB ranging from 0.75 to 1 T because the heat capacity for zero magnetic field is lower than that for a non-zero magnetic field. The peak is observed at 7.0 K for ΔB of 5 T and its position slightly increases toward higher temperatures with decreasing ΔB (7.3 and 7.6 K for ΔB of 2 and 1 T, respectively). The maximum ΔT_{ad} are 1.3, 1.9, 3.8 and 7.8 K for ΔB of 0.75, 1, 2, and 5 T, respectively.

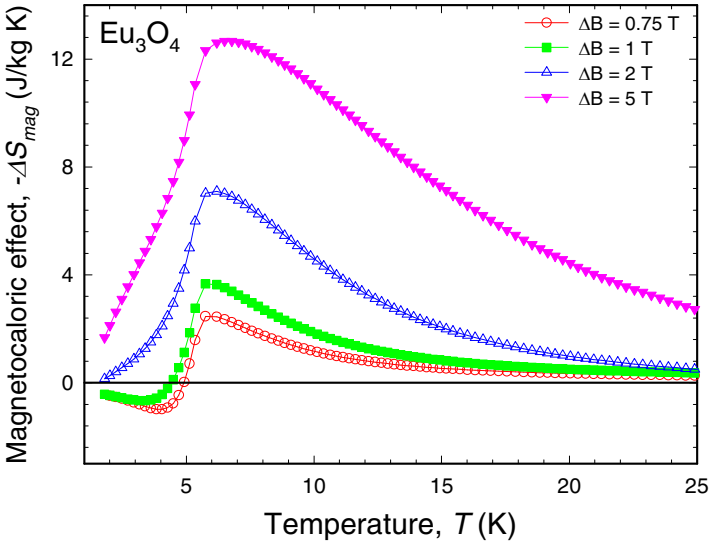

Fig. 3. The magnetic entropy change ($-\Delta S_{mag}$) of Eu_3O_4 calculated from the heat capacity data

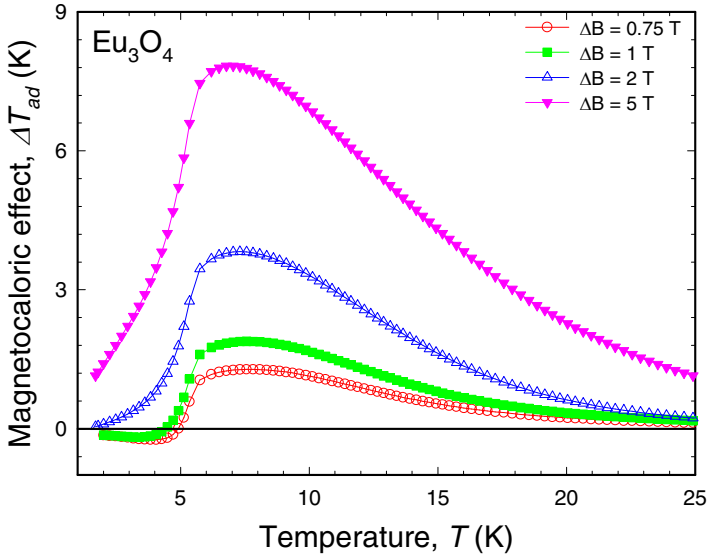

Fig. 4. The adiabatic temperature change (ΔT_{ad}) of Eu_3O_4 calculated from the heat capacity data

Figure 5 shows the magnetization (M) as a function of temperature (T) from 1.8 K to 10 K measured with the temperature interval of 0.2 K. The M versus T curve confirms that Eu_3O_4 exhibits an antiferromagnetic (AFM) ordering around 5 K. The M vs. T curves are plotted under various magnetic fields (0.05, 0.1, 0.2, 0.5, 1, and 2 T) for both zero-field cooled (ZFC) and field cooled (FC) conditions. For the magnetic fields of 0.05, 0.1, and 0.2 T nearly same behavior occurs in both the ZFC and FC conditions (see Fig. 5a), where the AFM ordering temperatures are 5.4, 5.4, and 5.2 K for 0.05, 0.1, and 0.2 T, respectively, and there are thermal hystereses with slight residual magnetizations, which is indicative of first-order transition. For a magnetic field of 0.5 T there is still AFM ordering around 4.4 K in the ZFC condition, but there is no sign of AFM ordering in the FC condition exhibiting conventional ferromagnetic ordering (see Fig.5b). For a magnetic field of 1 and 2 T, the signature of AFM ordering is no longer seen in both the ZFC and FC conditions. These experimental results indicate that magnetic fields above 1 T can switch the magnetic structure from AFM to FM state for Eu_3O_4.

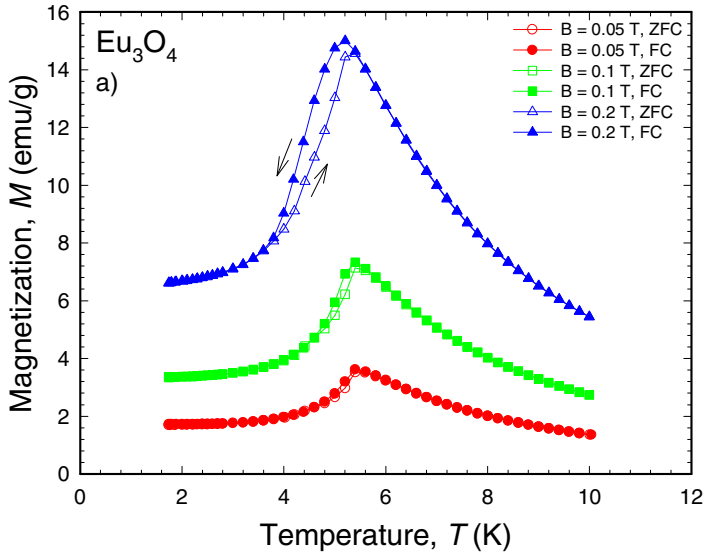

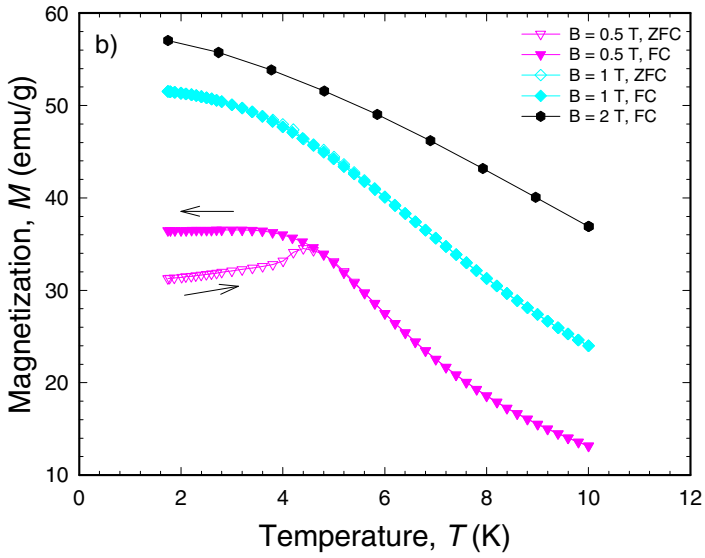

Fig. 5. The temperature dependencies of magnetization under various magnetic fields for Eu_3O_4: a) 0.05 to 0.2 T; b) 0.5 to 2 T

The ac magnetic susceptibility for Eu_3O_4 is shown as a function of temperature in Fig. 6. The ac magnetic susceptibility was measured for the amplitude of 5 x 10^{-4} T and frequency of 1000 Hz with the temperature interval of 0.1 K and 0.5 K for 1.8 K – 10 K and 10 K – 30 K, respectively. The real component (χ') of the ac magnetic susceptibility shows an AFM ordering at 5.4 K determined from a peak temperature.

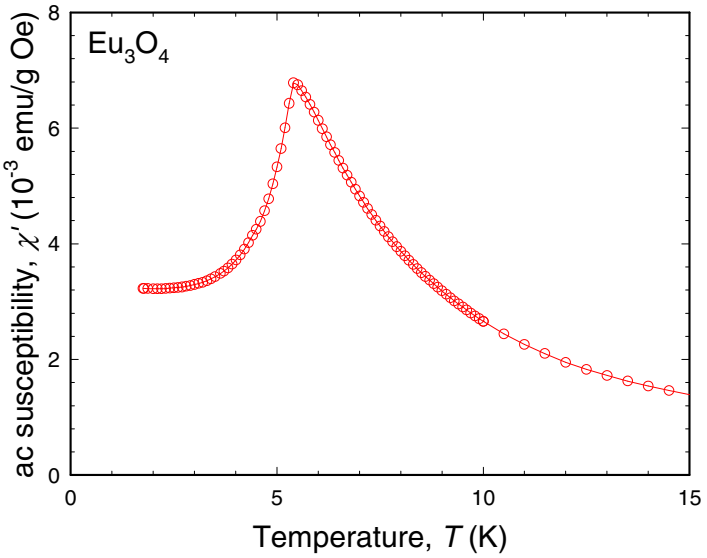

Fig. 6. The real part of the ac magnetic susceptibility of Eu_3O_4

Figure 7 shows the *B/M* as a function of temperature under the dc magnetic field of 20 kOe for Eu_3O_4. The negative paramagnetic Curie temperature (θ_p) of -36.9(2) K indicates dominant AFM interactions. The positive temperature-independent susceptibility χ_0 is 5.1 x 10^{-4} cm^3/Eu-mole (i.e. 2.9 x 10^{-2} emu/g T). Above 100 K, the *B/M* vs. *T* curve is nearly linear and it follows the Curie-Weiss law. According to the equation $p_{eff} = \left[z p_{eff1}^2 + (1-z) p_{eff2}^2 \right]^{1/2}$ where p_{eff} is the observed effective magnetic moment per Eu ion, p_{eff1} is the theoretical effective magnetic moment of free Eu^{2+} ion, p_{eff2} is the theoretical effective magnetic moment of free Eu^{3+} ion, z is the fraction of Eu^{2+} ion (the fraction of Eu^{2+} ion (z) in the unit cell of Eu_3O_4 is 1/3). Therefore, the observed effective magnetic moment of 5.34 μ_B/Eu atom, derived from the Curie-Weiss law using *M(T)* data measured between 240 and 340 K in a magnetic field of 2 T, is in excellent agreement with the theoretically expected effective magnetic moment of 5.38 μ_B/Eu atom from the assumption that there are one Eu^{2+} and two Eu^{3+} ions in Eu_3O_4, and the respective effective magnetic moments are 7.94 μ_B for Eu^{2+} and 3.45 μ_B[21,22] for Eu^{3+}, which was attained from the Van Vleck theory by considering small energy separation (Δ/k_B ~ 365 K for Eu^{3+})[23] between the ground state and the first excited state. Thus, the magnitude of the observed effective magnetic moment per Eu atom (i.e. 5.34 μ_B) confirms that Eu_3O_4 is a heterogeneous mixed-valence compound with two integral valence states:Eu^{2+} and Eu^{3+}.

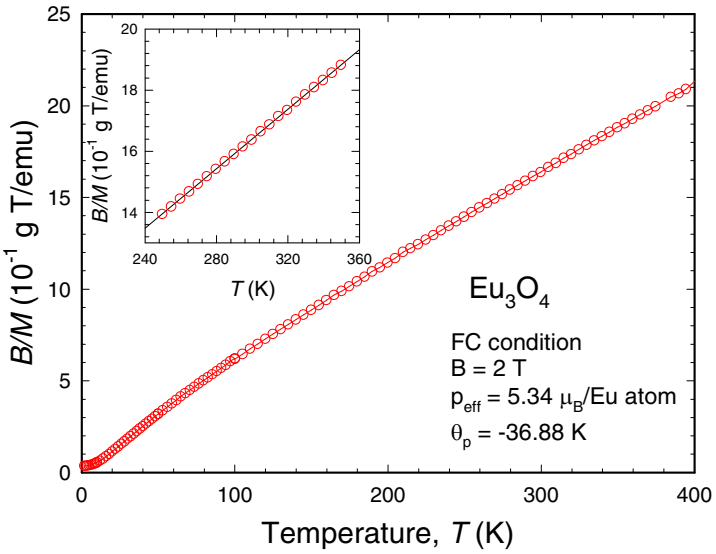

Fig. 7. The temperature dependence of inverse magnetic susceptibility (*B/M*) of Eu_3O_4

Figure 8 exhibits the magnetization (M) versus magnetic induction (B) curves at various temperatures. For 1.8 K and 2.5 K, the M vs. B curves show a metamagnetic transition ~ 0.3 T. It is hardly visible in the 5 K magnetization data. However, above 5 K, the metamagnetic transition is no longer observed. These behaviors are consistent with those reported earlier in Refs.11 and 12. Also, the ordered magnetic moment calculated by extrapolating the nearly linear behavior of $M(B)$ at T = 1.8 K observed above ~ 3 T to zero magnetic field is 1.9 μ_B/Eu atom. Under the plausible assumption that there is no population of first excited level in Eu^{3+} multiplets because 1.8 K is relatively low compared with the separation energy (~ 365 K), the expected ordered magnetic moment in Eu_3O_4 at 1.8 K is 2.3 μ_B/Eu atom (i.e, 1/3 x 7 μ_B) if the spins are collinear and thus it is in agreement with the observed ordered magnetic moment (i.e, 1.9 μ_B/Eu atom).

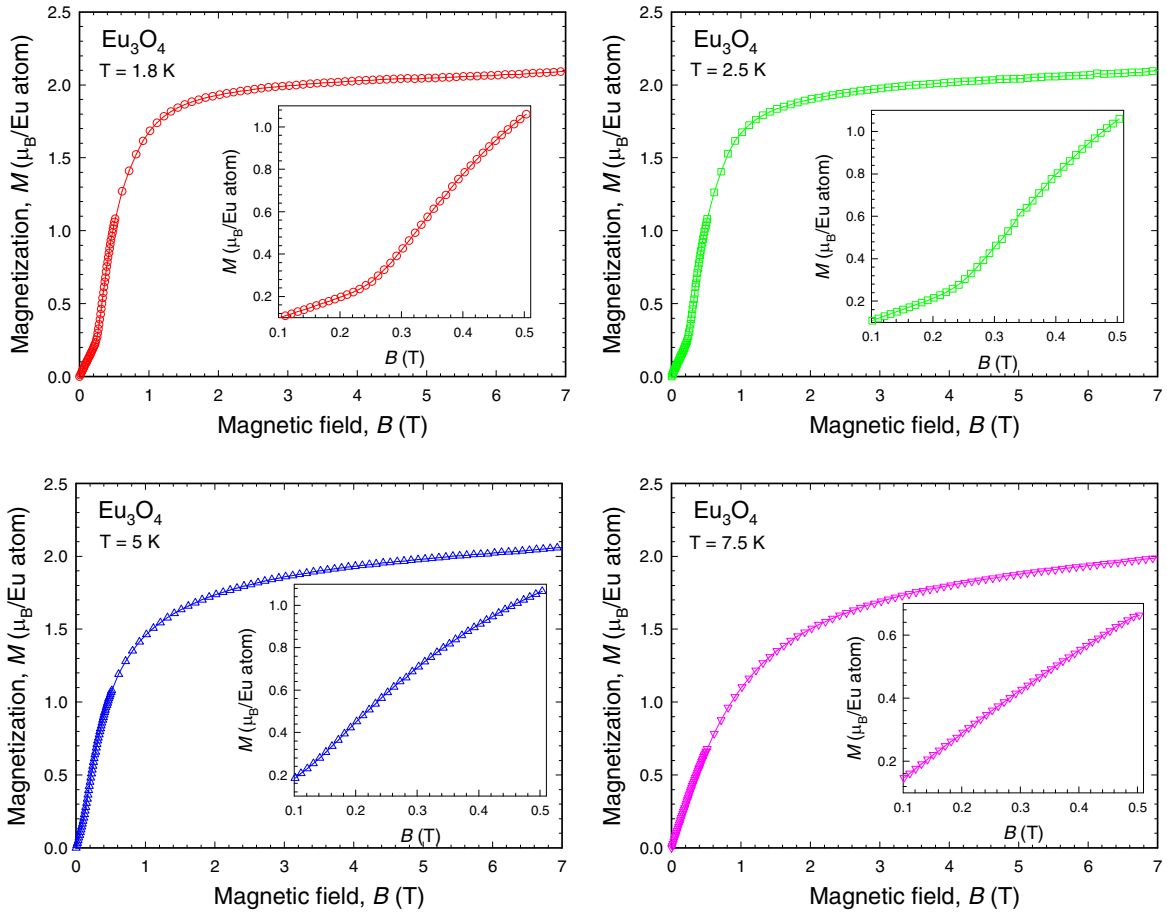

Fig. 8. The isothermal magnetization as a function of magnetic field for Eu_3O_4

Figure 9 shows the magnetic entropy change as a function of temperature for a magnetic field change of 1, 2, and 5 T calculated from both magnetization and heat capacity data. The peak of $-\Delta S_{mag}$ from magnetization data is observed at 6.3 K for magnetic field change of 5 T. The magnitude of maximum $|\Delta S_{mag}|$ from magnetization data are 3.9, 7.6, and 13.6 J/kg K for the magnetic field change of 1, 2, and 5 T, respectively. Also, the ΔS_{mag} from magnetization data have negative values below ~ 5 K for 1 T, which is in agreement with the ΔS_{mag} from heat capacity data. These values are approximately same as those calculated from the heat capacity data for 1 and 2 T and the $-\Delta S_{mag}$ for 5 T from magnetization data is slightly larger than that from heat capacity data for 5 T (i.e. the maximum $|\Delta S_{mag}|$ from magnetization and heat capacity data are 13.6 and 12.7 J/kg K, respectively). Thus, the $-\Delta S_{mag}$ from magnetization data is in good agreement with those from heat capacity data. The maximum magnetic entropy change $|\Delta S_{mag}|$ calculated from the magnetization and heat capacity data of Eu_3O_4 are 7.6 J/kg K (61 mJ/cm^3 K) at 6.3 K and 7.1 J/kg K (57 mJ/cm^3 K) at 6.2 K for a magnetic field change of 2 T, respectively. This value is lower than that of EuS (divalent europium valence state) for the same magnetic field change near its Curie temperature of ~17 K, i.e. 15 J/kg K (88 mJ/cm^3 K).[15]

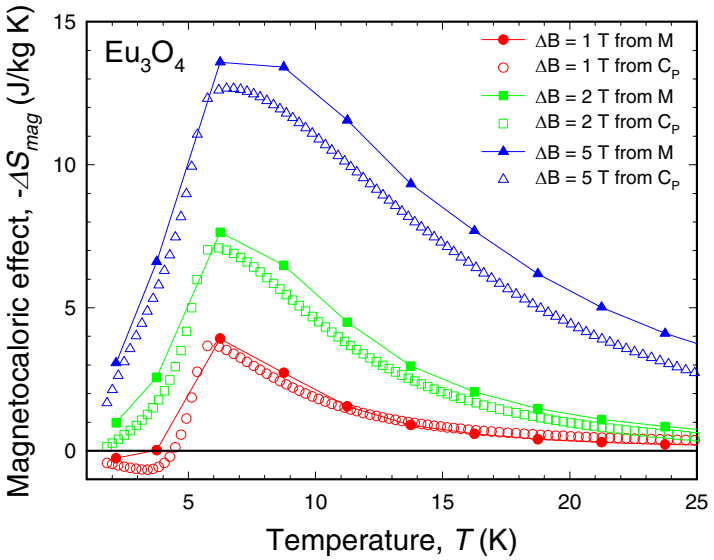

Fig. 9. The magnetic entropy change ($-\Delta S_{mag}$) calculated from magnetization (M) and heat capacity data (C_P) for Eu_3O_4

Conclusions

Polycrystalline Eu_3O_4 was successfully synthesized by heating EuO and Eu_2O_3 together at 1800 °C for 30 hours in a sealed tungsten crucible under high vacuum. The room temperature x-ray powder diffraction and Rietveld refinement for Eu_3O_4 confirm the existence of a single phase Eu_3O_4 with a complex orthorhombic structure. Magnetic and heat capacity measurements were carried out to characterize the magnetic and magneto-thermal properties of Eu_3O_4. We confirmed the mixed-valence character of Eu_3O_4 through the observed effective magnetic moment (5.34 μ_B/Eu atom) derived from the M vs. T curve. Additionally, a metamagnetic transition was detected at 0.3 T below 5 K, which is in good agreement with previous reports. Finally, the magnetocaloric effect of Eu_3O_4, both ΔS_{mag} and ΔT_{ad}, were calculated from both the magnetization and heat capacity data. The maximum magnetic entropy change $|\Delta S_{mag}|$ calculated from heat capacity data in Eu_3O_4 at 6.5 K is 12.7 J/kg K with the magnetic field change (ΔB) of 5 T. The maximum adiabatic temperature change ΔT_{ad} calculated from heat capacity data in Eu_3O_4 at 7.0 K is 7.8 K with the ΔB of 5 T. The $-\Delta S_{mag}$ from heat capacity data is in good agreement with those calculated from the magnetization data.

Acknowledgement

This work was supported by the Office of Basic Energy Sciences, Materials Sciences Division of the U.S. Department of Energy under contract No.DE-AC02-07CH11358 with Iowa State University.

References

[1] C. M. Varma, Rev. Mod. Phys. **48**, 219 (1976).

[2] D. T. Adroja and S. K. Malik, J. Magn. Magn. Mater. **100**, 126 (1991).

[3] J. M. Lawrence, P. S. Riseborough, and R. D. Parks, Rep. Prog. Phys. **44**, 1 (1981).

[4] P. Wachter, in *Handbook of the Physics and Chemistry of Rare Earths*, edited by K. A. Gschneidner, Jr., L. Eyring, and S. Hüfner (North-Holland, Amsterdam, 1994), Vol. 19, p. 177.

[5] K. A. Gschneidner, Jr., V. K. Pecharsky, A. O. Pecharsky, and C. B. Zimm, Mater. Sci. Forum **315-317**, 69 (1999).

[6] V. K. Pecharsky and K. A. Gschneidner, Jr., Phys. Rev. Lett. **78,** 4494 (1997).

[7] Y. C. Achard, Compt. Rend. Acad. Sci. **250**, 3025 (1960).

[8] H. Barnighausen and G. Brauer, Acta. Crystallog. **15**, 1059 (1962).

[9] R. C. Rau, Acta. Crystallog. **20**, 716 (1966).

[10] B. Batlogg, E. Kaldis, A. Schlegel, and P. Wachter, Phys. Rev. B **12**, 3940 (1975).

[11] L. Holmes and M. Schieber, Phys. Rev. **167**, 449 (1968).

[12] L. Holmes and M. Schieber, J. Appl. Phys. **37**, 968 (1966).

[13] O. Tegus, E. Brück, K. H. J. Buschow, and F. R. deBoer, Nature (London) **415**, 150 (2002).

[14] F. X. Hu, B. G. Shen, J. R. Sun, Z. H. Cheng, G. H. Rao, and X. X. Zhang, Appl. Phys. Lett. **78**, 3675 (2001).

[15] P. Bredy and P. Seyfert, Cryogenics **28**, 605 (1988).

[16] T. Hashimoto, T. Numasawa, M. Shino, and T. Okada, Cryogenics **21**, 647 (1981).

[17] K. Ahn, A. O. Pecharsky, K. A. Gschneidner, Jr., and V. K. Pecharsky, J. Appl. Phys. **97**, 063901 (2005).

[18] B. A. Hunter, Rietica – A visual Rietveld program, International Union of Crystallography Commission on Powder Diffraction, Newsletter No. 20 (Summer, 1998) http://www.rietica.org.

[19] V. K. Pecharsky, J. O. Moorman, and K. A. Gschneidner, Jr., Rev. Sci. Instrum. **68**, 4196 (1997).

[20] V. K. Pecharsky and K. A. Gschneidner, Jr., J. Appl. Phys. **86**, 565 (1999).

[21] J. H. Van Vleck and A. Frank, Phys. Rev. **34**, 1494 (1929).

[22] J. H. Van Vleck and A. Frank, Phys. Rev. **34**, 1625 (1929).

[23] J. H. Van Vleck, *The Theory of Electric and Magnetic Susceptibilities* (Oxford University Press, London, 1932), p. 245.

CHAPTER 6. GENERAL CONCLUSIONS

$Yb_5Si_xGe_{4-x}$

The crystallography, phase relationships, and physical properties of the $Yb_5Si_xGe_{4-x}$ alloys with $0 \leq x \leq 4$ have been examined by using single crystal and powder x-ray diffraction at room temperature, and dc magnetization and heat capacity measurements between 1.8 K and 400 K in magnetic fields ranging from 0 and 7 T. Unlike the majority of $R_5Si_xGe_{4-x}$ systems studied to date, where R is the rare earth metal, $Yb_5Si_xGe_{4-x}$ alloys preserve the same crystal structure (Gd_5Si_4-type) as x varies from 4 to 0, which leads to a continuous solid solubility between Yb_5Si_4 and Yb_5Ge_4. As a result, replacements of Ge by Si and vise versa have little effect on the magnetic properties of materials, which is a unique feature compared to all other R_5T_4 systems formed by lanthanides with an incompletely filled *4f* shell. Both the crystallographic and magnetic property data indicate that $Yb_5Si_xGe_{4-x}$ alloys are heterogeneous mixed valence systems, in which the majority (60%) of Yb atoms is divalent, while the minority (40%) is trivalent. Three different lattice sites accommodating lanthanides in the Gd_5Si_4-type crystal structure exhibit selectivity with respect to the valence states of Yb ions. The non-magnetic Yb^{2+} ions are located in the 4(c) and one of the 8(d) sites, while the Yb^{3+} ions are located exclusively in the 8(d) sites. $Yb_5Si_xGe_{4-x}$, therefore, may be considered to be a heterogeneous mixed valence system. All $Yb_5Si_xGe_{4-x}$ alloys exhibit weak antiferromagnetic correlations at temperatures between 2.4 K and 3.2 K.

^{170}Yb Mössbauer spectra of $Yb_5Si_xGe_{4-x}$ taken between 1.5 K and 40 K show that Yb is present as Yb^{2+} and Yb^{3+} in nearly equal amounts [51.6(3) % and 48.4(3) %, respectively] and that this balance is independent of temperature and composition. Magnetic order develops below 1.7 K with the zero temperature Yb^{3+} moments estimated to be $2.1\pm0.2\ \mu_B$ for x = 0 and 4. These results are in fair agreement with those observed by bulk magnetization data. Intermediate compositions (x = 1, 2, 3) exhibit two distinct ordered Yb^{3+} subcomponents which appear to have separate ordering temperatures. Furthermore, there is a break in magnetic behavior between x = 3 and x = 3.5, that does not appear to be associated

with any crystallographic changes. Final confirmation of magnetic structures will come in a future from neutron diffraction data. While neutrons are insensitive to valence, the neutron diffraction data should allow us to determine the amount and location of Yb^{3+} ions in $Yb_5Si_xGe_{4-x}$ since only Yb^{3+} carries a magnetic moment.

$Sm_5Si_xGe_{4-x}$

The crystallography, phase relationships, and physical properties of the $Sm_5Si_xGe_{4-x}$ alloys with $0 \leq x \leq 4$ have been investigated by using variable temperature x-ray powder diffraction, dc magnetization and heat capacity measurements between 3.5 K and 350 K in magnetic fields ranging from 0 and 10 T. Similar to the $Gd_5Si_xGe_{4-x}$ systems, there are three distinct phase regions in the $Sm_5Si_xGe_{4-x}$ system; the Gd_5Si_4-type for Si-rich compositions, the $Gd_5Si_2Ge_2$-type for intermediate range of concentrations, and the Sm_5Ge_4-type for Ge-rich alloys. Samarium ions in both Sm_5Si_4 and Sm_5Ge_4 compounds follow normal lanthanide contraction rule, thus indicating that Sm ions are in trivalent state. The dc magnetic susceptibilities for $Sm_5Si_xGe_{4-x}$ alloys can be well described with the consideration of the temperature-independent Van Vleck term because of the narrow energy separation between $J = 5/2$ and $J = 7/2$ multiplet states of Sm^{3+} ions. The reduced effective magnetic moment and saturated magnetic moment of $Sm_5Si_xGe_{4-x}$ alloys are likely due to CEF splittings. The magnetic behaviors with the replacement of Ge by Si in $Sm_5Si_xGe_{4-x}$ alloys are similar to those observed in $Gd_5Si_xGe_{4-x}$ alloys (second order FM for Si-rich regions, first-order FM for intermediate regions, and AFM for Ge-rich regions). Interestingly, the paramagnetic Curie temperature of Sm_5Si_4 (θ_p = 220(2) K) is approximately two times higher than the expected temperature estimated from de Gennes factor scaling with the other corresponding R_5Si_4 systems for light rare earth elements. The external magnetic field of 10 T cannot suppress the specific heat peaks, which are clearly of magnetic origin in the $Sm_5Si_xGe_{4-x}$ system ($Sm_5Si_2Ge_2$ also has a structural phase change), while those in other $R_5Si_xGe_{4-x}$ system are significantly affected (either reduced and broadened or shifted) by high magnetic fields. Thus, the magnetocaloric effect values are expected to be negligible in the $Sm_5Si_xGe_{4-x}$ system. Moreover, *in-situ* x-ray powder diffraction measurements as a function of

temperature indicate that there is the coupling of magnetic and structural phase transition for $Sm_5Si_2Ge_2$.

EuO

Polycrystalline EuO was successfully synthesized through the thermal reduction of Eu_2O_3 by a stoichiometric quantity of metallic Eu. The room temperature crystal structure of the material was confirmed by the room temperature x-ray powder diffraction. According to the heat capacity and magnetic measurements, EuO undergoes a second-order phase transformation at ~69 K from the ferromagnetic to the paramagnetic state on heating. The magnetocaloric effect (MCE) of EuO, both as the isothermal magnetic entropy change (ΔS_{mag}) and the adiabatic temperature change (ΔT_{ad}), was obtained from the heat capacity data. Also, the magnetization isotherms were used to calculate ΔS_{mag}. EuO exhibits the MCE with a peak in the vicinity of the magnetic phase transition temperature (~69 K), the amplitude of which is comparable to other known magnetocaloric materials such as $DyAl_2$. The ΔS_{mag} calculated from the heat capacity data is in excellent agreement with that calculated from the magnetization data. The $|\Delta S_{mag}|$ maximum in EuO near T_C (69 K) are 4.6, 8.4, 17.5, 22.3, and 27.6 J/kg K for ΔH of 10, 20, 50, 75, and 100 kOe, respectively. The ΔT_{ad} maximum of EuO are 1.6, 3.2, 6.8, 8.8, and 11.2 K for the same magnetic field changes, respectively.

Eu_3O_4

Polycrystalline mixed-valence compound Eu_3O_4 was successfully synthesized by heating EuO and Eu_2O_3 together at 1800 °C for 30 hours in the sealed tungsten crucible under the high vacuum. The room temperature x-ray powder diffraction and Rietveld refinement for Eu_3O_4 confirm the existence of a single phase Eu_3O_4 with a complex orthorhombic structure. Magnetic and heat capacity measurements were carried out to characterize the magnetic and magneto-thermal properties of Eu_3O_4. The mixed-valence character of Eu_3O_4 was confirmed from the observed effective magnetic moment (5.34 μ_B/Eu atom) derived from the *M(T)* data.

A metamagnetic transition is detectable below 5 K at a magnetic field of 0.3 T, which is in good agreement with earlier reported results. To our best knowledge, the heat capacity study of Eu_3O_4 was performed in this work for the first time. The magnetocaloric effects (MCE) in Eu_3O_4, both the magnetic entropy change (ΔS_{mag}) and the adiabatic temperature change (ΔT_{ad}), were measured when subjected to applied magnetic fields. The magnetic entropy change ($-\Delta S_{mag}$) from the heat capacity data in Eu_3O_4 near 6.5 K is around 12.7 J/kg K with the magnetic field change (ΔB) of 5 T. The adiabatic temperature change (ΔT_{ad}) in Eu_3O_4 near 7 K is around 7.0 K with the ΔB of 5 T. Also, the magnetic entropy change ($-\Delta S_{mag}$) calculated from the magnetization data in Eu_3O_4 near 6.3 K is around 13.6 J/kg K with the magnetic field change (ΔB) of 5 T, which is roughly same as that from heat capacity data.

Recommendations for future work

(1) Other probes may be needed in order to understand the evident reason of not having FM state in the presence of interslab bonds in all $Yb_5Si_xGe_{4-x}$ compounds while neutron diffraction work is in progress to identify the magnetic structures. Element-specific x-ray magnetic circular dichroism (XMCD) and x-ray absorption fine structure (XAFS) measurements may be good choices of probe.

(2) The stabilization of the Gd_5Si_4-type structure by reduced valence electron density is valid in the $Yb_5Si_xGe_{4-x}$ system and thus the replacement of tetravalent germanium by either trivalent gallium or pentavalent antimony in Yb_5Ge_4 could be interesting. This project is in progress and Mössbauer spectroscopy and neutron diffraction works will be performed on $Yb_5Ga_xGe_{4-x}$ and $Yb_5Sb_xGe_{4-x}$.

(3) Inelastic neutron scattering work may be considered to clarify the CEF level in the $Sm_5Si_xGe_{4-x}$ system.

(4) EuO is a ferromagnetic semiconductor and has been reported to show the insulator-metal transition below T_C. Detail investigations of the insulator-metal transition in EuO may be interesting.

ACKNOWLEDGEMENTS

First of all, I cannot help mentioning my sincere appreciation to my major professors Vitalij K. Pecharsky and Karl A. Gschneidner, Jr. This work and my Ph. D. degree would not be accomplished without their thoughtful guidance and support. Also I would like to give thanks to my committee members who are professors David C. Johnston, Paul C. Canfield, and R. William McCallum. And I would like to thank Mrs. Carol Smith, Mr. Roger Rink, Dr. Yaroslav Mudryk, all the graduate students, and postdocs in the group for their help in experiments and useful discussions.

Finally, I would like to share my accomplishments and happiness with my wife, Hye-Gyung, and my son, Daniel. Their encouragement and cheer were great to me and I was always happy with them. Also I am very thankful to encouragements of my parents, parents-in-law, sisters, and brothers.

This work was supported by the Office of Basic Energy Sciences, Materials Sciences Division of the U.S. Department of Energy under contract No.DE-AC02-07CH11358 with Iowa State University.